BIFURCATION OF BUOYANT JETS IN CROSS FLOW

by

Mohamed S.T. Abdelwahed

A Thesis submitted to the Faculty of Graduate Studies and Research in partial fulfilment of the requirements for the Degree of Master of Engineering

Department of Civil Engineering and Applied Mechanics
McGill University
Montreal, Canada

March 1978

TO MY BELOVED WIFE

ABSTRACT

Experiments were performed by discharging hot water upward through an orifice at the channel bottom into an open channel cross-flow with a free water surface. The buoyant jet was observed to bend over and form a pair of vortex-like circulations within a short distance from the exit. As the vortex pair approaches the free surface it bifurcates into two turbulent vortex elements; between them a clear space could be observed extending continuously. This phenomenon has been pointed out by Hayashi (1971) as one possible mechanism through which pollutant effluent disposed off-shore may drift back toward the shore line and contaminate the coastal environment.

In the experiments, cross-section and trajectory of the bifurcated jet were determined from visual observations. The results were correlated by dimensionless variables derived from a line impulse model. With proper interpretation of the results, the development of the bifurcated jet was shown to follow essentially the same behaviour as a non-bifurcated jet, undeflected by the free surface. The mean vortex circulation in each of the turbulent element was found to decay with distance from the bifurcated point. The observations have invalidated the theoretical models proposed by Hayashi (1971) and by Turner (1960) in which circulation in each of the separated elements was assumed to remain constant.

RESUME

Des expériences ont été éxécutées en déchargeant de l'eau chaude, par un orifice pratiqué dans le fond d'un canal découvert, dans un écoulement transversal d'eau à surface libre. Il fut observé que le jet flottant adoptait une forme courbe et bifurquait en une paire de circulations semblables à des tourbillons en deçà d'une courte distance de l'orifice. En s'approchant de la surface libre, la paire de tourbillons se transforme en deux tourbillons turbulents; entre ces tourbillons l'on remaique un espace continu. Ce phénomène a été signalé par Hayashi (1971) comme étant un mécanisme possible par lequel un effluent polluent déchargé au large des côtes puisse se r'abattre et contaminer l'environnement côtier.

Dans les experiences, les profils et les trajectoires furent déterminés par observations visuelles. Les resultats furent mis en corrélation par des variables sans dimensions dérivées à portir d'un modèle de pulsations alignées. Une interprétation appropriée des résultats a montré que le développement du jet bifurqué suivait essentiellement le même comportement qu'un jet non-bifurqué, non-dévié par la surface libre. Il fut constaté que la circulation moyenne du tour billon dans chaque élément turbulent diminuait en fonction de la distance du point de bifurcation. Les observations ont invalidé les modèles théoriques proposés par Hayashi (1971) et par Turner (1960) dans lesquels il est supposé que la circulation dans chacun des élements séparés demeure constante.

ACKNOWLEDGEMENTS

The author is indebted to Professor V.H. Chu for his guidance, advice and encouragement throughout the course of this work.

The technical assistance of Mr. B. Cockayne, Mr. T. Rigby and the Fluid Mechanics Laboratory staff is much appreciated.

In addition, the interest and helpful suggestions of fellow graduate students contributed significantly to this thesis.

Sincere thanks are also due to Miss J.M. Richards for typing the manuscript.

TABLE OF CONTENTS

LIST OF FIGURES

LIST OF TABLES

LIST OF SYMBOLS

A = cross sectional area of the jet = $r_n\ r_s$

B = breadth of the open channel

d = jet diameter at the nozzle

D = characteristic dilution ratio

F = buoyancy flux

F_r = densimetric Froude number

g = gravitational constant

g' = buoyancy force per unit mass

H = water depth above the exit

k = added mass coefficient

ℓ_b = buoyancy length scale

ℓ_m = momentum length scale

ℓ_{m_B} = momentum length scale based on the momentum at the bifurcation point

ℓ_q = volume length scale

ℓ_s = length scale of the line impulse model

m = momentum flux per unit length

M = momentum flux

q = volume per unit length

Q = volume flux

r = characteristic radius of the jet

r_s = jet width (see Fig. 1)

r_n = jet width (see Fig. 1)

R = exit to cross-flow velocity ratio = $\frac{V}{U}$

$(Re)_a$ = Reynolds number of the cross-flow

$(Re)_o$ = jet Reynolds number at the exit

Ri = Richardson number

$(Ri)_B$ = Richardson number at the bifurcation point

R_x = Reynolds number based on the nozzle length $x = \frac{V_{av}x}{\nu}$

s = lateral migration distance (see Fig. 1c)

s_i = inner migration distance

s_o = outer migration distance

t = time

t_s = time scale of the line impulse model

T_a = temperature of the cross-flow

T_o = temperature of the discharging jet at the exit

u = characteristic velocity of the two-dimensional element

U = velocity of the cross-flow along the centerline of open channel

U_i = U_1, U_2, U_3 = velocity of the cross-flow

V = exit velocity at the nozzle

V_{av} = the average velocity in the nozzle

V_{max} = the maximum velocity in the nozzle

x = horizontal coordinate along the channel

x_B = longitudinal bifurcated distance

y = horizontal coordinate in the transverse direction

y_o = the outer boundary of the bifurcated jet

z = vertical coordinate

z_p = length of the potential core

α, β, β_s, β_n = entrainment coefficients

δ^* = displacement thickness of the laminar boundary layer

Γ = circulation

ν = kinematic viscosity

Θ = momentum thickness of the laminar boundary layer

Θ_B = angle of impingement

ρ = fluid density

Subscripts

B = conditions at the bifurcation point

o = conditions at the exit

CHAPTER 1

INTRODUCTION

The bifurcation phenomenon of turbulent buoyant jets in a cross-flow was investigated here experimentally. Hot and cold water were discharged upward through an orifice at the channel bottom into an open channel cross-flow with free water surface as shown in Figs. 1 and 2. The turbulent jet was first observed to bend over and form a pair of vortex-like turbulent elements. As the jet approached the free water surface it bifurcated into two separate regions; between them a clear space can be seen extending continuously.

The bifurcation phenomenon described above has been considered by Hayashi (1971). He suggested that this could be one possible mechanism through which sewage effluents, disposed off-shore may drift back toward the shore line and contaminate the coastal environment. Similar bifurcation process is expected when buoyant clouds of pollutants are impinged on strongly stratified regions such as inversion layers or thermoclines in both the atmosphere and the oceans. Bifurcation of stack plumes has also been observed in a neutrally stable atmosphere by Scorer (1958). He pointed out that such phenomenon is often observed in washed thermal plumes in cold weather when rapid evaporation of condensed water droplets occur.

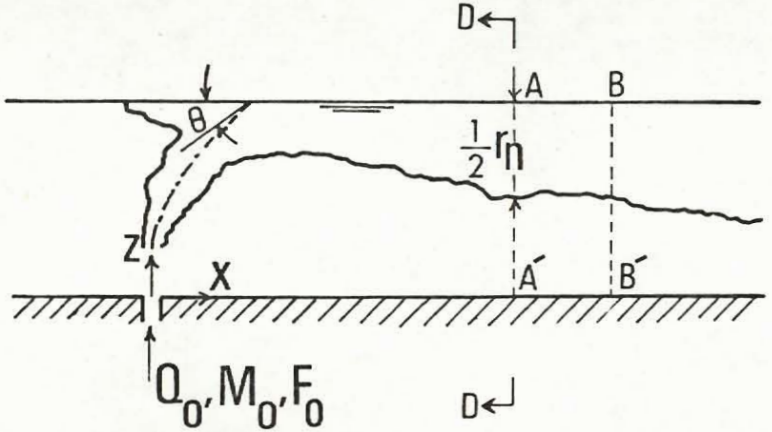

(a)

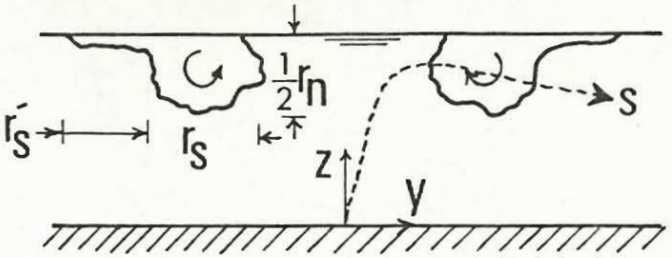

(c) Section D – D

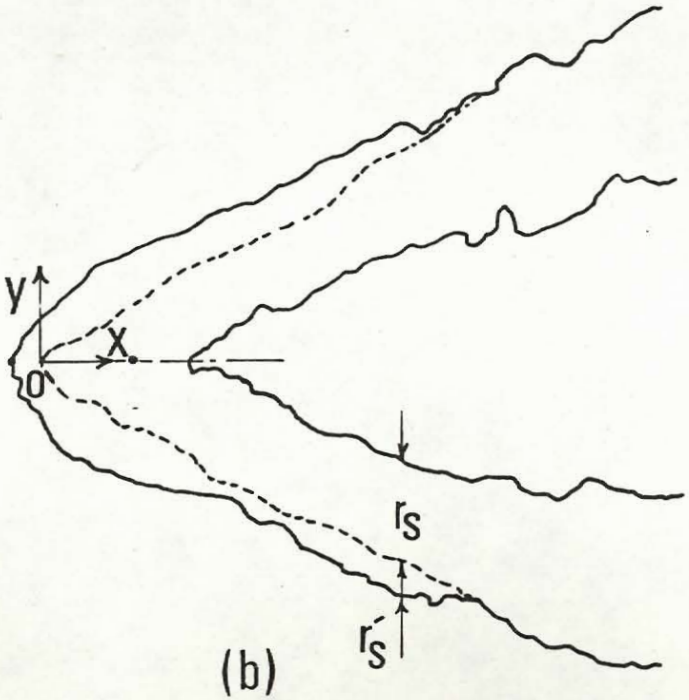

(b)

Fig. 1 Definition Sketch of the Bifurcated Jet

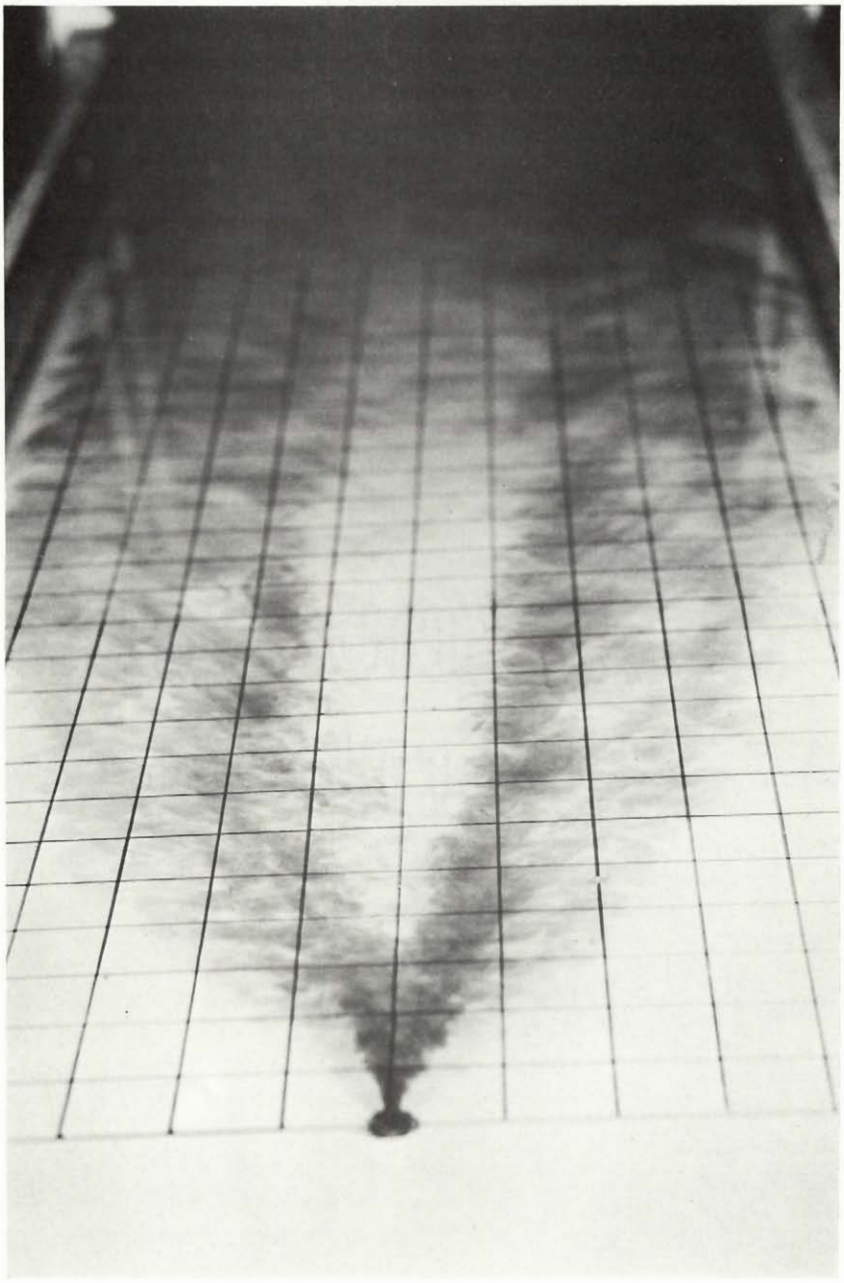

Fig. 2 Photograph of the Bifurcation Phenomena

A theoretical model was introduced by Turner (1960) for bifurcated plumes (a buoyant jet with no exit momentum flux) in a uniform surrounding. He suggested that circulation in each of the vortex elements should remain constant, once the elements are clearly separated. Based on this assumption, he then predicted that the separating distance between the buoyant vortex elements would increase exponentially with height. However, the exponential behaviour has not been supported by experimental observations. To study the effect of a free surface on the bifurcated jet, Hayashi (1971) has introduced a theoretical model in which the free surface was simulated by an image vortex pair. Assuming again that the circulation remains constant, as in Turner (1960), he found the separating distance to vary linearly with distance from certain virtual origin. Although his theoretical solution was shown to be in qualitative agreement with experimental observation, it gave an incorrect limit, namely: bifurcation is not predicted in the limiting case when buoyancy vanishes to zero (i.e., the case of momentum jet).

Bifurcation phenomena will be considered in this thesis for both buoyant and non-buoyant jets. The experimental results will be correlated by dimensionless variables derived from a line impulse model. Comparisons will be made with existing experimental results of non-bifurcated turbulent jets and plumes in cross-flow. Finally, a number of analytical models for buoyant jets in uniform cross-flows will be reviewed in the light of our experimental observations on bifurcated jets.

CHAPTER 2

THEORETICAL CONSIDERATION

Theoretical solutions are obtained in this chapter to describe the bifurcation phenomena of buoyant jets in cross-flow. Considerable simplification of the problem can be achieved by introducing a number of simplifying concepts. These concepts are the "line impulse model", the "point source model", and the "momentum redirection model" to be illustrated later in this chapter.

We shall begin with dimensional consideration to bring out the important length scales and dimensionless variables. Then the formulation of the problem will follow from an entrainment hypothesis.

2.1 Dimensional Analysis

The purpose of this section is to show how dimensional reasoning together with the concept of a "line impulse model" and the concept of a "point source model" could simplify the problem. We shall begin with a simple minded dimensional analysis to bring out some of the important length scales and dimensionless variables that are commonly used in the literature. Consider, for example, the trajectory of the jet. It can be expressed in a functional form as follows:

$$s = f\,(U,\ Q_o,\ M_o,\ F_o,\ \rho,\ H,\ x) \qquad (1)$$

where the important physical variables are:

s = transverse migrating distance (see Fig. 1(c))

U = cross-flow velocity

Q_o = volume flux at the exit

M_o = momentum flux at the exit

F_o = buoyancy flux at the exit

ρ = fluid density

H = depth of the cross-flow

x = longitudinal distance along the direction of the cross-flow.

In deriving Eq. 1, the fluid is assumed to be uniform in density but variable in specific weight following the Boussinesq approximation. The jet trajectory is defined on a curved surface as shown in Fig. 1(c). The transverse migration distance s follows initially along the vertical plane of symmetry and is eventually directed along the free water surface after bifurcation. Three basic length scales can be defined in terms of the variables in Eq. 1 as follows:

$$\ell_q = \text{volume length scale} = \left[\frac{4\, Q_o}{\pi U} \right]^{\frac{1}{2}}$$

$$\ell_m = \text{momentum length scale} = \left[\frac{4\, M_o}{\pi \rho U^2} \right]^{\frac{1}{2}} \qquad (2a,b,c)$$

$$\ell_b = \text{buoyancy length scale} = \left[\frac{4\, F_o}{\pi \rho U^3} \right]$$

Now the jet trajectory can be expressed in dimensionless form:

$$\frac{s}{\ell_m} = f\left(\frac{H}{\ell_m}, \frac{x}{\ell_m}, \frac{\ell_b}{\ell_m}, \frac{\ell_q}{\ell_m}\right) \tag{3}$$

If the buoyant fluid is injected into the cross-flow through a circular pipe of diameter d , and if the buoyancy per unit mass $g' = (g\Delta\rho/\rho)$ and the velocity V are both assumed uniform at the exit, the length scales in Eq. 2 will give two dimensionless parameters as follows:

$$\text{Exit to cross-flow velocity ratio } R = \frac{V}{U} = \left(\frac{\ell_m}{\ell_q}\right)^2 \tag{4a,b}$$

$$\text{Densimetric Froude number (based on cross-flow velocity)} \qquad F_r = \frac{U}{(g'd)^{\frac{1}{2}}} = \left(\frac{\ell_m}{\ell_b}\right)^{\frac{1}{2}}$$

In terms of these parameters, Eq. 3 can be expressed alternatively by

$$\frac{s}{d} = f\left(\frac{x}{d}, R, F_r, \frac{H}{d}\right) \tag{5}$$

The dimensionless parameters in Eqs. 3 and 5 are the most commonly used in the literature. Obviously, these are too many parameters for systematic correlation with the experimental results. An attempt will be made to simplify the problem further by introducing the concept of a "line impulse model" and the concept of a "point source model".

We shall now describe the concept of the "line impulse model" following Priestley (1956), Scorer (1958) and Chu (1976). In this model, the motion of the jet will be considered in a coordinate system moving with the cross-flow. In the moving coordinate system, the ambient fluid is stationary. The jet is seen to be resulting from a continuous source which ejects buoyant fluid and is moving with a velocity U equal and opposite in direction to the cross-flow. This continuous source is characterized by its volume flux Q_o , momentum flux M_o , and buoyancy flux F_o at the exit. The velocity distribution along the jet will be assumed to be "top-hat"*. Thus, it is possible to follow a segment of the jet AB by moving along the path line A'A and B'B as shown in Fig. 1a. The segment AB could be chosen such that A left the source A' at a unit time earlier than B left B'. In such a manner the volume, momentum and the buoyancy force associated initially with the segment are defined and are equal to the volume flux Q_o, the momentum flux M_o, and the buoyancy flux F_o at the source.

As the segment moves away from the source, it gradually rotates towards the direction of the cross-flow. The length of the segment is equal to the magnitude of the cross-flow velocity U. The problem is now two-dimensional and is reduced to the determination of the motion of a line turbulent element in a stationary ambient fluid. The initial

---

* The assumption of a top-hat profile is no more restrictive than the assumption of any similarity profiles for velocity and buoyancy distribution. Top-hat profiles and Gaussian profiles have been shown to be equivalent by Morton, Taylor and Turner (1956).

impulse per unit length of the line element is Q_o/U, M_o/U and F_o/U. The relevant physical variables for a "line impulse model" are depth of cross-flow H, the fluid density ρ , and the strength of the impulse Q_o/U, M_o/U and F_o/U. These basic variables will generate two independent length scales,

$$\ell_q = \left[\frac{4\, Q_o}{\pi U} \right]^{\frac{1}{2}}$$

$$\ell_s = \left[\frac{4\, M_o^{\,2}}{\pi \rho F_o U} \right]^{1/3} = \left[\frac{\ell_m^{\,4}}{\ell_b} \right]^{1/3} \qquad (6a,b,c)$$

and a time scale,

$$t_s = \frac{M_o}{F_o} = \frac{\ell_m^{\,2}}{\ell_b U}$$

In the moving coordinate system the ambient fluid is stationary. The transverse distance of the line segment s is a function of time t. Expressing in dimensionless form,

$$\frac{s}{\ell_s} = f\left(\frac{t}{t_s} , \frac{\ell_q}{\ell_s} , \frac{H}{\ell_s} \right) \qquad (7a)$$

Since time is related to longitudinal coordinate in the direction of cross-flow by $x = Ut$, the jet trajectory can be expressed in terms of coordinates fixed with the source as follows:

$$\frac{s}{\ell_s} = f\left(\frac{x\ell_b}{\ell_m^2}, \frac{\ell_q}{\ell_s}, \frac{H}{\ell_s}\right) \qquad (7b)$$

At this stage the "point source model" should be introduced. It is argued that at some far field region, due to turbulent entrainment of ambient fluid, the volume flux of the jet will eventually become very large compared with the initial volume flux at the exit. The effect of exit volume flux Q_o may be negligible (i.e., $\ell_q \to o$) and Eq. 7b reduced to:

$$\frac{s}{\ell_s} = f\left(\frac{x\ell_b}{\ell_m^2}, \frac{H}{\ell_s}\right) \qquad (8)$$

This approximation is referred to as a "point source model". For a fixed ℓ_m and ℓ_b the limit $\ell_q \to o$ is equivalent to $D \to o$ (point source) and $R \to \infty$.

The trajectory of the buoyant jet before bifurcation is rather unaffected by the free surface. Under this condition, the depth dependence will be eliminated from Eq. 8 and

$$\frac{s}{\ell_s} = f\left(\frac{x\ell_b}{\ell_m^2}\right) \qquad (9)$$

The explicit dependency on H/ℓ_s in Eq. 8 could be eliminated also for the region after bifurcation. This can be done by introducing the "momentum

redirection model" at the bifurcation point. Further details on this model will be illustrated in the later sections when the problem is formulated based on entrainment hypothesis.

2.2 Formulation

A number of assumptions will be made to simplify the formulation. One of these assumptions is to neglect the loss of momentum and buoyancy from the jet into the wake. In a neutrally stable cross-flow, this means that the buoyancy force F/U associated with unit length of the line segment is conserved, i.e.,

$$\frac{F}{U} = \frac{F_o}{U} \tag{10}$$

Before jet bifurcation, the rate of change of momentum per unit length is given by:

$$(1 + k)\,\frac{dm}{dt} = \frac{F_o}{U} \qquad \text{for } t > t_B \tag{11}$$

where

m = momentum per unit length of the two-dimensional element

k = the added mass coefficient

t = time.

The subscript "o" refers to the condition at the exit and the subscript "B" refers to the conditions at the bifurcation point. Eq. 11 includes the added mass effect which was virtually neglected in all other analytical models for jets and plumes in cross-flows. The importance of the added mass effect has been pointed out recently by Escudier and Maxworthy (1973) in formulating the rise of axisymmetrical thermals.

Integrating Eqs. 10 and 11 with respect to time,

$$m = \frac{F_o t}{U(1+k)} + \frac{M_o}{U} \qquad \text{for } t < t_B \tag{12}$$

Once the turbulent element reaches the free surface, bifurcation occurs, momentum will be redirected sideways and from then on the momentum in the horizontal direction associated with each of the bifurcated elements will remain constant. The momentum, per unit length, just before bifurcation is:

$$m_B = \frac{F_o t_B}{U(1+k)} + \frac{M_o}{U} \tag{13}$$

If the bifurcation is assumed to occur rather rapidly, then the fluid motion around the point of bifurcation could be treated as invicid and follows the Bernoulli equation along a stream line. The horizontal momentum associated with each of the bifurcated element will be half m_B.

Since the buoyancy force is acting in the vertical direction, the horizontal momentum of each of the bifurcated elements will remain half m_B for all time after bifurcation occurs.

To proceed further it is now necessary to introduce an entrainment hypothesis. According to Morton, Taylor and Turner (1956):

$$\frac{dq}{dt} = 2 \pi \alpha r u \tag{14}$$

where q = volume per unit length of the two-dimensional element

α = entrainment coefficient

r, u = characteristic radius and characteristic velocity of the element respectively, and are defined by:

$$q = \pi r^2 \tag{15}$$

$$u = \frac{ds}{dt} = \frac{m}{q} \tag{16}$$

Initially, before bifurcation occurs, the travelling distance of the element s is measured along the vertical direction, i.e., $s = z$. After the jet has bifurcated into two separated elements, the distance s following one of the elements is $s = s_B + y$ (see Fig.1(c). Note that the volume per unit length of each of the bifurcated elements is $\frac{1}{2} q$; but, the characteristic radius r is defined based on the total volume of both elements.

Substituting Eqs. 15 and 16 into Eq. 14,

$$\alpha = \frac{dr}{ds} \tag{17}$$

This defines the entrainment coefficient as the rate of change of the characteristic radius with distance. The entrainment coefficient will remain constant if the rate of change of radius r with distance s is linear.

The entrainment coefficient is known to remain essentially constant before the bifurcation of the jet, i.e., for non-bifurcated jets (see Chu and Goldberg (1974) and Chu (1978)). Once the bifurcated elements are directed along the free surface in the horizontal direction, entrainment will be affected by the stable density stratification along the turbulent and laminar interface. The entrainment coefficient may depend on the local Richardson number. The turbulent entrainment may collapse at certain critical Richardson number as in the surface jet experiments of Ellison and Turner (1959) and Chu and Vanvari (1976).

For simplicity, an analytical solution will be developed here assuming the entrainment coefficient to remain constant before and after bifurcation. Such an assumption is expected to be valid at least for momentum jets that are unaffected by buoyancy. The solution will be compared with experimental results in a later chapter. The deviation of the solution with experiment will possibly determine how the entrainment coefficient of a bifurcated jet may be affected by the buoyancy effects.

For constant entrainment coefficient Eq. 17 can be integrated and gives:

$$r = \alpha s \tag{18}$$

in which the distance s is measured from a virtual origin where r = o. Making use of Eqs. 15, 16 and 18, and the fact that x = Ut, Eqs. 12 and 13 can be rewritten as follows:

For $x \leq x_B$, before the bifurcation

$$\pi\alpha^2 s^2 \frac{ds}{dx} = \frac{F_o}{(1+k)U^3} x + \frac{M_o}{U^2} \tag{19}$$

and for $x > x_B$, after bifurcation

$$\pi\alpha^2 s^2 \frac{ds}{dx} = \frac{F_o}{(1+k)U^3} x_B + \frac{M_o}{U^2} \tag{20}$$

Further simplification is obtained by introducing the dimensionless variables:

$$\tilde{s} = \frac{s}{\ell_s} \quad \text{and} \quad \tilde{x} = \frac{x\ell_b}{\ell_m^2} \tag{21}$$

In dimensionless form Eqs. 19 and 20 are:

$$\frac{4\alpha^2}{3}\frac{d\tilde{s}^3}{d\tilde{x}} = \frac{\tilde{x}}{(1+k)} + 1 , \quad \text{for } \tilde{x} \le \tilde{x}_B \tag{22}$$

$$\frac{4\alpha^2}{3}\frac{d\tilde{s}^3}{d\tilde{x}} = \frac{\tilde{x}_B}{(1+k)} + 1 , \quad \text{for } \tilde{x} > \tilde{x}_B \tag{23}$$

These equations can be integrated to give trajectories of the jet before and after bifurcation as follows:

$$\tilde{s}^3 = \left(\frac{3}{4\alpha^2}\right)\left[\frac{\tilde{x}^2}{2(1+k)} + \tilde{x}\right] , \quad \text{for } \tilde{x} \le \tilde{x}_B \tag{24}$$

$$\tilde{s}^3 - \tilde{s}_B^3 = \left(\frac{3}{4\alpha^2}\right)\left[\frac{\tilde{x}_B}{(1+k)} + 1\right](\tilde{x}-\tilde{x}_B) , \quad \text{for } \tilde{x} > \tilde{x}_B \tag{25}$$

At the bifurcation point, according to Eq. 24,

$$\tilde{s}_B^3 = \left(\frac{3}{4\alpha^2}\right)\left[\frac{\tilde{x}_B^2}{2(1+k)} + \tilde{x}_B\right] \tag{26}$$

Substituting into Eqs. 24 and 25,

$$\tilde{s} = \left(\frac{3}{4\alpha^2}\right)^{1/3}\left[\frac{\tilde{x}^2}{2(1+k)} + \tilde{x}\right]^{1/3} , \quad \text{for } \tilde{x} \le \tilde{x}_B \tag{27}$$

and

$$\tilde{s} = \left(\frac{3}{4\alpha^2}\right)^{1/3}\left[\frac{2\tilde{x}\tilde{x}_B - \tilde{x}_B^2}{2(1+k)} + \tilde{x}\right]^{1/3} , \quad \text{for } \tilde{x} > \tilde{x}_B \tag{28}$$

where the longitudinal location of the bifurcation point

$$\tilde{x}_B = -(1+k) + \sqrt{(1+k)^2 + \frac{8\alpha^2}{3}(1+k)\,\tilde{s}_B^3} \qquad (29)$$

Now the jet trajectory before and after bifurcation point is determined. The location of the bifurcation point remains to be determined. According to the estimate given in section 4.2, $s_B \approx 0.78$ H.

It should be mentioned again that the solution Eqs. 27 and 28 were obtained based on the assumption that the entrainment coefficient remains constant. For non-bifurcated jet, the entrainment coefficient is known to remain approximately a constant (see, for example, Chu and Goldberg, 1974). Once the jet bifurcates and spreads along the free surface,the entrainment coefficient will be affected by stable stratification and may possibly depend on the local Richardson number. The limitation of the solution given by Eqs. 27 and 28 will be discussed in a later chapter where they are compared with the experimental observations.

At this stage, two limiting cases may be mentioned. For momentum jet in which buoyancy effect is negligible (i.e., $\ell_b \to o$), both Eqs. 27 and 28 reduce to a one-third power law:

$$\frac{s}{\ell_m} = \left(\frac{3}{4\alpha^2}\right)^{1/3} \left[\frac{x}{\ell_m}\right]^{1/3} \qquad (30)$$

On the other hand, for the buoyant plume in which the exit momentum is negligible (i.e., $\ell_m \to 0$), a two-thirds power law is obtained for the non-bifurcated region of the jet, i.e.,

$$\frac{s}{\ell_b} = \left(\frac{3}{8(1+k)\alpha^2}\right)^{1/3} \left(\frac{x}{\ell_b}\right)^{2/3} , \quad \text{for } x \leq x_B \tag{31}$$

There is, however, no simple power law for $x > x_B$. The one-third and the two-thirds laws will be used in a later section (§4.1) for the determination of the entrainment coefficient and the added mass coefficient from experiments of non-bifurcated jets. Note that the jet trajectory for a momentum jet is independent of the added mass coefficient.

We are now in a position to determine the dilution and concentration decay along the jet axis. Due to turbulent entrainment of ambient fluid, the radius of the jet increases continuously as it penetrated through the cross-flow. According to the entrainment hypothesis (Eq. 18), the volume per unit length of the vortex element is given by,

$$\frac{Q}{U} = \pi r^2 = \alpha^2 \pi s^2 \tag{32}$$

where Q is a characteristic volume flux.

The jet dilution is characterized by the dilution ratio,

$$D = \frac{Q}{Q_o} = \frac{\alpha^2 \pi s^2 U}{Q_o} \tag{33}$$

Note that concentration of certain conserved substances discharged through the jet is equal to the inverse of dilution ratio. A characteristic concentration could be defined as $D^{-1} = Q_o/Q$. Eq.(33) can be rewritten in dimensionless form:

$$\frac{DQ_o}{U\ell_s^2} = \alpha^2 \pi \tilde{s}^2 \tag{34}$$

Experimental observation of the concentration distribution in a cross-section of the vortex element has shown that there are two maxima of concentration and they are located at the vortex cores. According to Fan (1967) the maximum concentration at the cores is 50 to 75% higher than the maximum at the plane of symmetry.

CHAPTER 3

EXPERIMENTAL SET-UP AND PROCEDURES

3.1 Experimental Set-Up

Experiments were performed in a wide rectangular channel 800 cm long, 60 cm wide and 15 cm deep. Due to the construction of the channel, only a section of the jet can be observed through the side window. The side window is 40 cm long and is located at 20 cm downstream of the discharging nozzle as shown in Fig. 3.

Hot and cold water were discharged from a nozzle located at the bottom of the channel. Two nozzles of different inside diameters were used in the experiments. There were two stages of flow contraction before the fluid was discharged through the nozzles. This reduces the non-uniformity of the velocity distribution at the exit. Most of the experiments were carried out with the nozzle flush with the channel bottom. A short stack (3 cm in length and with the same diameter as the nozzle) was added on top of the nozzle in one series of the test (series 2000). The purpose of the stack was to study the effect of the channel bottom on the development of the bifurcated jet. The nozzles and the stack are shown in Fig. 4.

To trace the jet paths photographically, the jet fluids were mixed with dye (potassium permanganate solution). A pressurized dye injector was built. It consists of two inter-connected plexiglass boxes

and a venturi-meter as shown in Fig. 5. The injector can be pressurized by opening valve #1 and closing valve #2. During the experiments, valve #1 was closed and the dye was injected through valve #2. The dye concentration in the jet was generally low and it is believed to have little effect on the observed phenomena.

For buoyant jet experiments, the water was heated by using two electric water heaters (model Cascade 60, John Wood). The maximum water temperature gained from the water heater was 170°F. The discharging water temperature was recorded by a calibrated thermistor probe (Earling model 19-0140 Thermistor Thermometer) which was connected to the nozzle as shown in Fig. 4. To eliminate heat losses, all piping , hoses, the thermistor probe and the nozzle were thermally insulated.

The discharge through the nozzle was determined by using a small rotameter (Brooks - tube size R-6-25-B) which was calibrated and cleaned several times during the course of the experiments.

To reduce the swirling and secondary currents in the cross-flow, a screen and a series of flow straighteners were installed at the upstream end of the open channel. Within the range of velocity in our experiments, the cross-flow was practically laminar and the streamlines were essentially parallel to each other.

Pictures of the top and side views of the experiments were taken by two cameras, one located at 150 cm above the channel and the other 200 cm from the side window. At least four pictures of the dyed jet were taken for each run of the test.

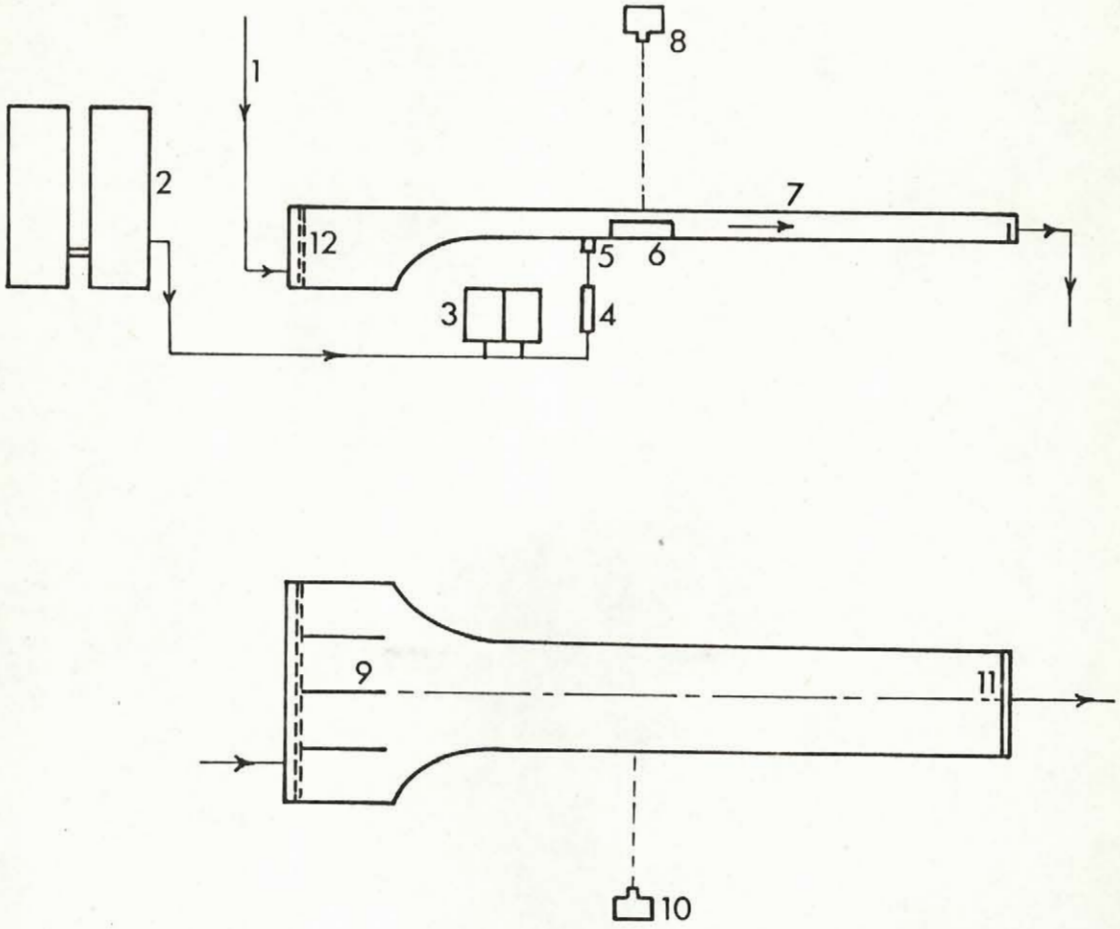

(1) Water Supply

(2) Electric Water Heaters

(3) Pressurized Dye Injector

(4) Rotameter

(5) Thermistor Probe

(6) Side Window

(7) Open Channel

(8) Top Camera

(9) Flow Straighteners

(10) Side Camera

(11) Weir

(12) Vertical Screen

Fig. 3 Experimental Set-Up

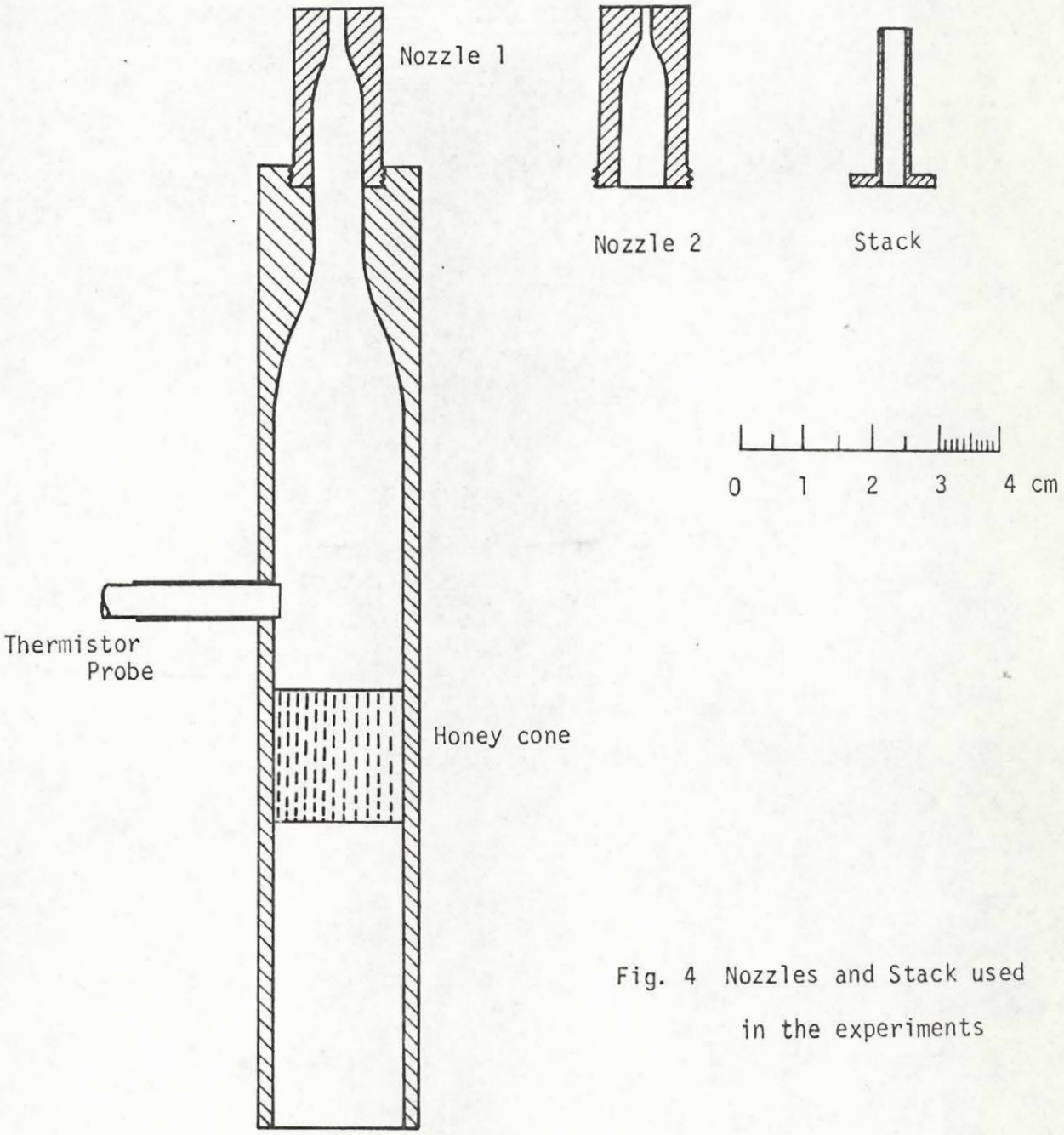

Fig. 4 Nozzles and Stack used in the experiments

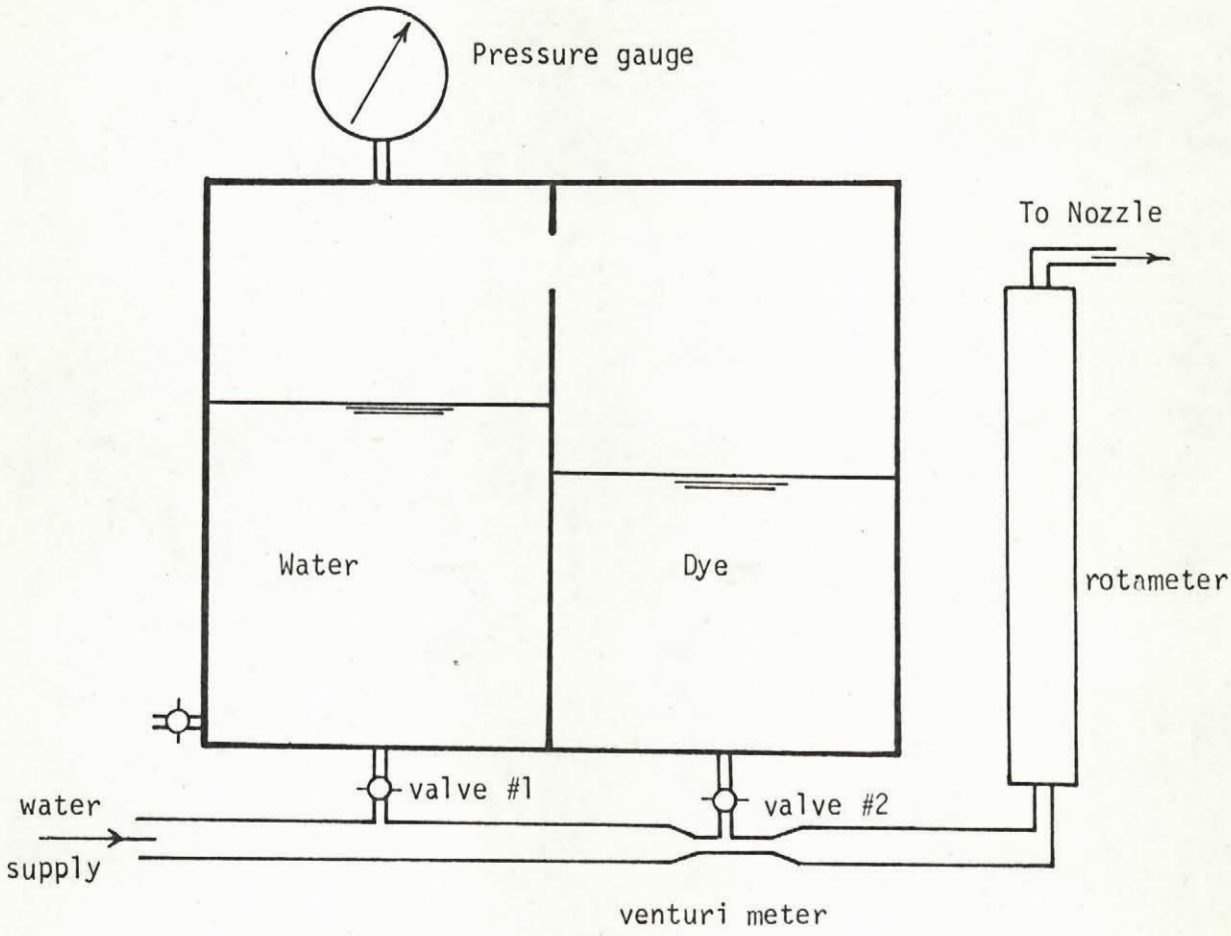

Fig. 5 Pressurized Dye Injector

3.2 Experimental Procedure

There were six series of experiments being carried out for different exit and cross-flow conditions. Test series 1000, 2000 and 3000 were for momentum jets with no temperature difference between the discharging jet and the cross-flow. The other tests, series 4000, 5000 and 6000 were carried out for hot jets with buoyancy.

Test series 2000 were performed with a stack added on top of the nozzle (see Fig. 4). Test series 1000 and 6000 had almost the same flow conditions except for temperature differences. All the test conditions are summarized in Tables 1 and 2.

Cross-flow velocities U shown in the tables were determined on the free water surface along the center line of the channel. Experimental observations were made in the central region where the velocity distribution is relatively uniform. Vertical and horizontal velocity distributions in a cross-section of the open channel were determined. Horizontal cross-flow velocity distribution was obtained from photographs of small floating pieces of paper (punched out by an IBM key-punching machine) which were dropped on the water surface at some upstream stations. For the vertical velocity distribution, fine particles of potassium permanganate were dropped into the open channel. The velocities were determined from photographs of the dye trace as observed through the side window. Velocity distributions obtained in this manner are shown in Figs. 6, 7, 8 and 9.

The exit velocity distribution from the nozzle is not exactly uniform. The boundary layer thickness inside the nozzle was estimated and the exit momentum flux was calculated with a correction factor as described in Appendix II.

The jet trajectories (s versus x) and the jet widths r_s and r_n were determined from the photographs (see Fig. 1 for definitions of r_s and r_n). The results were corrected for parallax and they are presented in the tables given in Appendix III.

All the experimental results in Appendix III were obtained in a region downstream of the point of bifurcation. Due to the size and construction of the experimental channel, it was not possible for us to determine the jet development in the region upstream of the bifurcation point with acceptable accuracy. Some unpublished experimental results of a non-bifurcated momentum jet obtained previously in a deeper tilting flume at McGill are also included here for discussion. The tilting flume for these non-bifurcated jet experiments is 30 cm wide and 45 cm deep. The injection was made by using a two-foot long stack of 1.42 cm inside diameter. The cross-flow velocity was 10.1 cm/sec. Test conditions for these previous non-bifurcated jet experiments are summarized in Table 3.

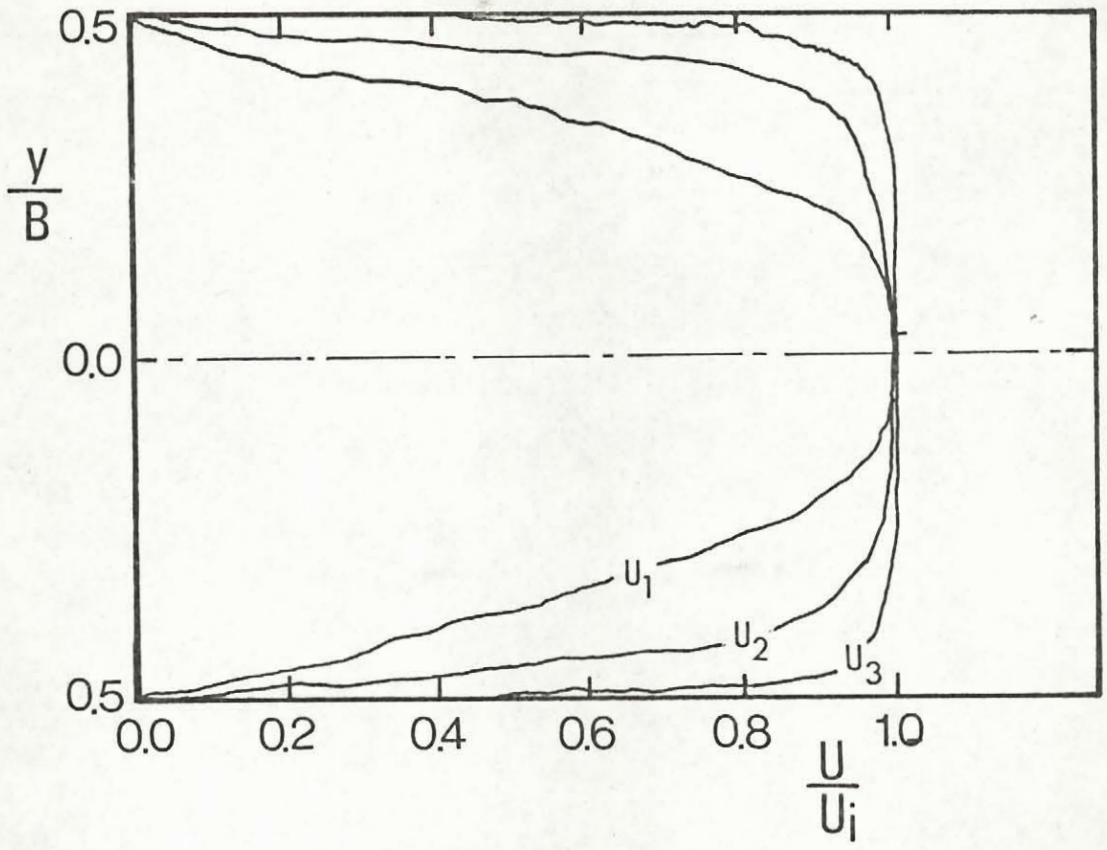

Fig. 6 Horizontal Velocity Distribution.

H = 7.6 cm, U_1 = 3 cm/sec, U_2 = 6 cm/sec, U_3 = 12 cm/sec.

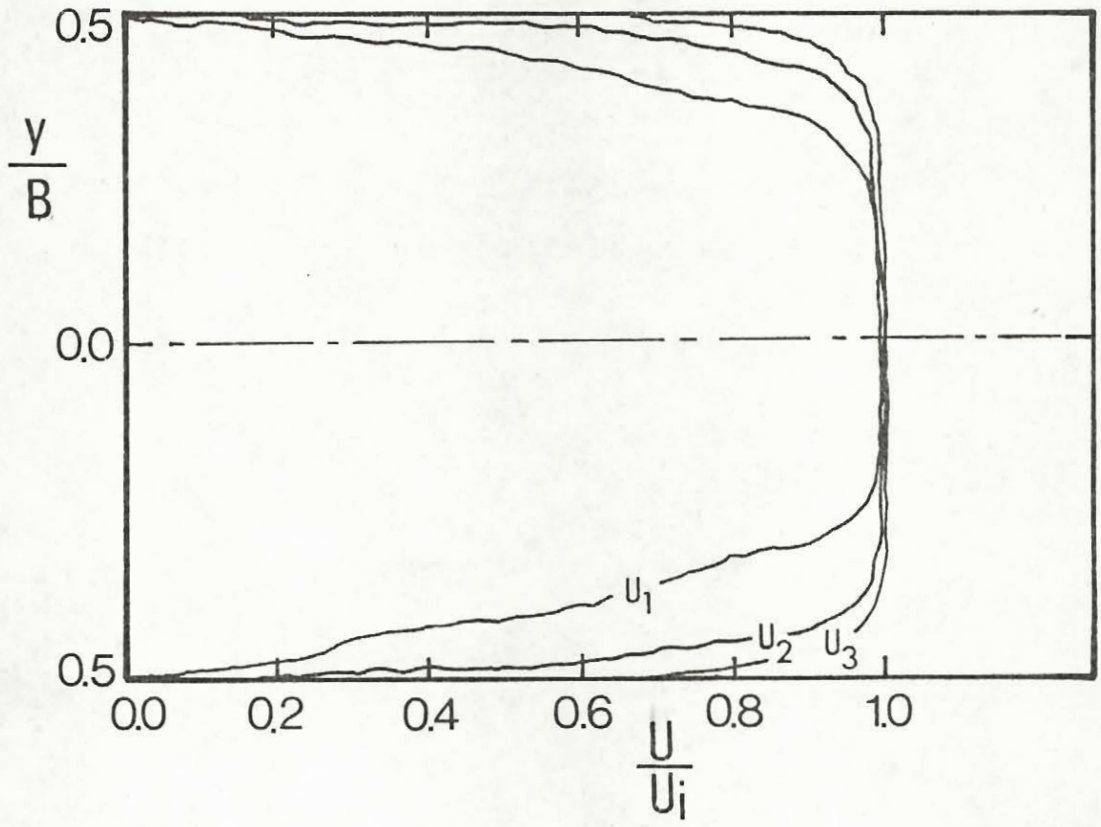

Fig. 7 Horizontal Velocity Distribution.

H = 10.4 cm, U_1 = 3 cm/sec, U_2 = 6 cm/sec, U_3 = 12 cm/sec

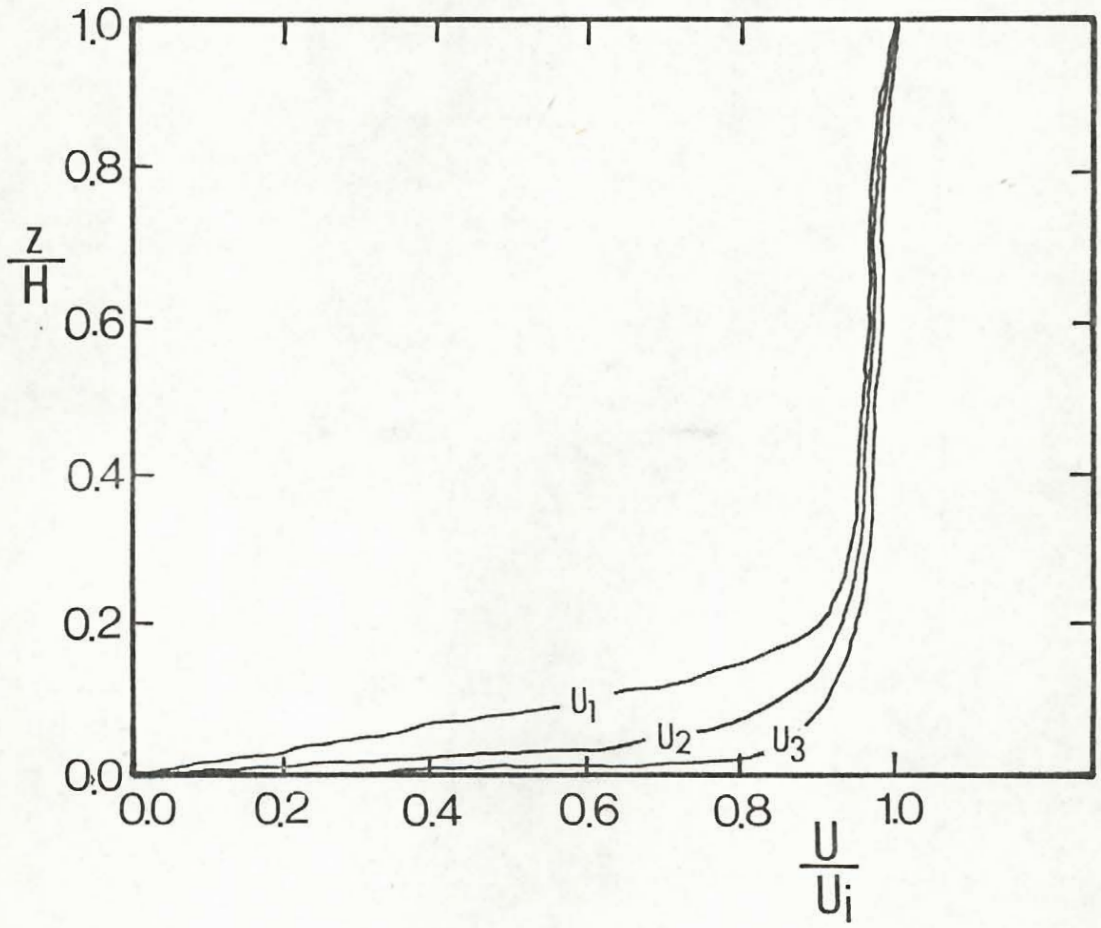

Fig. 8 Vertical Velocity Distribution.

H = 7.6 cm, U_1 = 3 cm/sec, U_2 = 6 cm/sec, U_3 = 12 cm/sec.

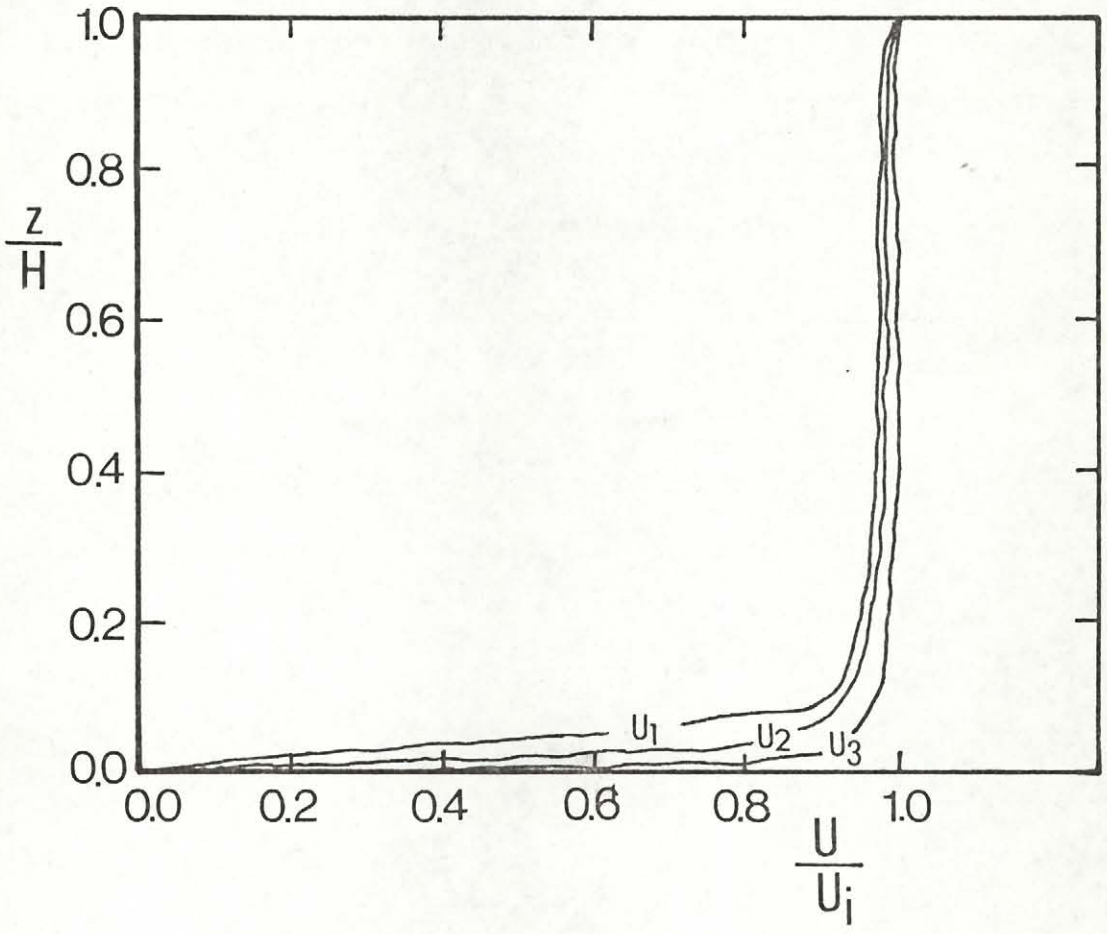

Fig. 9 Vertical Velocity Distribution.

H = 10.4 cm, U_1 = 3 cm/sec, U_2 = 6 cm/sec, U_3 = 12 cm/sec.

TABLE 1. Test Conditions for Bifurcated Momentum Jets

Test No	Symbols	d (cm)	U (cm/sec)	H cm	R	T_o (°C)	T_a (°C)	ℓ_m (cm)	ℓ_b (cm)	x_B (cm)	Θ_B (degree)	$(Ri)_B$
1001	◆	0.20	8.43	14.29	28	23.5	23.5	5.75	-	13.76	15.02	-
1002	■	0.20	4.13	14.76	28	23.5	23.5	5.81	-	14.86	14.4	-
1003	▲	0.40	8.18	14.76	14	23.5	23.5	5.81	-	14.86	14.4	-
1004	▼	0.40	4.09	14.76	14	23.5	23.5	5.90	-	14.42	14.81	-
1005	●	0.20	8.43	14.29	32	23.5	23.5	6.56	-	10.57	19.25	-
1006	◆	0.20	4.15	14.76	32	23.5	23.5	6.63	-	11.43	18.45	-
1007	■	0.40	8.49	14.76	16	23.5	23.5	6.62	-	11.44	18.44	-
1008	●	0.40	4.19	14.76	16	23.5	23.5	6.72	-	11.13	18.92	-
1009*	△	0.20	8.46	14.29	36	23.5	23.5	7.37	-	8.374	23.78	-
1010*	▽	0.40	4.06	14.76	18	23.5	23.5	7.54	-	8.83	23.37	-
1011*	○	0.20	8.49	14.29	40	23.5	23.5	8.18	-	6.80	28.49	-
1012*	○	0.20	4.16	14.76	40	23.5	23.5	8.25	-	7.37	27.37	-
1013*	□	0.40	4.23	14.76	20	23.5	23.5	8.35	-	7.19	27.94	-

TABLE 1 (continued)

Test No	Symbols	d (cm)	U (cm/sec)	H cm	R	T_o (°C)	T_a (°C)	ℓ_m (cm)	ℓ_b (cm)	x_B (cm)	θ_B (degree)	$(Ri)_B$
2001	◈	0.20	12.20	7.62	12	24	24	2.48	-	11.21	9.96	-
2002	◨	0.20	6.11	7.62	12	24	24	2.51	-	10.92	10.22	-
2003	▲	0.40	12.03	7.62	6	24	24	2.51	-	10.91	10.22	-
2004	▼	0.40	6.21	7.62	6	24	24	2.56	-	10.55	10.57	-
2005	◑	0.20	11.87	7.62	16	24	24	3.29	-	6.35	17.21	-
2006	⊠	0.20	6.38	7.62	16	24	24	3.33	-	6.23	17.54	-
2007	◐	0.40	12.53	7.62	8	24	24	3.33	-	6.22	17.55	-
2008	◈	0.40	6.10	7.62	8	24	24	3.38	-	6.02	18.10	-
2009*	◇	0.20	11.70	7.62	20	24	24	4.11	-	4.09	25.70	-
2010*	□	0.20	6.15	7.62	20	24	24	4.15	-	4.01	26.13	-
2011*	△	0.40	12.30	7.62	10	24	24	4.15	-	4.01	26.13	-
2012*	▽	0.40	5.71	7.62	10	24	24	4.21	-	3.89	26.86	-

TABLE 1 (continued)

Test No	Symbols	d (cm)	U (cm/sec)	H cm	R	T_o (°C)	T_a (°C)	ℓ_m (cm)	ℓ_b (cm)	x_B (cm)	θ_B (degree)	$(Ri)_B$
3001	◐	0.40	3.09	7.65	6	25.5	25.5	2.64	-	10.00	11.18	-
3002	◧	0.40	6.05	7.65	6	25.5	25.5	2.64	-	10.00	11.18	-
3003	▲	0.40	2.98	7.65	8	25.5	25.5	3.52	-	5.62	19.36	-
3004	▼	0.40	6.03	7.65	8	25.5	25.5	3.52	-	5.62	19.36	-
3005	◐	0.40	11.87	7.50	8	25.5	25.5	3.52	-	5.30	20.05	-
3006*	◪	0.40	3.06	7.55	10	25.5	25.5	4.40	-	3.46	29.41	-
3007*	◪	0.40	6.06	7.60	10	25.5	25.5	4.40	-	3.53	29.09	-
3008*	◇	0.40	11.62	7.60	10	25.5	25.5	4.41	-	3.53	29.09	-
3009*	◇	0.40	3.02	7.55	12	25.5	25.5	5.29	-	2.40	39.07	-

* Tests with θ_B >20°

TABLE 2. Test Conditions for Bifurcated Buoyant Jets

Test No	Symbols	d (cm)	U (cm/sec)	H cm	R	T_o (°C)	T_a (°C)	ℓ_m (cm)	ℓ_b (cm)	x_B (cm)	θ_B (degree)	$(Ri)_B$
4001	◑	0.40	6.06	7.78	6	39.5	25.5	2.56	0.12	10.28	11.96	0.0478
4002	◨	0.40	5.88	7.78	8	39.5	25.5	3.39	0.16	6.13	18.86	0.0246
4003	▲	0.40	11.80	7.62	6	38	25.5	2.52	0.02	10.73	10.62	0.0114
4004	◆	0.40	11.92	7.62	8	38	25.5	3.33	0.03	6.16	17.86	0.0050
4005*	○	0.40	5.986	7.78	10	36.5	25.5	4.21	0.17	4.06	26.75	0.0114
4006*	□	0.40	6.04	7.78	12	36.5	25.5	5.03	0.20	2.87	35.29	0.0069
4007*	△	0.40	11.91	7.62	10	36.5	25.5	4.15	0.04	3.97	26.35	0.0026

TABLE 2 (continued)

Test No	Symbols	d (cm)	U (cm/sec)	H cm	R	T_o (°C)	T_a (°C)	ℓ_m (cm)	ℓ_b (cm)	x_B (cm)	θ_B (degree)	$(Ri)_B$
5001	●	0.40	3.04	10.30	6	66.5	24	2.62	1.79	10.47	21.84	0.2466
5002	■	0.40	5.90	10.40	6	65.5	24	2.56	0.48	16.65	12.50	0.1833
5003	▲	0.40	6.00	10.40	9	67.5	24	3.80	0.76	9.70	18.42	0.1092
5004	◆	0.40	11.90	10.35	8	66.5	24	3.33	0.16	14.12	11.69	0.0530
5005	▼	0.40	11.85	10.35	10	69.5	24	4.15	0.20	9.51	16.49	0.0332
5006*	◇	0.40	3.03	10.30	10	68.5	24	4.29	2.91	6.21	29.68	0.1652
5007*	▽	0.40	3.04	10.30	14	67.5	24	5.94	4.20	3.89	39.12	0.1040
5008*	-○-	0.40	5.97	10.40	12	67.3	24	5.03	0.99	6.19	25.69	0.0613
5009*	○	0.40	12.01	10.30	12	68.3	24	4.96	0.24	6.69	22.30	0.0189

TABLE 2 (continued)

Test No	Symbols	d (cm)	U (cm/sec)	H cm	R	T_o (°C)	T_a (°C)	ℓ_m (cm)	ℓ_b (cm)	x_B (cm)	θ_B (degree)	$(Ri)_B$
6001		0.40	6.08	7.62	6	66.5	23	2.56	0.45	8.21	16.32	0.1180
6002		0.40	6.08	7.62	7	67.5	23	2.97	0.54	6.51	19.45	0.0919
6003		0.40	12.01	7.62	6	67.5	23	2.51	0.12	9.97	12.10	0.0496
6004		0.40	12.01	7.62	7	66.5	23	2.92	0.14	7.58	15.33	0.0340
6005		0.40	12.01	7.62	8	67.5	23	3.33	0.16	5.96	18.94	0.0235
6006		0.40	12.01	7.62	9	67.5	23	3.74	0.17	4.79	22.93	0.0171
6007*		0.40	6.08	7.62	8	67.5	23	3.38	0.62	5.365	22.76	0.0706
6008*		0.40	6.08	7.62	9	66.5	23	3.80	0.68	4.344	26.35	0.0531
6009*		0.40	6.08	7.62	10	66.5	23	4.21	0.78	3.62	30.32	0.0425
6010*		0.40	12.01	7.62	10	66.5	23	4.15	0.19	3.93	27.143	0.0128

* Tests with θ_B >20°

Test No	Symbols	d (cm)	U (cm/sec)	R	$(Re)_o$	ℓ_m (cm)
9201	○	1.42	10.1	2	2869	2.84
9202	-○-	1.42	10.1	4	5738	5.68
9203	●	1.42	10.1	6	8607	8.52
9204	-●-	1.42	10.1	8	11476	11.36

TABLE 3. Test Conditions for Previous Non-Bifurcated Jet Experiments

CHAPTER 4

EXPERIMENTAL RESULTS AND DISCUSSION

4.1 Non-Bifurcated Jets

Due to the relatively shallow water depth in the present experiments and the construction of the channel, it is not possible to determine the development of the jet in the region upstream of the bifurcation with acceptable accuracy. An attempt is made in this chapter to establish a number of basic properties of the non-bifurcated jets based on some unpublished experimental results obtained previously at McGill University and other published works made by Pratte and Baines (1967), Fan (1967), Margason (1968), Chu and Goldberg (1974), Wright (1977) and others (see Table 4). These results will be used as standard and reference in the discussion of bifurcated jets to be presented later in this chapter.

The McGill unpublished results of momentum jets will be considered first. The experiments were carried out in a tilting flume 30 cm wide and 45 cm deep. The momentum jets were made visible by injected dyed water vertically downward into a horizontal open channel cross-flow. The trajectory (s versus x) and widths r_s and r_n of the jet were determined from photographs of the top and the side views of the jet. A series of tests for exit to cross-flow velocity ratios R = 2,4,6,8 and 10 were made. The test conditions are summarized in Table 3.

The jet trajectory was defined in the photographs as the mid-point between the upper and the lower visual boundaries. The trajectory (z versus x) for each exit to cross-flow velocity ratio is seen in Fig. 10 to follow essentially a one-third slope in a logarithmic plot. Comparing this with Eq. 30, the entrainment coefficients are determined and the results are presented in Fig. 11. The entrainment coefficients are seen to decrease with increase in velocity ratios R. For large velocity ratios, the entrainment coefficient is known to approach a constant (see, for example, Chu and Goldberg, 1974) and this asymptotic value can be estimated from Fig.11 to be $\alpha \simeq 0.45$.

The entrainment coefficient can be determined alternatively from the growth of jet widths r_s and r_n with height s (or z). According to Eq. 17, the entrainment coefficient is equal to the rate of growth of characteristic radius r with distance s. In the experiments, two jet widths r_s and r_n measured along and perpendicular to the direction of travel, were determined from top view and side view photographs. Since these jet widths r_s and r_n are in proportion to the characteristic radius r defined in the theoretical model, several other entrainment coefficients can be defined as follows:

$$r_s = \beta_s s$$

$$r_n = \beta_n s \qquad (35a,b,c)$$

$$r_s r_n = \beta^2 s^2$$

It is anticipated that all these entrainment coefficients β_s, β_n and β

are proportional to the entrainment coefficient α determined from jet trajectories. The cross-sectional area ($r_s . r_n$) as determined from the experiments is presented in Fig. 12. The entrainment coefficient was obtained for each velocity ratio by fitting the experimental data by the quadratic relation, Eq. 35c; the results are presented in Fig. 13. Also presented in this figure are the entrainment coefficients β_s and β_n as defined in Eqs. 35a,b. All three coefficients are seen to decrease with increase in velocity ratio R. The extrapolated values for large R are: $\beta_s = 0.58$, $\beta_n = 0.77$ and $\beta = 0.66$.

Although the two entrainment coefficients α and β are determined from jet paths and jet cross-sections independently, the ratio of these two coefficients is approximately a constant independent of the velocity ratio R. This not only gives confidence to the value of the entrainment coefficient determined from the experiment, but it also points out the correctness of the theoretical formulation which leads to the one-third power law mentioned in Eq. 30.

Similar experiments on momentum jets in a cross-flow have been performed by a very large number of previous investigators. A review of some of these previous works was given by Rajaratnam (1976). Most of the experiments were concerned with the path of the jet. The only other experiment that has included measurement of jet widths was by Pratte and Baines (1967, see also Correction, 1968). The coefficients obtained from fitting their results are included in Table 4 for comparison. Note that the coefficients β_s, β_n and β of Pratte and Baines in Table 4 were obtained based on the averages of four experiments of R = 5, 15, 25, 35.

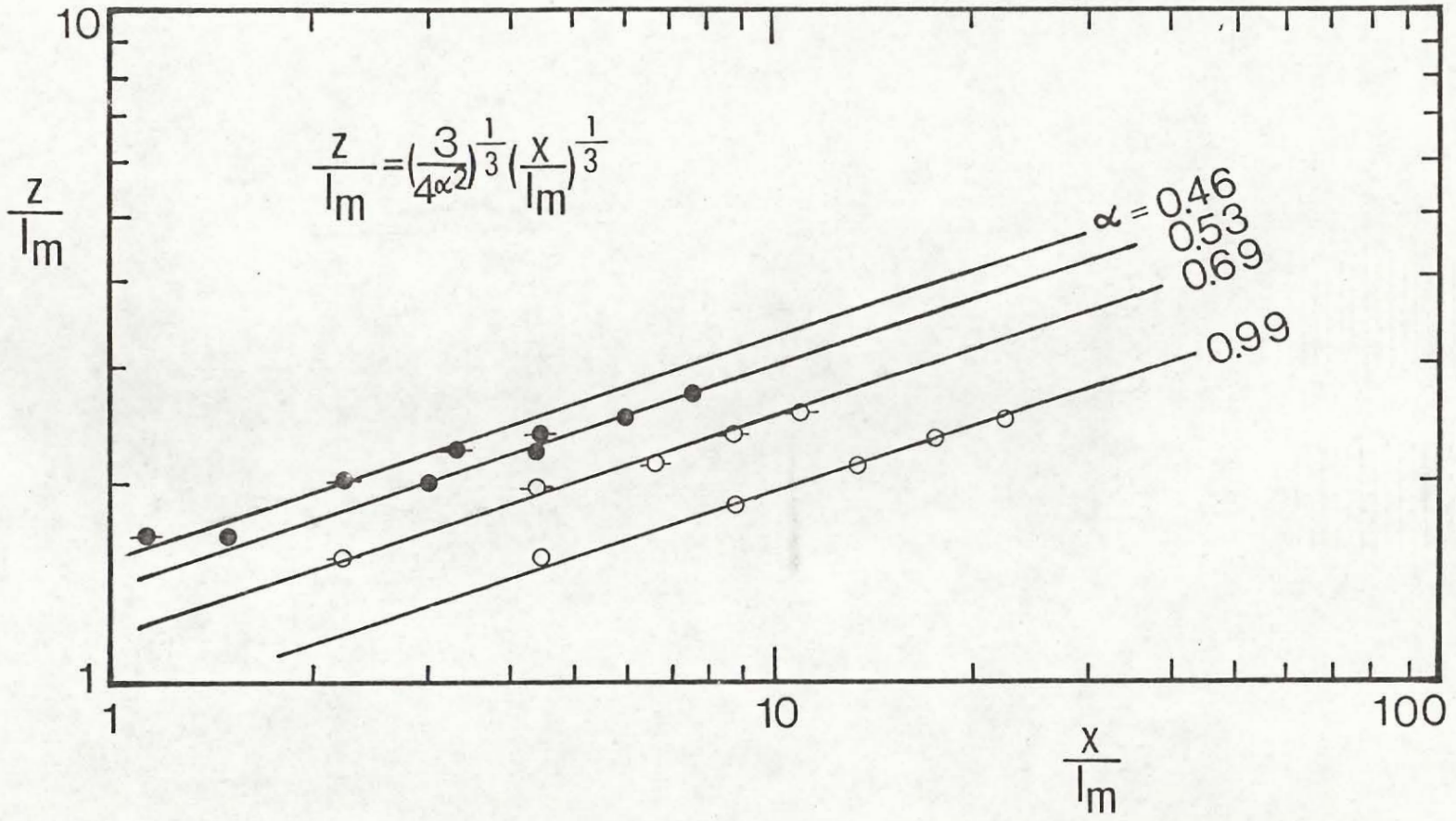

Fig. 10 Jet Trajectory of Non-Bifurcated Jets

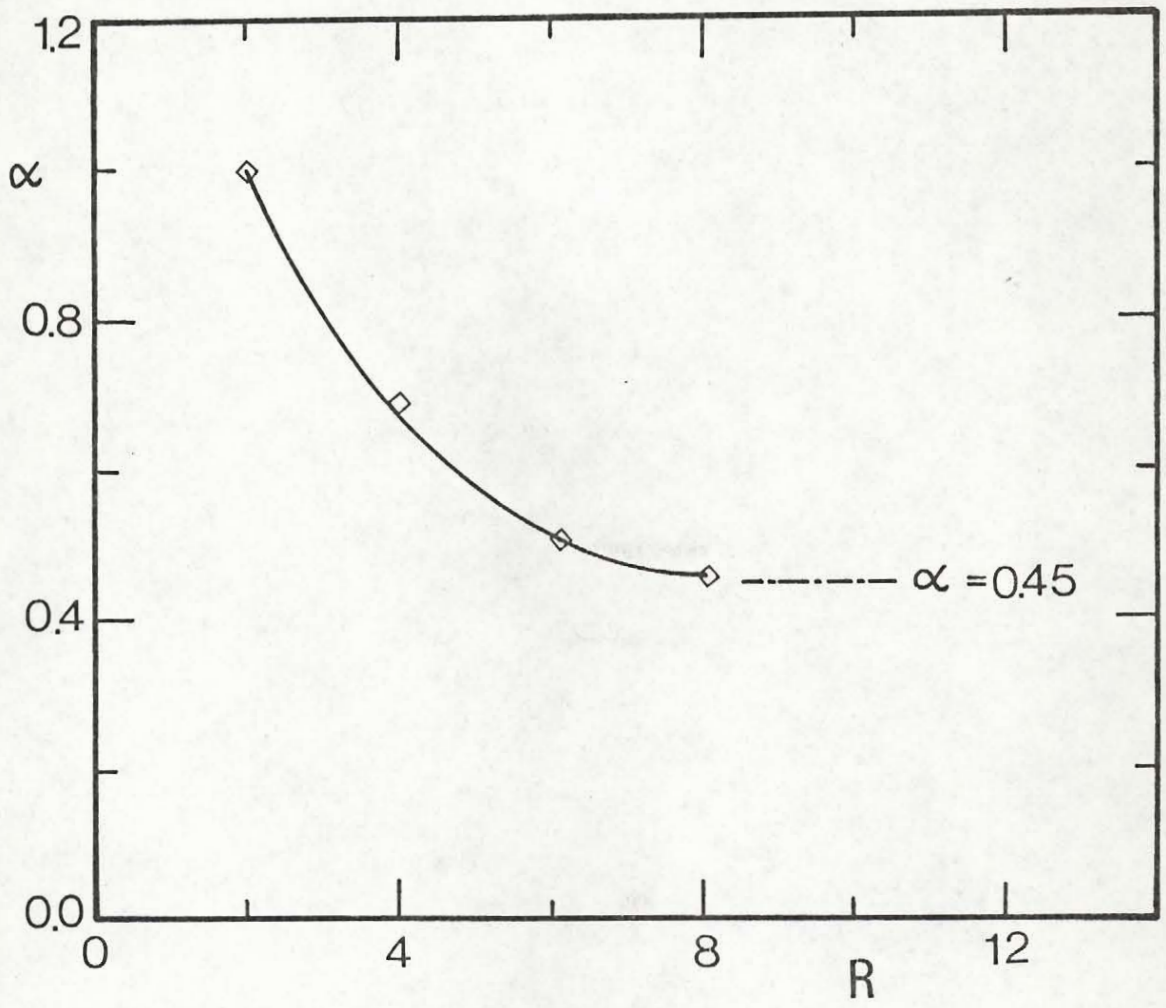

Fig. 11 Entrainment Coefficient α for Non-Bifurcated Jets

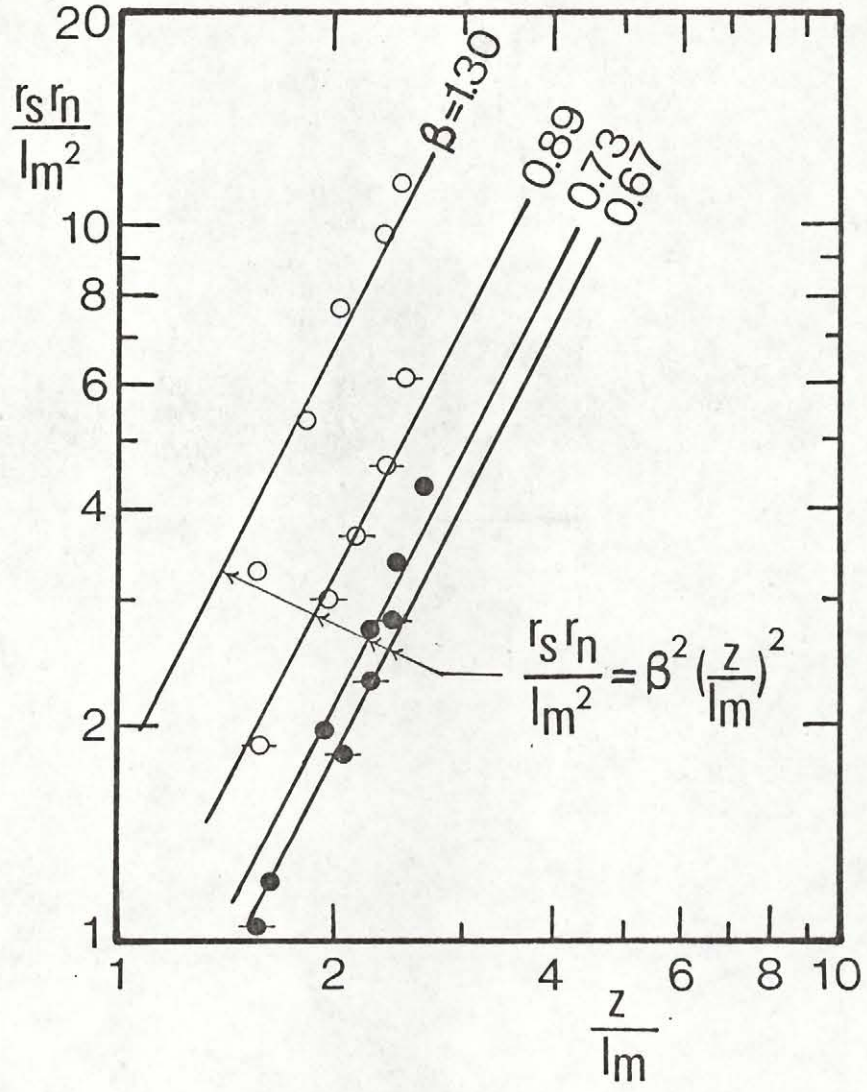

Fig. 12 Cross-sectional Area of Non-Bifurcated Jets

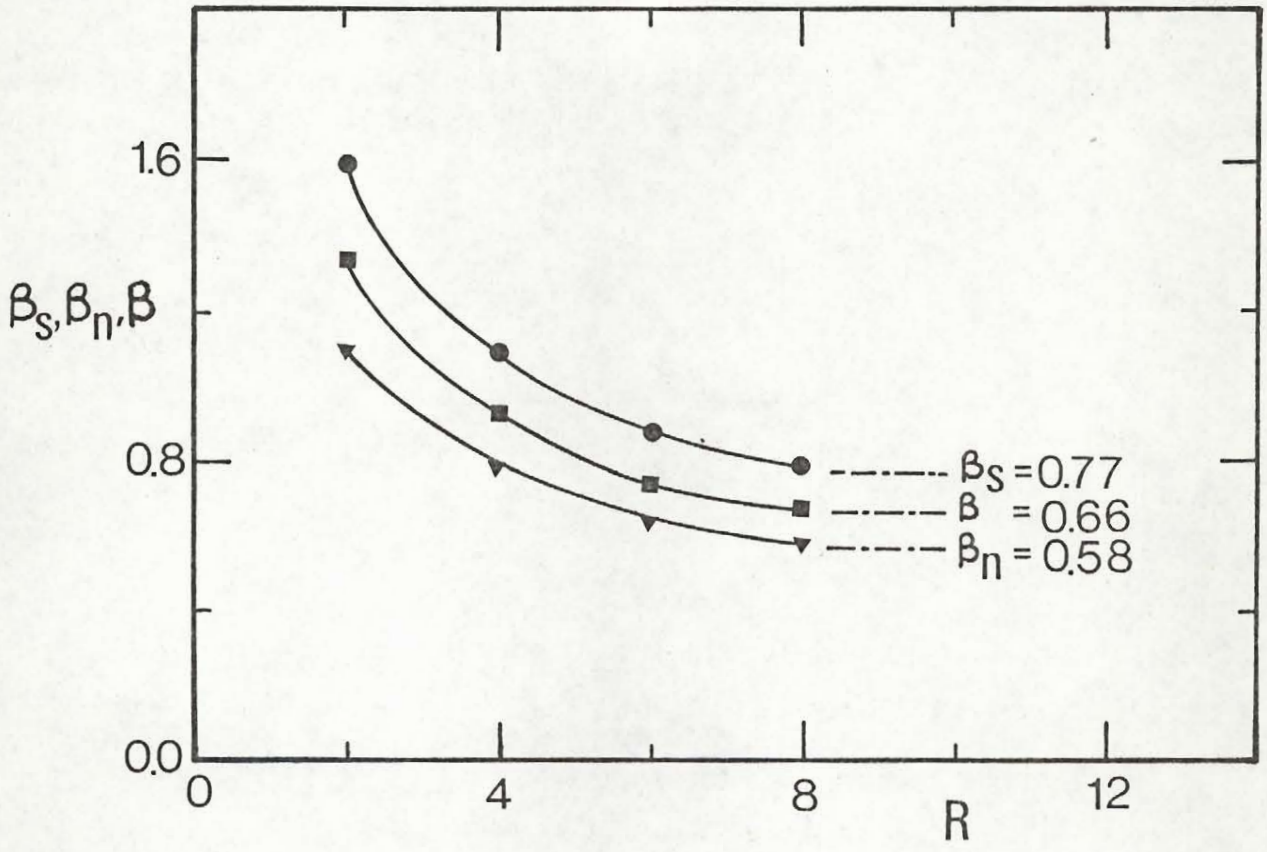

Fig. 13 Entrainment Coefficients β_s, β_n and β for Non-Bifurcated Jets

Investigators	α	β_s	β_n	β	Remarks
McGill unpublished results	0.45	0.58	0.77	0.66	Momentum jets; asymptotic values for $R \to \infty$
Pratte & Baines (1967, see also Correction, 1968)	0.42	0.68	0.89	0.78	Momentum jets; R = 5, 15, 25, 35
Margason (1968)	0.43	-	-	-	Momentum jets; R = 2 to 10
Fan (1967, see also Chu, 1978)	0.50	0.68	-	-	Buoyant jets; R = 8, 16
Chu & Goldberg (1974)	0.50	-	-	-	Momentum and buoyant jets; R = 5 to 40
Wright (1977)	0.43	-	-	-	Momentum and buoyant jets
Fay, Escudier & Hoult (1970)	0.57	-	-	-	Stack plumes; field data of TVA and Bringfelt (1968)
Hewett, Fay & Hoult (1971)	0.50	-	-	-	Plumes in stably stratified wind tunnel

TABLE 4. Entrainment Coefficients for Non-Bifurcated Jets and Plumes in Cross-Flow.

It is, therefore, not surprising that they are slightly higher than the asymptotic values of McGill presented in the same table. The entrainment coefficients α of Pratte and Baines (1967), Margason (1968), Chu and Goldberg (1974), and of Wright (1977) are not significantly different from the asymptotic value of $\alpha = 0.45$ obtained from McGill's results.

The motion of buoyant jets and plumes in cross-flow are affected by both entrainment and acceleration of ambient fluid. Chu (1978) has recently re-analyzed the experimental data of buoyant jets by Fan (1967). The entrainment coefficient β (which can be determined independently of the added mass coefficient k) was found to be the same constant for both momentum-dominated and buoyancy-dominated regions of the jets. The added mass coefficient k was found to be equal to 1.0 (the same as for a two-dimensional solid circular cylinder). Taking $k = 1.0$, the entrainment coefficients were determined from results of several other previous investigators. The values are listed in Table 4. They are generally not significantly different from the entrainment coefficient obtained from momentum jet experiments. It should be pointed out that the path of a buoyant jet is rather insensitive to the choice of value of added mass coefficient k. The value $k = 1.0$ was not determined in Chu (1978) with great certainty (see discussion of Chu (1976)).

Many other experimental investigations are not included in Table 4 for comparison. This is because some of the other experimental results are not readily converted into the same theoretical formula derived in this thesis. A rather extensive review on momentum jets has been given by Rajaratnam (1976). Jet trajectory obtained by all the

other investigators was found to be not significantly different from Pratte and Baines (1967).

There has been also a great deal of previous work on stack plumes but only the work of Fay, Escudier and Hoult (1970) which is believed to be most reliable, is being mentioned in Table 4. A review of the entrainment coefficients obtained from stack plume studies is summarized in Table 5. Again, for comparison purposes, the added mass coefficient k is taken to be 1.0. As the results are arranged in chronological order, it appears that the entrainment coefficients determined by various investigators in the past years have been increasing continuously to approach the value given in Table 4.

Investigator	Entrainment Coefficient
Csanady (1961)	$\alpha = 0.15$
Briggs (1965)	$\alpha = 0.17$
Slawson and Csanady (1965)	$\alpha = 0.14$
Bringfelt (1968)	$\alpha = 0.20$
Hoult, Fay and Forney (1969)	$\alpha = 0.36$
Fay, Escudier and Hoult (1970)	$\alpha = 0.57$

TABLE 5. Entrainment Coefficients obtained from Stack Plume Studies; k = 1.0.

In conclusion, the coefficients obtained from McGill's unpublished work are believed to be acceptable. The set of coefficients given in Table 6 will be referred to in the later chapter as NB (the "non-bifurcated" results). They will be used as a reference for comparison with the experimental results of bifurcated jets in later sections of this chapter.

$$k = 1.0$$

$$\alpha = 0.45$$

$$\beta_s = 0.58$$

$$\beta_n = 0.77$$

$$\beta = 0.66$$

TABLE 6. Coefficients for NB (the "Non-Bifurcated" Jets)

4.2 Separation of the Vortex Element in the Vicinity of the Bifurcated Point

Theoretical solutions were obtained in the previous chapter for regions of the jet upstream and downstream of the bifurcation point. Since the pressure drag is neglected in the formulation, the solution is not strictly applicable in the region where the jet is just beginning to split up into separated elements. A simplified description of the bifurcation phenomena is necessary here in order that the solution obtained for the upstream and the downstream regions can be joined together.

Let us begin with a review of the vortex model of Hayashi (1971). In his model the free surface is simulated by a pair of image vortices as shown in Fig. 14. If the separation of the pair is half of r_n, the trajectory of the vortex pair (in a coordinate system moving with the cross-flow) will be given by:

$$\frac{1}{y'^2} + \frac{1}{z'^2} = \frac{16}{r_n^2} \tag{36}$$

where y' and z' are the coordinates originated from the mid-point at the free surface. From the symmetrical properties of Eq. 36, it is possible to show that the horizontal momentum associated with each of the separated elements is equal to half of the vertical momentum

initially associated with the non-bifurcated vortex pair; i.e., half m_B . Once the jet is bifurcated into separated elements, the momentum associated with the element will remain constant.

Due to the turbulent entrainment, the velocity scale will decay as m_B/q or m_B/r^2 and the circulation associated with the separated vortex element will not remain constant but decay as m_B/r . For this reason, the model of Hayashi (1971) is not applicable far away from the bifurcation point.

In fact, as we shall see in the experimental results, the region influenced by pressure drag is rather small, and for all practical purposes can be treated as a point. This leads us to the more simplified description of the bifurcated jet as described in Fig. 15.

In this model the jet will be assumed to behave as a non-bifurcated jet until the top edge of the jet touches the free surface. This point is defined as the bifurcation point. It occurs at

$$s_B = H - \frac{r_s}{2} \tag{37}$$

since according to NB

$$r_s = 0.58\, s_B \tag{38}$$

at the bifurcation point. Substituting into the former equation yields,

$$s_B = 0.775\, H \tag{39}$$

The vortex element is assumed to move along the free surface immediately after the jet reaches the bifurcation point. Thus,

$$s = z \tag{40a}$$

upstream of the bifurcation point, and

$$s = 0.775\ H + y \tag{40b}$$

downstream of the bifurcation point. Eq. 40 will be used to calculate the lateral migration distance s for all the experimental results to be presented in the later sections. It is interesting to note that the lateral migration s calculated by the Hayashi model, Eq. 36, gives:

$$s = 0.780\ H + y \tag{41}$$

for the jet far downstream of the bifurcation region. This result is almost in exact agreement with Eq. 40 which is based on a more simplified model.

Once the lateral bifurcation distance s_B is determined, the longitudinal location of the bifurcation point can be obtained from Eq. 29:

$$\frac{x_B \ell_b}{\ell_m^2} = -2 + \sqrt{4 + 0.503 \left(\frac{H}{\ell_s}\right)^3} \tag{42}$$

The inclination angle of the non-bifurcated jet at the bifurcation point is

$$\Theta_B = \tan^{-1}\left(\frac{dz}{dx}\right)_B = 2.052\left(\frac{\ell_m}{H}\right)^2\sqrt{1 + 0.125\left(\frac{H}{\ell_s}\right)^3} \qquad ((43)$$

This angle θ_B will be referred to as the "angle of impingement".

In the limiting case of a momentum jet, $\ell_b \to 0$, Eqs. 42 and 43 reduce to

$$\frac{x_B}{\ell_m} = 0.126\left(\frac{H}{\ell_m}\right)^3 \qquad (42a)$$

$$\Theta_B = 2.052\left(\frac{\ell_m}{H}\right)^2 \qquad (43a)$$

On the other hand, in the limiting case of a buoyant plume ($\ell_m \to 0$),

$$\frac{x_B}{\ell_b} = \sqrt{0.503\left(\frac{H}{\ell_b}\right)^3} \qquad (42b)$$

$$\Theta_B = 2.052\sqrt{0.125\left(\frac{\ell_b}{H}\right)} \qquad (43b)$$

It should be pointed out at this stage that the bifurcation phenomenon at the jet impingement is in general more complicated than the simplified description given in Figs. 14 and 15. This is particularly so when the jet inclination angle Θ_B is large, say larger than 20°. Under this condition, a thin layer of upstream wedge is observed to form, in which the jet fluid can be seen to flow in all radial directions. Owing to this, the experimental results to be presented in the later sections are divided into two groups according to whether the jet impingement angle is smaller or larger than 20°.

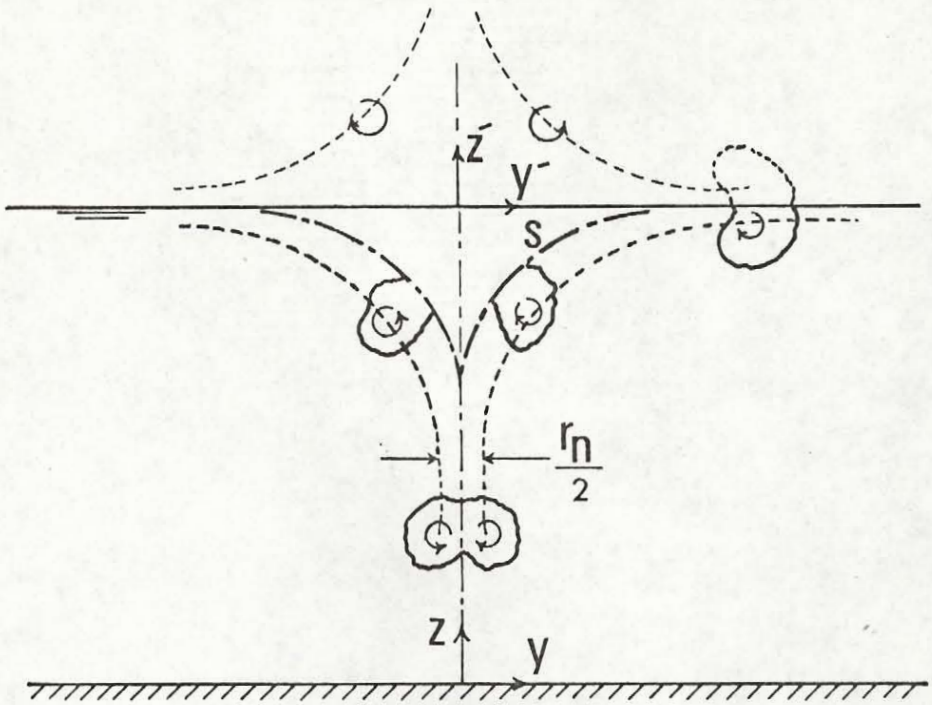

Fig. 14 The Vortex Model of Hayashi (1971)

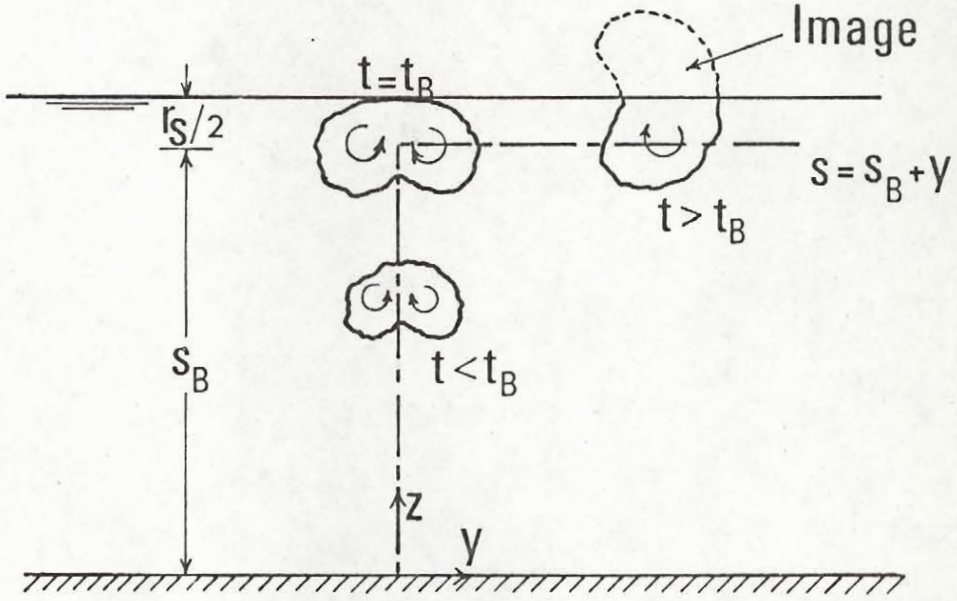

Fig. 15 A Simplified Model at the Bifurcation Point

4.3 Bifurcation of Momentum Jets

The first three series of experiments were carried out for momentum jets in which there was no temperature difference between the exit and the cross-flow. The test conditions are summarized in Table 1. Two basic differences between the three series of tests should be mentioned:

(i) Test series 1000 and 2000 were both performed in the same range of H/ℓ_m varied from 2 to 3; series 1000 were performed at a higher depth, H = 14.7 cm, in comparison with series 2000 which has a depth of H = 7.6 cm;

(ii) The two series of tests 2000 and 3000 have exactly the same test conditions except that series 3000 were performed with short stack (see Fig. 4) attached on top of the nozzle. Although both series have the same H = 7.6 cm, the total depth of the cross-flow in test series 3000 is 10.7 cm deep.

The typical behaviour of the bifurcated momentum jets is shown in a series of top view photographs in Figs. 16, 17 and 18.

Fig. 16 shows a comparison between a series of bifurcated momentum jets with the same ℓ_m and H but with different cross-flow velocities and nozzle diameters. The purpose of this figure is to show the importance of both scale lengths H and ℓ_m. As long as H and ℓ_m are maintained the same, other parameters do not have any significant effect on the jet bifurcation. Also compared in the same figure are the results of series 2000 and 3000. The addition of the stack and the change of total water depth in test series 3000 are shown to have negligible effect on jet bifurcation.

Fig. 17 is a series of photographs taken from test series 1000. In comparing with the test conditions in Fig. 16, we find that both length scales H and ℓ_m are double but the ratio H/ℓ_m is maintained. The increase in length scale has resulted in increasing the scale of turbulent motion. Furthermore, since x_B is double, what is seen in the pictures of Fig. 17 are, in fact, rather earlier stages of bifurcation (compare also Figs. 18(a) and 18(b)). In this early stage of bifurcation, clear separation of the two vortex elements is sometimes not observed.

The behaviour of the jet at various impingement angles θ_B is shown in Figs. 18(a) and 18(b). When the angle θ_B is large, the jet near the bifurcation point is seen to form a spreading layer flowing in all radial directions along the free surface. For a test with large θ_B, it is sometimes difficult, at least in the region near the bifurcation point, to define the inner boundary of the bifurcating jet. For this reason, experimental results with high and low angles of θ_B are presented separately. The results for $\theta_B < 20°$ are presented in Figs. 19, 20, 21 and 22. The results for $\theta_B > 20°$ are shown in Figs. 23 and 24.

Jet widths r_s, r_n and cross-sectional area $r_s r_n$ as determined from photographs of the bifurcated jets were plotted against the lateral migration distance s in Figs. 19, 20 and 21. The results are seen to follow closely the linear and quadratic relationships proposed in Eqs. 35 (a,b,c). The jet trajectories are presented in Fig. 22 and they are seen to follow the one-third law of Eq. 30.

There are no noticeable differences between the two sets of results of test series 2000 and 3000. This suggests that the addition of a stack

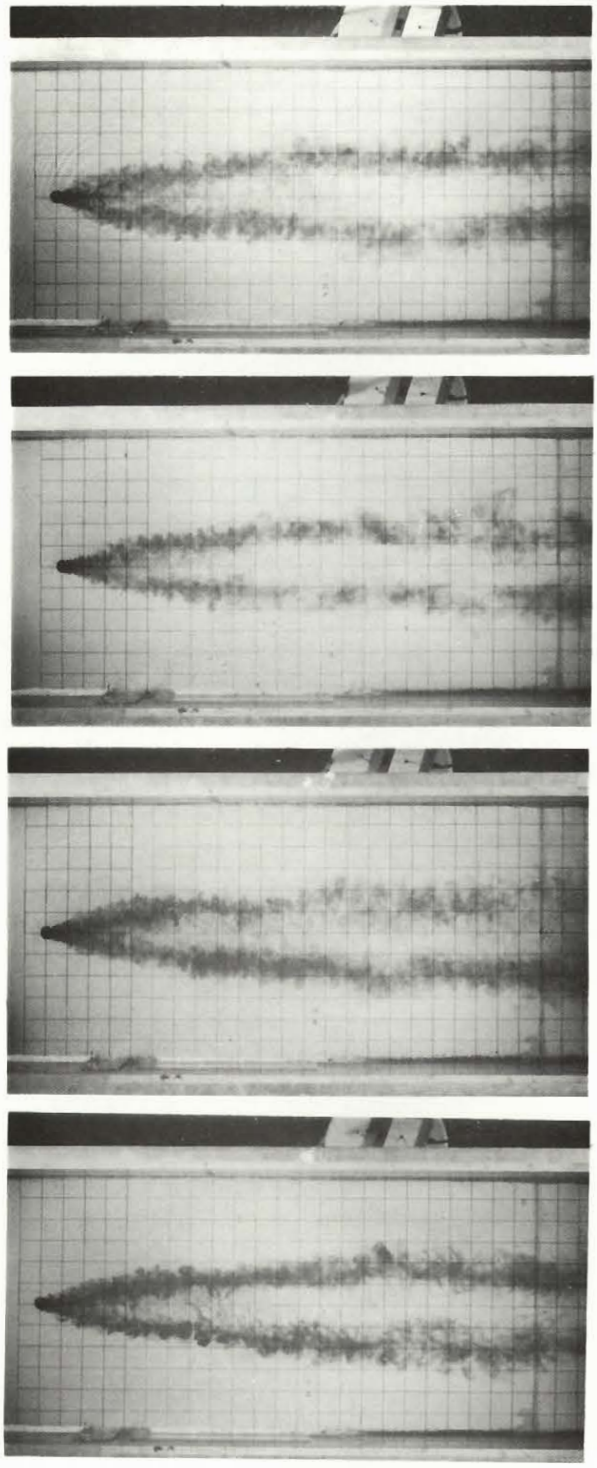

Test 2005

d = 0.2 cm

U = 11.9 cm/sec

Test 2006

d = 0.2 cm

U = 6.4 cm/sec

Test 2007

d = 0.4 cm

U = 12.5 cm/sec

Test 2008

d = 0.4 cm

U = 6.1 cm/sec

Fig. 16(a) Photographs of Bifurcated Momentum Jets without stack; ℓ_m = 3.4 cm, H = 7.6 cm, Θ_B = 19°

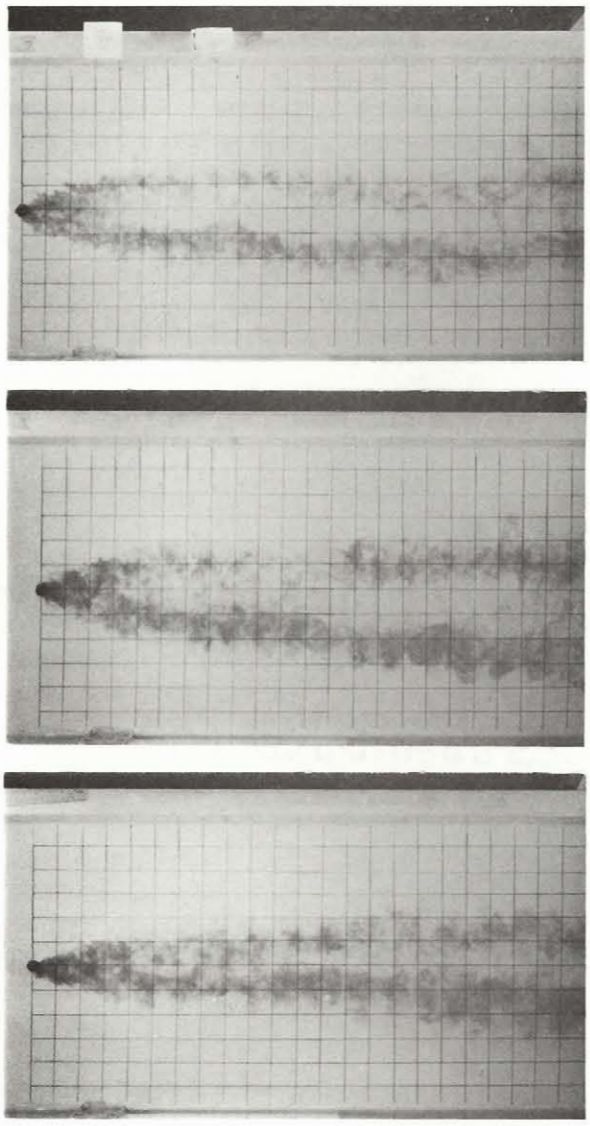

Test 3003

d = 0.40 cm

U = 2.98 cm/sec

Test 3004

d = 0.40 cm

U = 6.03 cm/sec

Test 3005

d = 0.40 cm

U = 11.87 cm/sec

Fig. 16 (b) Photographs of Bifurcated Momentum Jets with stack; ℓ_m = 3.4 cm, H = 7.6 cm, Θ_B = 19°

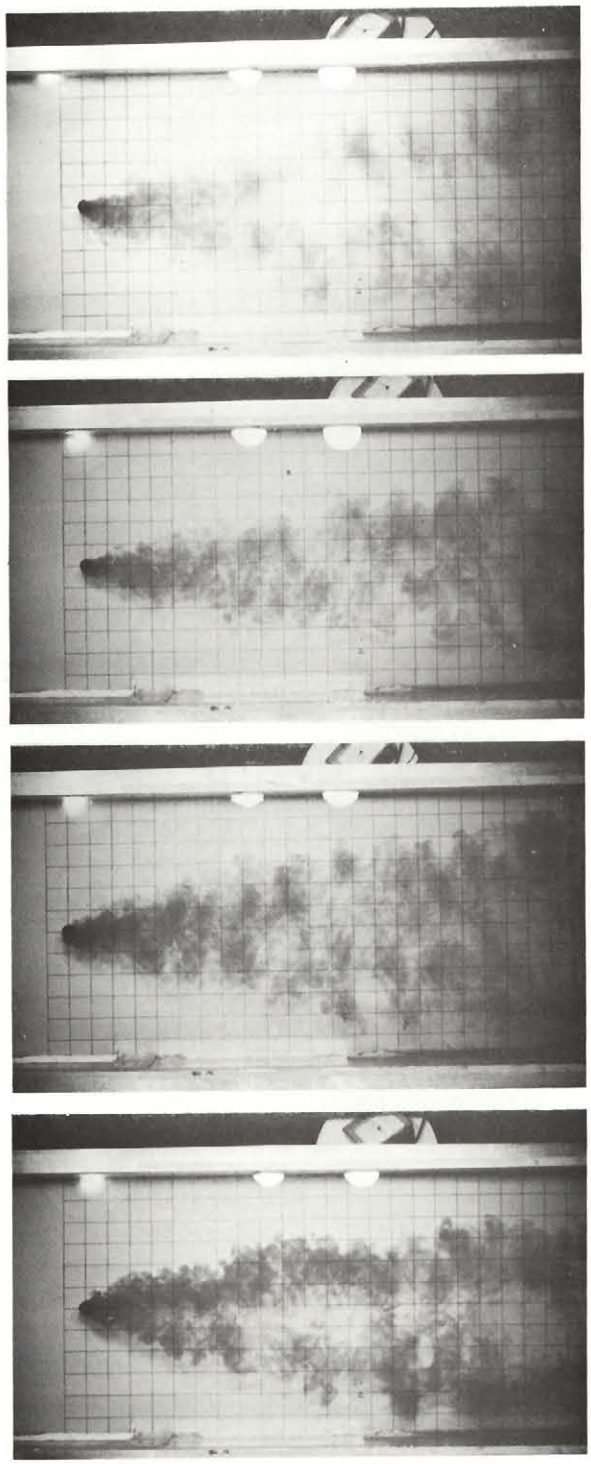

Test 1005

U = 8.45 cm/sec

d = 0.2 cm

Test 1006

U = 4.15 cm/sec

d = 0.20 cm

Test 1007

U = 8.49 cm/sec

d = 0.40 cm

Test 1008

U = 4.19 cm/sec

d = 0.40 cm

Fig. 17 Photographs of Bifurcated Momentum Jets;

ℓ_m = 6.60 cm, H = 14.7 cm, Θ_B = 19°

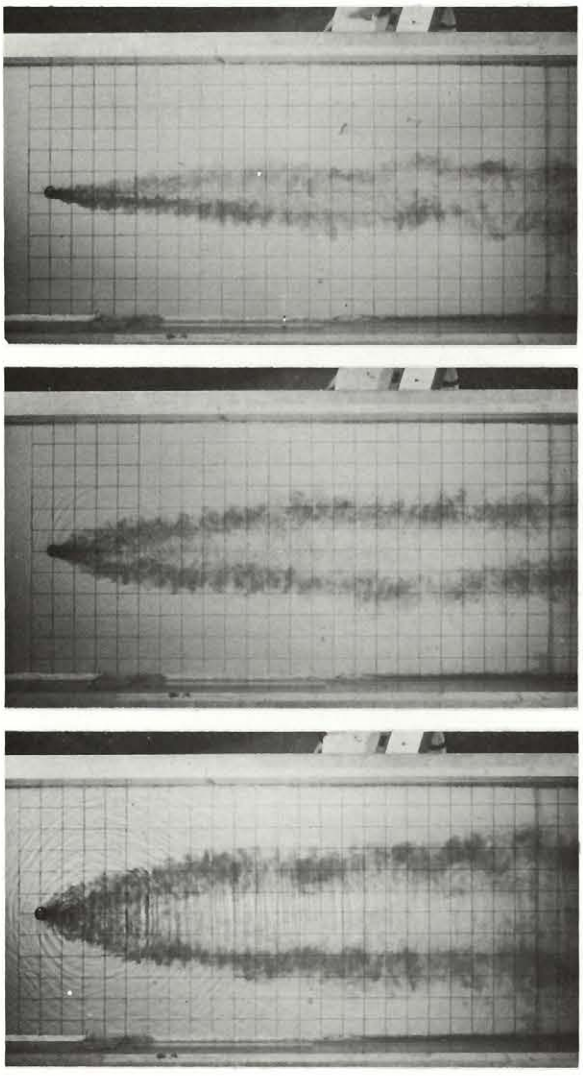

Test 2001

Θ_B = 10°

U = 12.2 cm/sec

d = 0.20 cm

Test 2005

Θ_B = 19°

U = 11.87 cm/sec

d = 0.20 cm

Test 2009

Θ_B = 26°

U = 11.70 cm/sec

d = 0.2 cm

Fig. 18(a) Photographs of Bifurcated Momentum Jets at various Θ_B

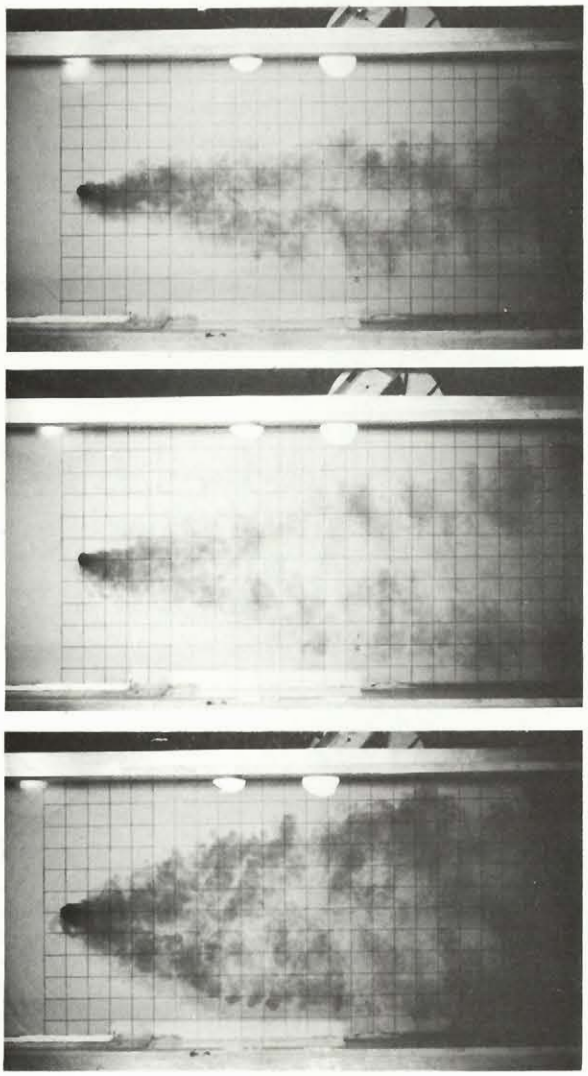

Test 1001

Θ_B = 15°

U = 8.43 cm/sec

d = 0.20 cm

Test 1005

Θ_B = 19°

U = 8.43 cm/sec

d = 0.20 cm

Test 1009

Θ_B = 24°

U = 8.45 cm/sec

d = 0.2 cm

Fig. 18 (b) Photographs of Bifurcated Momentum Jets at various Θ_B

and the change of total depth of the cross-flow in test series 3000 do not affect the jet (at least, this is true for the present range of test conditions). The growth of jet width for test series 1000 is somewhat larger. This could be due to the presence of a larger scale of turbulent motion; or it could be due to the way in which s is defined. In fact, a slight adjustment of the coefficient in Eq. 40(b) (say, $s = 0.70\ H + y$) would bring the three series of experiments to closer agreement and a better fit to the linear and quadratic relationships of Eq. 35 (a,b,c).

The entrainment coefficients α, β, β_s and β_n determined from best fit of experimental results are summarized in Table 7. The set of coefficients will be referred to as BM ("Bifurcated Momentum" jets).

$$\alpha = 0.50$$

$$\beta = 0.65$$

$$\beta_s = 0.55$$

$$\beta_n = 0.77$$

TABLE 7. Entrainment Coefficients for BM

The entrainment coefficients in Table 7 for BM are not significantly different from the coefficients in Table 6 for NB. This shows that entrainment characteristics for non-bifurcated jets and for bifurcated jets are essentially similar, at least in the region sufficiently far away from the bifurcation point.

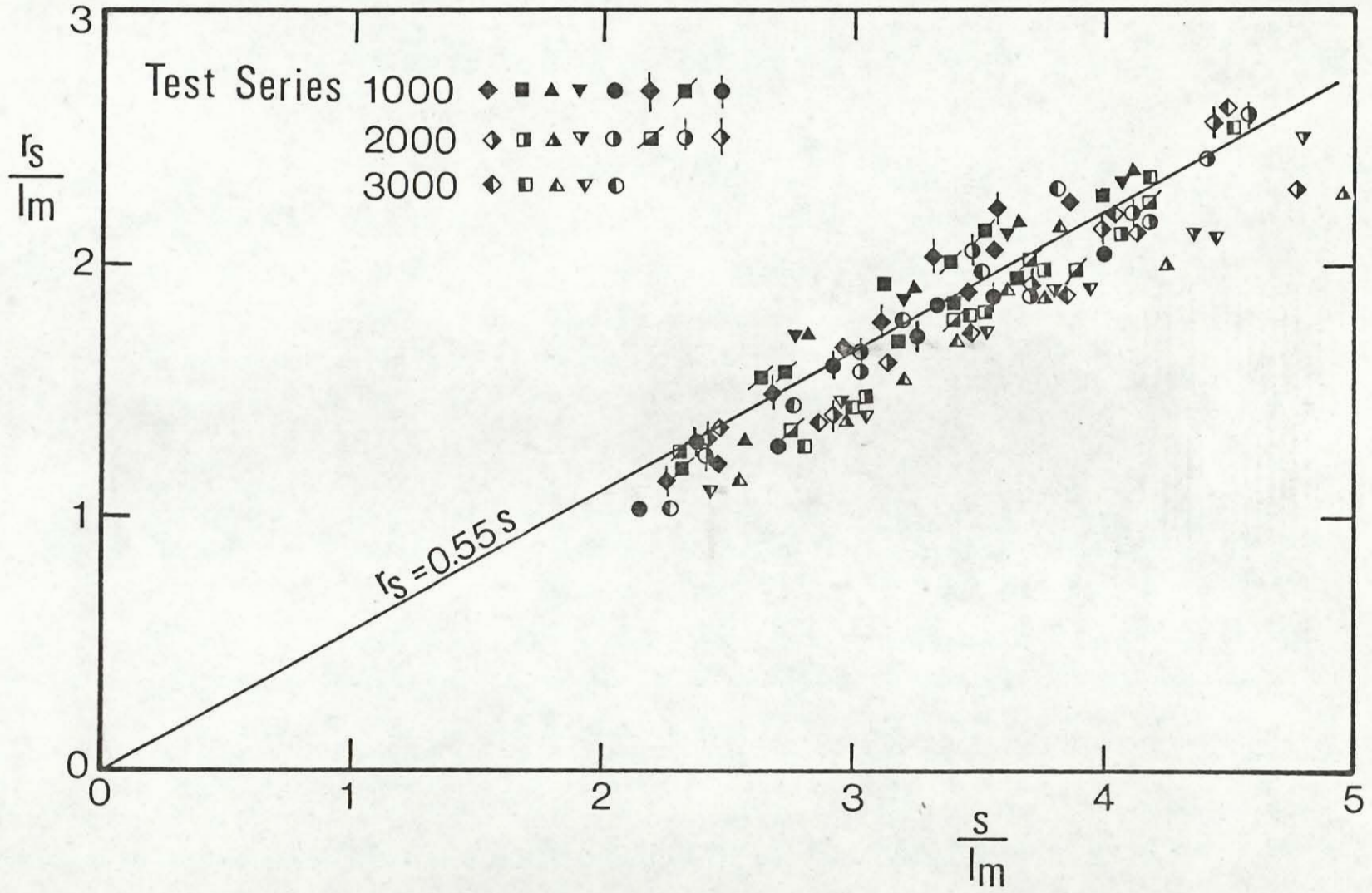

Fig. 19 Jet Width r_s for Bifurcated Momentum Jets ($\theta_B < 20°$)

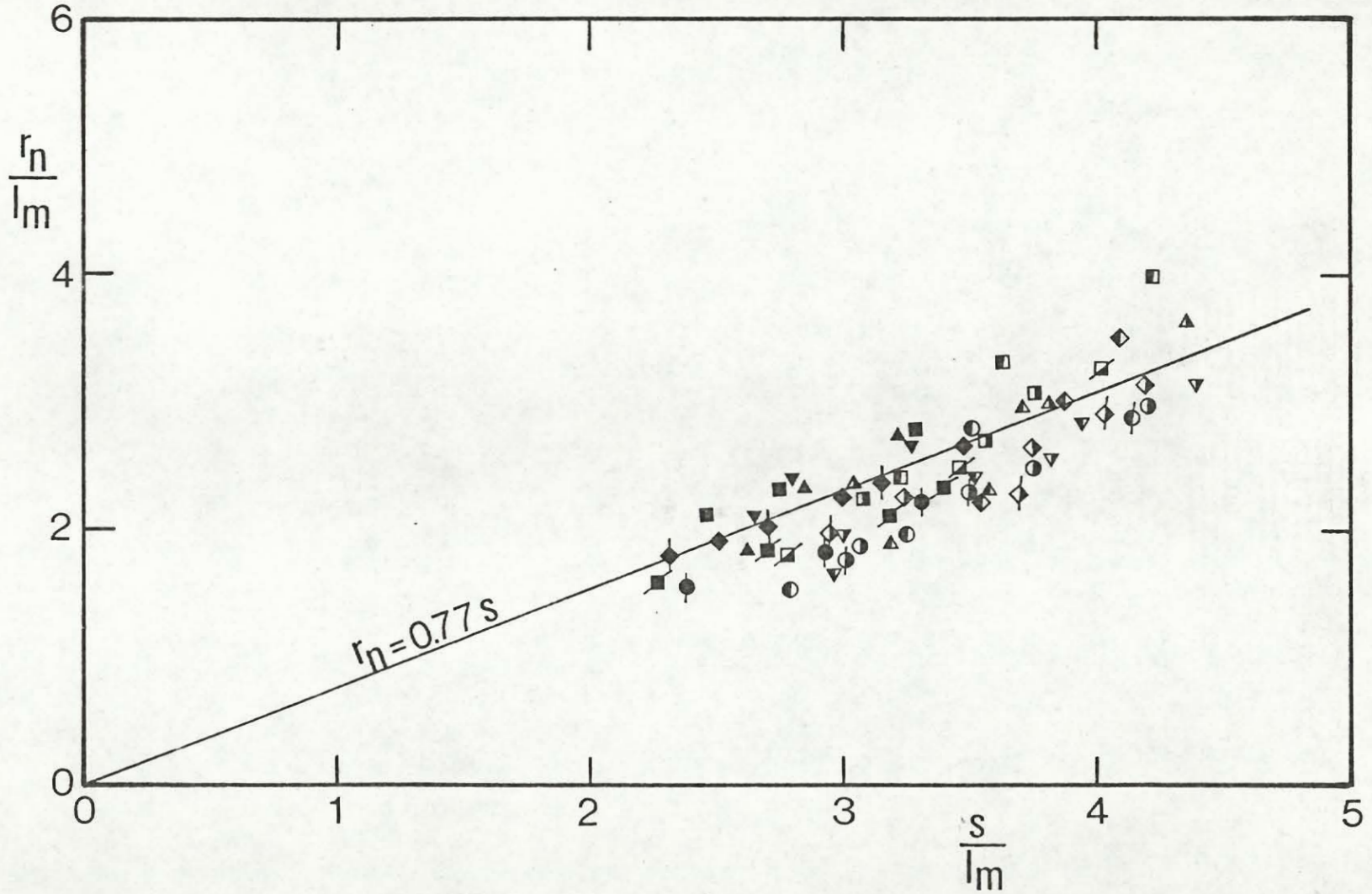

Fig. 20 Jet Width r_n for Bifurcated Momentum Jets ($\theta_B < 20°$)

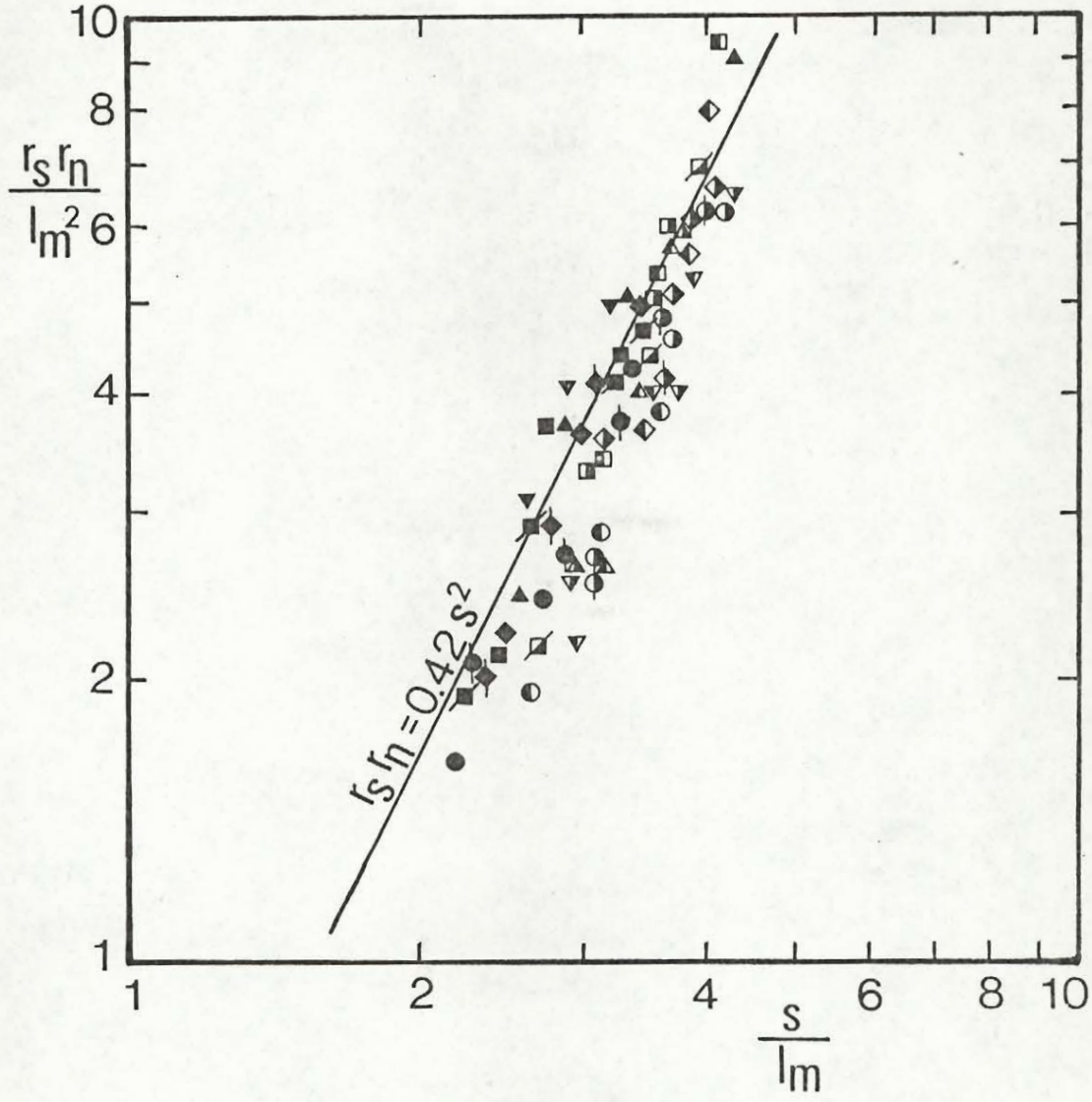

Fig. 21 Cross-sectional Area of Bifurcated Momentum Jets ($\theta_B < 20°$)

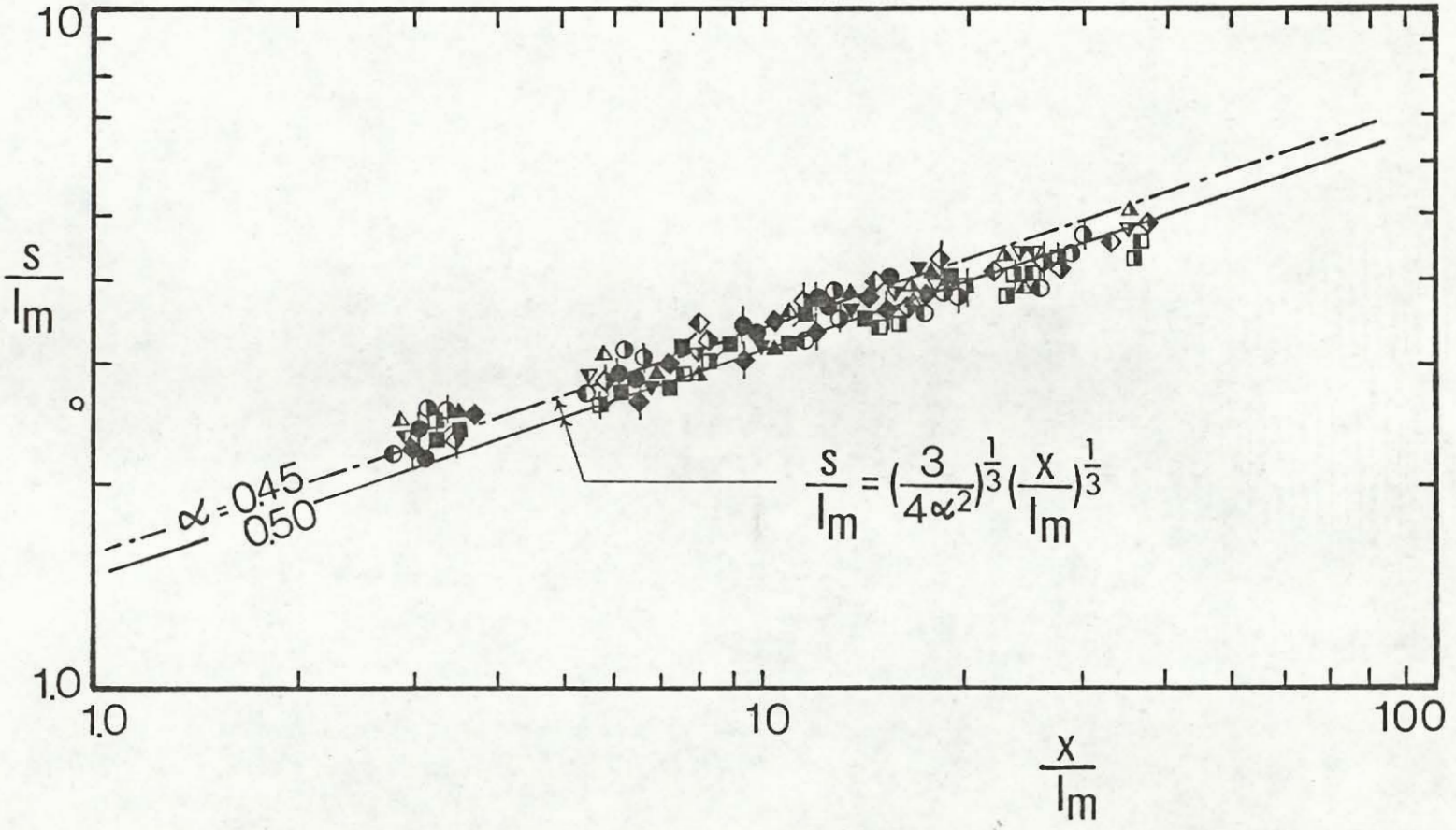

Fig. 22 Jet Trajectory of Bifurcated Momentum Jets ($\theta_B < 20°$)

The behaviour of the impinging jet near the bifurcation point is somewhat different. A surface layer was observed near the impinging point where the jet fluid spreads in all radial directions. Fig. 23 presents the configuration of such a spreading layer for tests with $\Theta_B > 20°$. The locus of the outer jet boundary is plotted in a coordinate system originated from the bifurcation point. An upstream wedge can be seen to form, the extent of which is approximately one to two times the momentum length scale ℓ_m.

Similar spreading layer was observed in tests with $\Theta_B < 20°$. But the extent of the layer appears to be smaller and the boundary was not so clearly defined in the photographs.

The same set of experimental data in Fig. 23 is replotted in Fig. 24 to compare with the results obtained for low impinging angles ($\Theta_B < 20°$). The result for the low impinging angle is represented in the figure by the one-third law:

$$\frac{s_o}{\ell_m} = \frac{s + r_s/2}{\ell_m} = \left(1 + \frac{1}{2}\beta_s\right)\left(\frac{3}{4\alpha^2}\right)^{1/3}\left(\frac{x}{\ell_m}\right)^{1/3} \qquad (44)$$

with $\alpha = 0.50$ and $\beta_s = 0.55$. Despite the dependency on Θ_B in the region near the bifurcation point, the two sets of data for low and high angles Θ_B are seen in the figure to approach each other in the far field region.

The jet width r_n/H for the whole range of impinging angles is plotted against x/x_B in Fig. 25. Note that r_n is equal to twice the thickness of the surface layer (see Fig. 1(c)). Again, some dependency on the angle θ_B can be observed, particularly for tests with $\theta_B > 20°$. The reduction of the jet thickness in these cases could be explained by the fact that the jet fluid at high impinging angles distributed more evenly in all directions rather than concentrated along two vortex elements, as in the case with low impinging angles.

For low angles of impingement, the experimental results are seen to follow the one-third law:

$$\frac{r_n}{s_B} = \beta_n \left(\frac{x}{x_B}\right)^{1/3} \tag{45}$$

Since $\beta_n = 0.77$ and $s_B = 0.775\ H$,

$$\frac{r_n}{H} = 0.596 \left(\frac{x}{x_B}\right)^{1/3} \tag{46}$$

The coefficient β_n has been determined previously in Fig. 20.

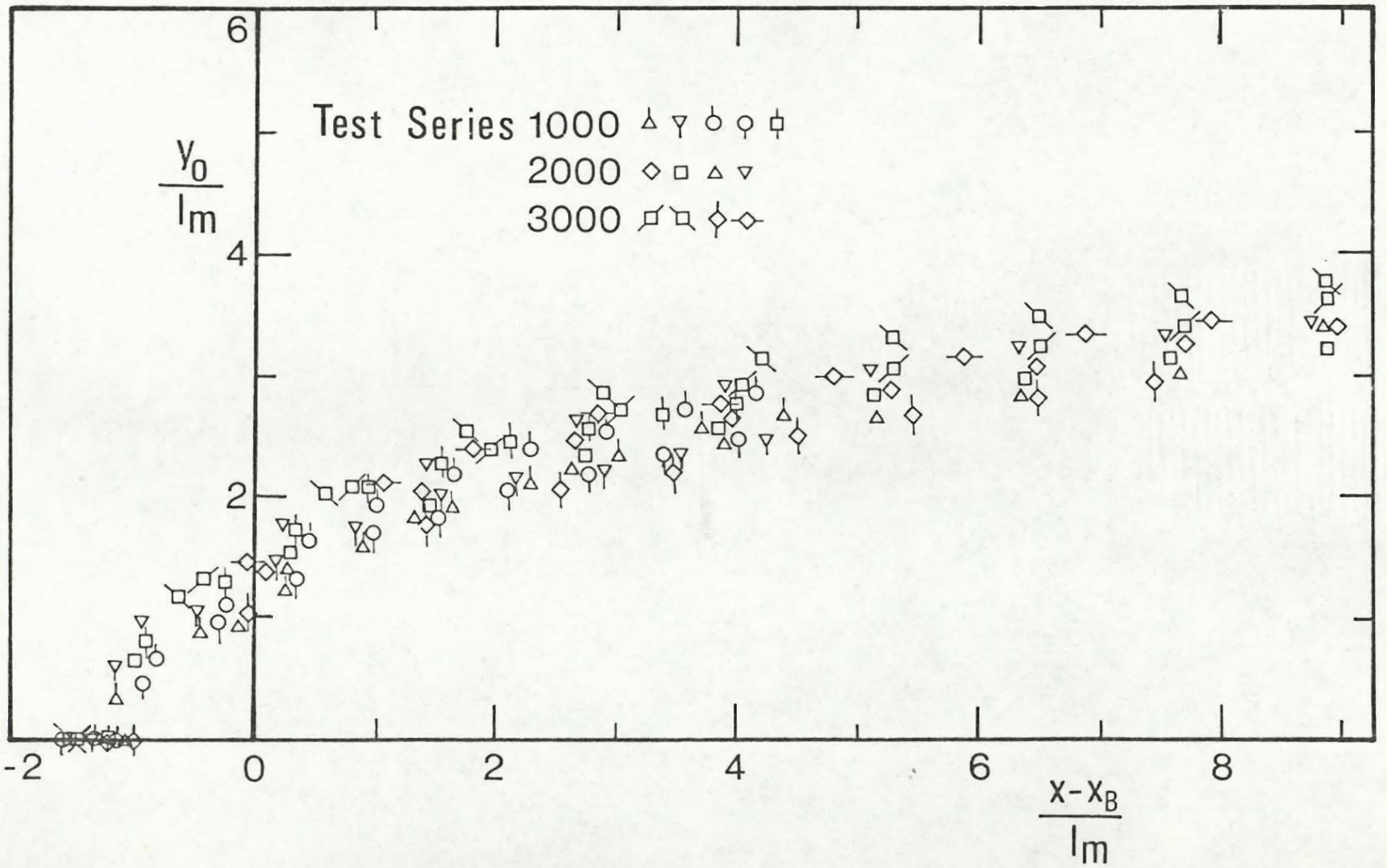

Fig. 23 Radially Spreading Layer Around the Bifurcation Point ($\theta_B > 20°$)

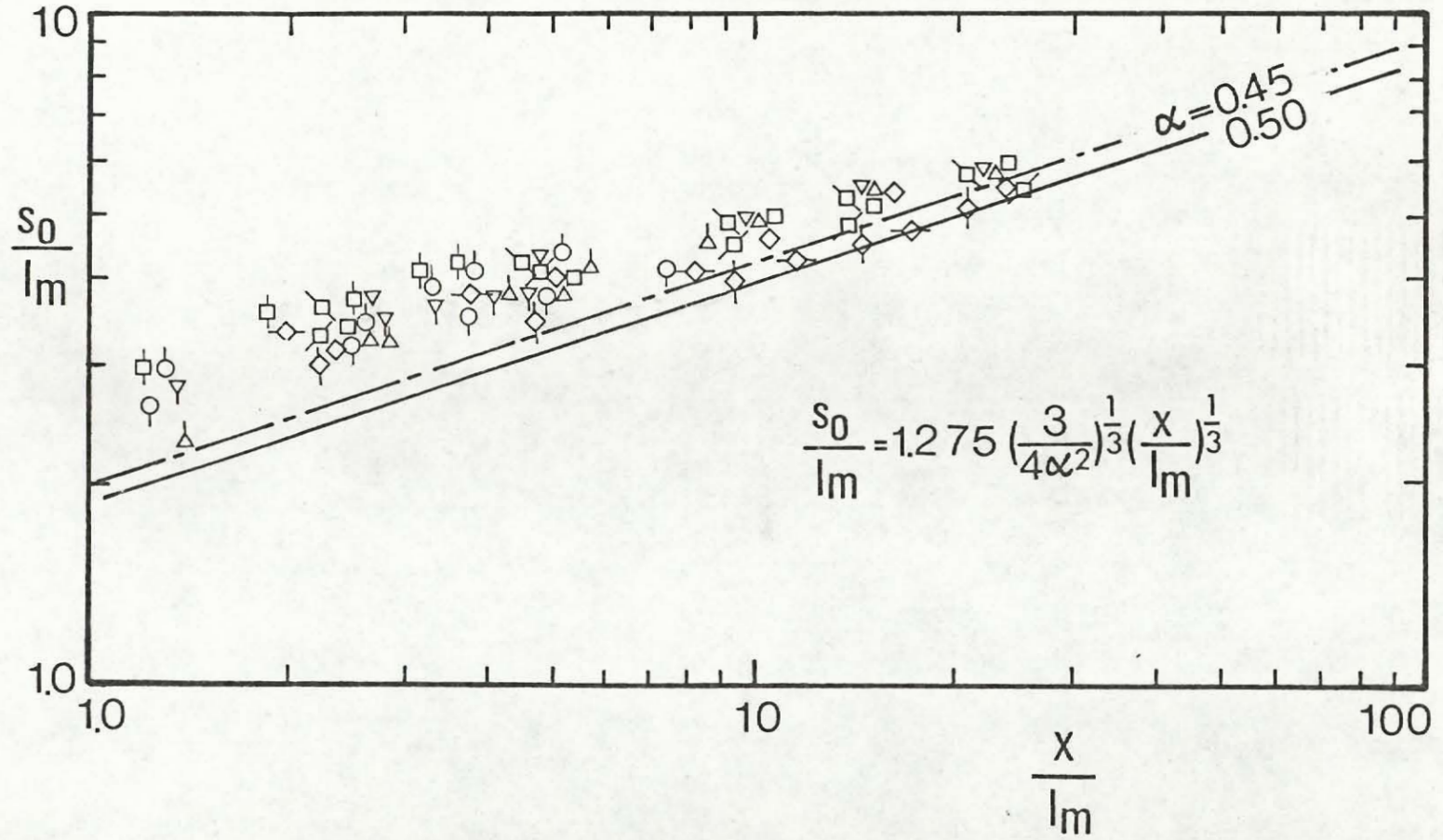

Fig. 24 Outer Boundary of the Bifurcated Momentum Jets (θ_B > 20°)

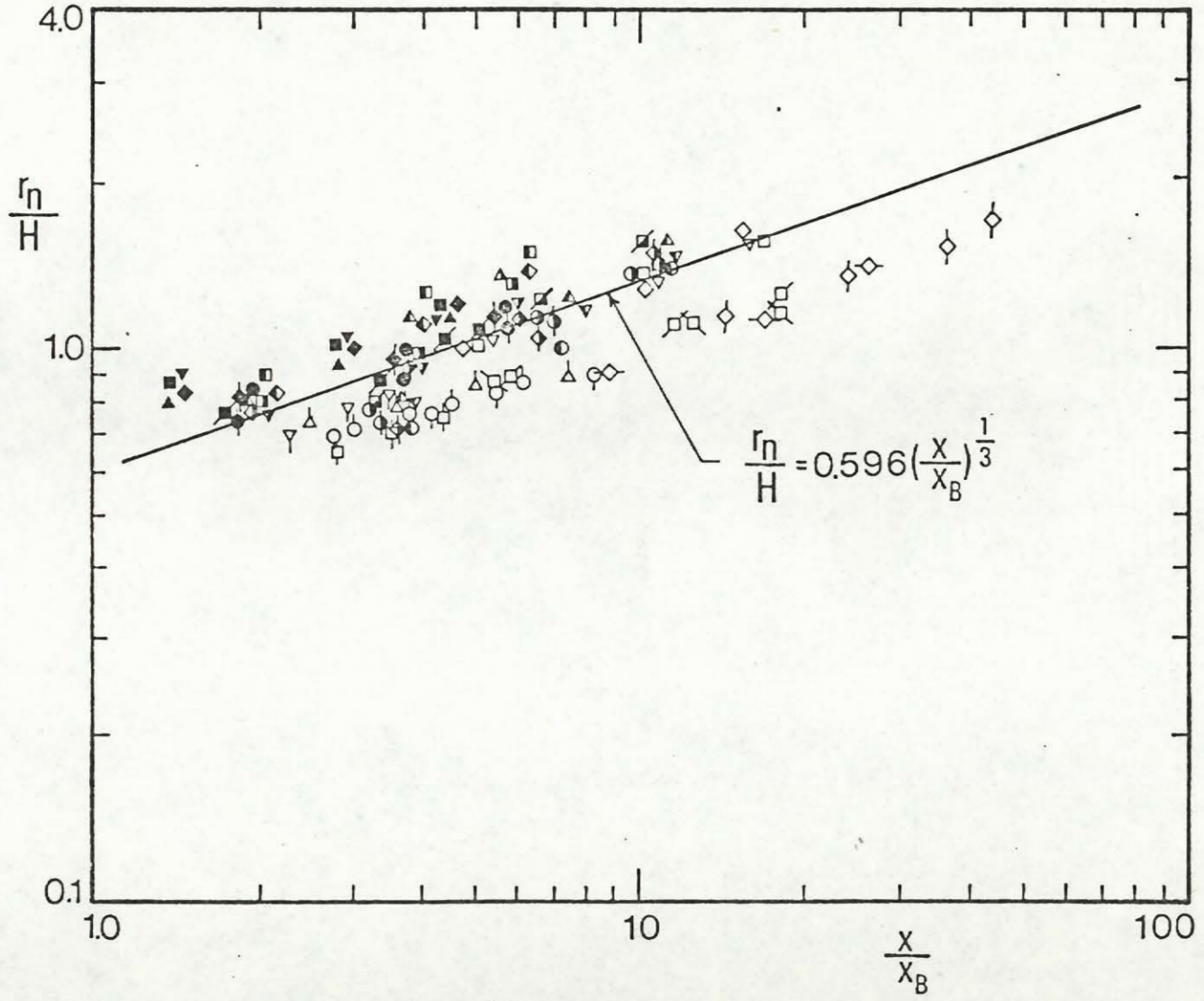

Fig. 25 Thickness of the Spreading Layer at Various Angles of Impingement

4.4 Bifurcation of Buoyant Jets

Three series of tests were carried out to study the bifurcation phenomena of buoyant jets. The excess temperature ΔT at the exit and the depth of cross-flow H are as follows:

Test series 4000: $\Delta T = 15°C$, $H = 7.6$ cm

Test series 5000: $\Delta T = 44°C$, $H = 10.4$ cm

Test series 6000: $\Delta T = 44°C$, $H = 7.6$ cm

Test conditions for each test in the series are summarized in Table 2.

A selection of top view photographs of the bifurcated jets is presented in Figs. 26 and 27. Fig. 26 compares a series of tests with different exit temperatures but keeping all other conditions exactly the same. The effect of buoyancy induced by temperature difference can be seen to have a rather significant influence on the jet bifurcation.

The cross-section of a bifurcated buoyant jet was observed to have a rather different shape. In general, a thin layer was observed attaching in front of the vortex element as shown schematically in Fig. 1(c). Fig. 27 compares tests with different depths while keeping other conditions identical. Thin spreading layer is observed in cases when the depth is shallower. The spreading layer in the present experiment was generally observed to be rather thin. It also has a tendency to merge with the vortex element and disappear at some downstream region.

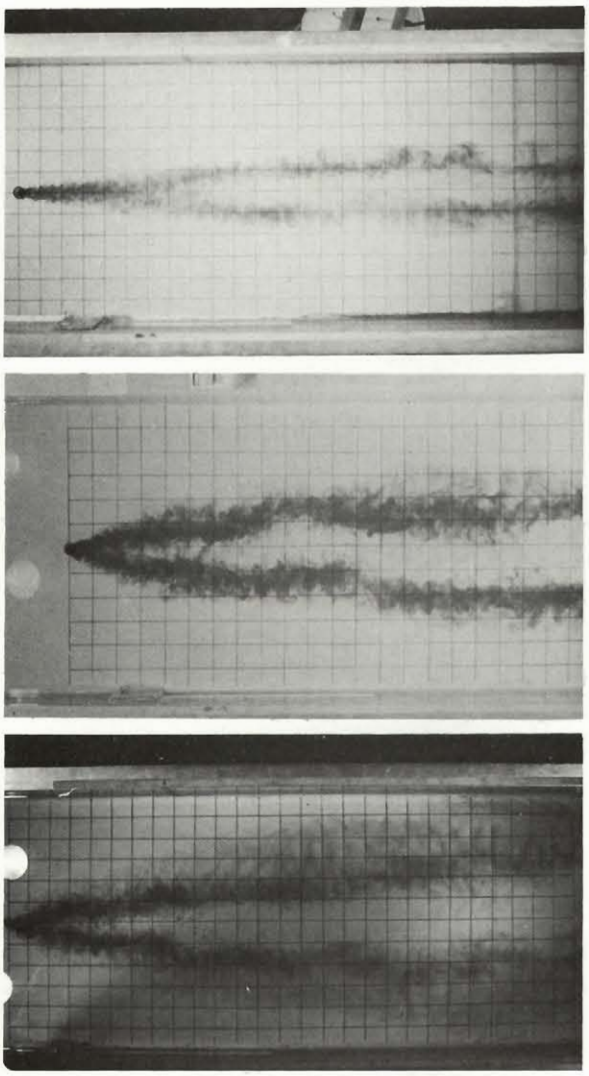

Test 2004

$\Delta T = 0°C$

Test 4001

$\Delta T = 14°C$

Test 6001

$\Delta T = 44°C$

Fig. 26 Effect of Buoyancy on Bifurcated Jets;

$U = 6.1$ cm/sec, $d = 0.40$ cm, $\ell_m = 2.6$ cm

$H = 7.6$ cm, $R = 6$

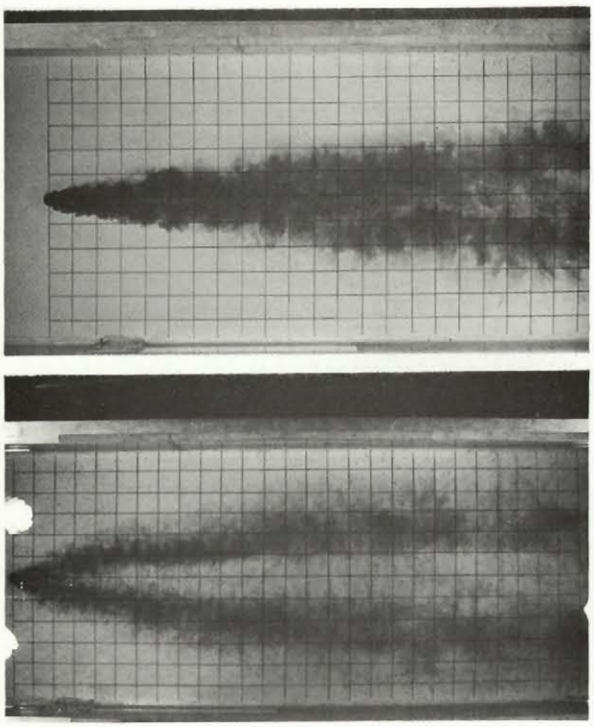

Test 5004

H = 10.4 cm

ΔT = 44°C

U = 12 cm/sec

d = 0.40 cm

R = 8

Test 6005 ℓ_m = 3.30 cm

H = 7.62 cm ℓ_b = 0.16 cm

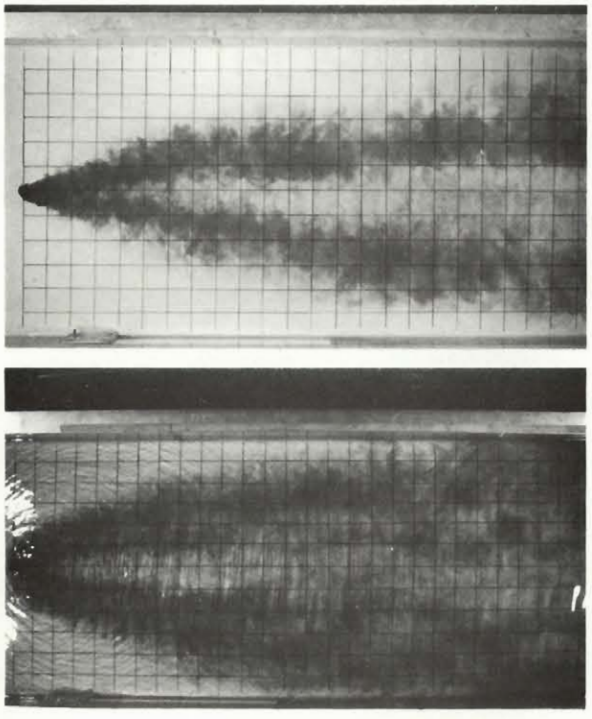

Test 5005

H = 10.40 cm

ΔT = 44°C

U = 12 cm/sec

d = 0.40 cm

R = 10

Test 6010 ℓ_m = 4.20 cm

ℓ_b = 0.20 cm

H = 7.62 cm

Fig. 27 Photographs of Bifurcated Buoyant Jets

To distinguish the thin layer from the main bulk of the vortex element, two jet widths can be defined from the top view photograph. As shown in Fig. 1(c), the jet width of the main bulk, ignoring the thin layer, is r_s. The total width including the thin layer is r_s'. Both r_s and r_s' are presented in Fig. 28. The jet width of the main bulk r_s is observed to grow linearly with the transverse migration distance s (following a 45° slope in a log-log plot). This gives an entrainment coefficient $\beta_s = 0.52$ which is slightly below the value of 0.58 and 0.55 for NB and BM, respectively. The apparent reduction of β_s could be the result of ignoring the thin layer. The width of the thin layer appears to vary in a rather complex manner, and we have not been successful in providing a proper description of the phenomena.

The jet width r_n is presented in Fig. 29. The individual test can be seen to relate to the distance s by a linear relationship. But the entrainment coefficient β_n appears to vary somewhat from test to test; the values are generally below the value of 0.77 for NB and BM. The reduction in entrainment coefficient β_n in this case is believed to be affected by stable density stratification and it may be related to the local Richardson number

$$Ri = \frac{g \frac{\Delta\rho}{\rho} r}{4u^2} \qquad (47)$$

Since $u = ds/dt$ and $r = \alpha s$, the Richardson number defined in Eq. 47 can be expressed in dimensionless form and related to the jet trajectory as follows:

$$Ri = [16\alpha\tilde{s}\ (\frac{d\tilde{s}}{d\tilde{x}})^2]^{-1} \tag{48}$$

where

$$\tilde{s} = \frac{s}{\ell_s} \quad \text{and} \quad \tilde{x} = \frac{x\ell_b}{\ell_m^2}$$

for a jet trajectory given by Eq. 27. The Richardson number at the bifurcation point is

$$(Ri)_B = \frac{3\alpha}{4} \frac{[\frac{\tilde{x}_B^2}{2(1+k)} + \tilde{x}_B]}{[\frac{\tilde{x}_B}{(1+k)} + 1]^2} \tag{49}$$

The maximum value of $(Ri)_B$ is equal to $3\alpha/4$ and it occurs at $\tilde{x}_B = \infty$. Richardson number $(Ri)_B$ is calculated in Table 2 based on $\alpha = 0.40$. The entrainment coefficient β_n is correlated with the Richardson number $(Ri)_B$ in Fig. 30. The reduction of β_n is rather small even when the $(Ri)_B$ reaches its maximum. It is not certain whether the turbulent entrainment would eventually collapse as in other density stratified shearing flows (see, for example, Chu and Vanvari (1976)). Some evidence of collapse is apparent at least in test No. 5001 with the highest $(Ri)_B$. The growth of jet widths in this test can be seen to level off in the far field region.

In one or two tests performed under very low cross-flow velocity ($U \simeq 1.5$ cm/sec, not listed in Table 2), the bifurcated vortex elements were observed to break down and to form a vortex street as vorticity vectors rotating toward the vertical direction. The vortex street was also observed to have a tendency to merge back into a single thin layer at some downstream region. The merge at this low cross-flow velocity was, however, affected by the boundary layer development alongside the channel. It was not possible to establish with certainty whether the merging is, indeed, the result of vortex interaction within the street.

It should be pointed out that merging of the vortex street was not observed, at least within the test section, in any of the tests listed in Table 2. The phenomenon, if it exists at all, would probably occur only in cases when $(Ri)_B$ is very close to its maximum of 0.3 or, in a region very far downstream from the bifurcation point.

Since the dependency of entrainment coefficient on the Richardson number has not been established with satisfaction, from now on our analysis will be based on an averaged coefficient. The variation of β_n is not large. It is possible to fit the experimental data in Fig. 29 by a single linear relationship and obtain an averaged coefficient $\overline{\beta}_n = 0.54$.

The cross-sectional area of the bifurcated buoyant jet $r_s r_n$, ignoring the thin spreading layer, is plotted in Fig. 31 against the lateral migration distance s. An average coefficient $\overline{\beta} = 0.53$ is obtained by fitting the data with a quadratic relationship.

The jet trajectory is presented in Fig. 32. In evaluating the centerline, the thin layer was ignored. The experimental results were found to follow very closely Eq. 28 if an average entrainment coefficient $\overline{\alpha} = 0.40$ and an added mass coefficient $k = 1.0$ are chosen. In the range of $H/\ell_s = 0.5$ to 4.0 of the present experiments, Eq. 28 is seen to follow essentially a one-third law. In fact, Eq. 28 would eventually approach a one-third law in the far field region. Note that $\overline{\alpha}$ and ($\overline{\beta}_n$, $\overline{\beta}$) are determined independently based on jet path and jet width, respectively. The reduction of $\overline{\alpha}$ is consistent with a similar reduction of $\overline{\beta}$ and $\overline{\beta}_n$. Average coefficients for BB ("Bifurcated Buoyant" jets) are summarized in Table 8.

$$k = 1.00$$

$$\overline{\alpha} = 0.40$$

$$\overline{\beta}_s = 0.52$$

$$\overline{\beta}_n = 0.54$$

$$\overline{\beta} = 0.53$$

TABLE 8. Average Coefficients for BB ("Bifurcated Buoyant" jets)

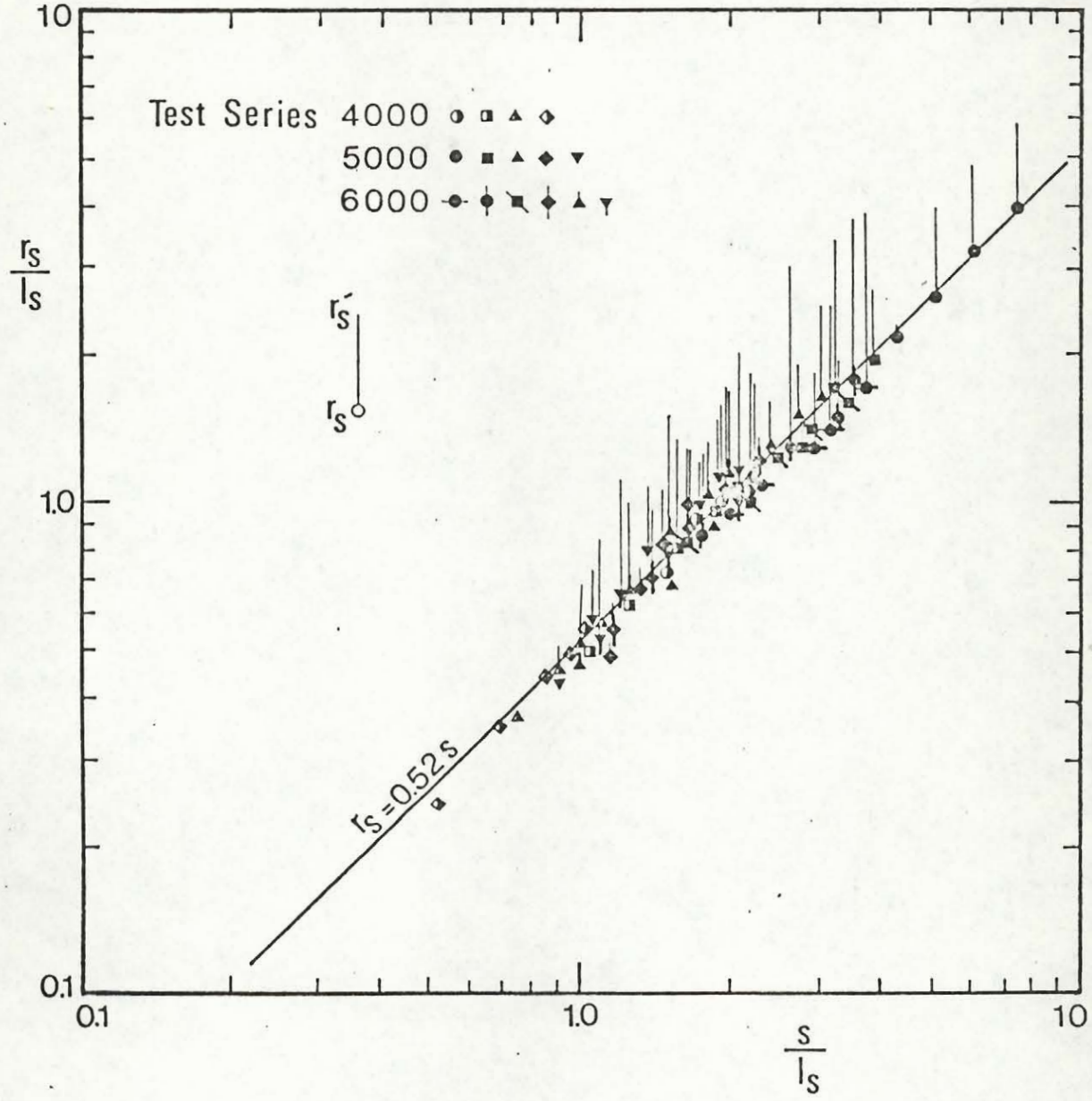

Fig. 28 Jet Width r_s of Bifurcated Buoyant Jets ($\theta_B < 20^\circ$)

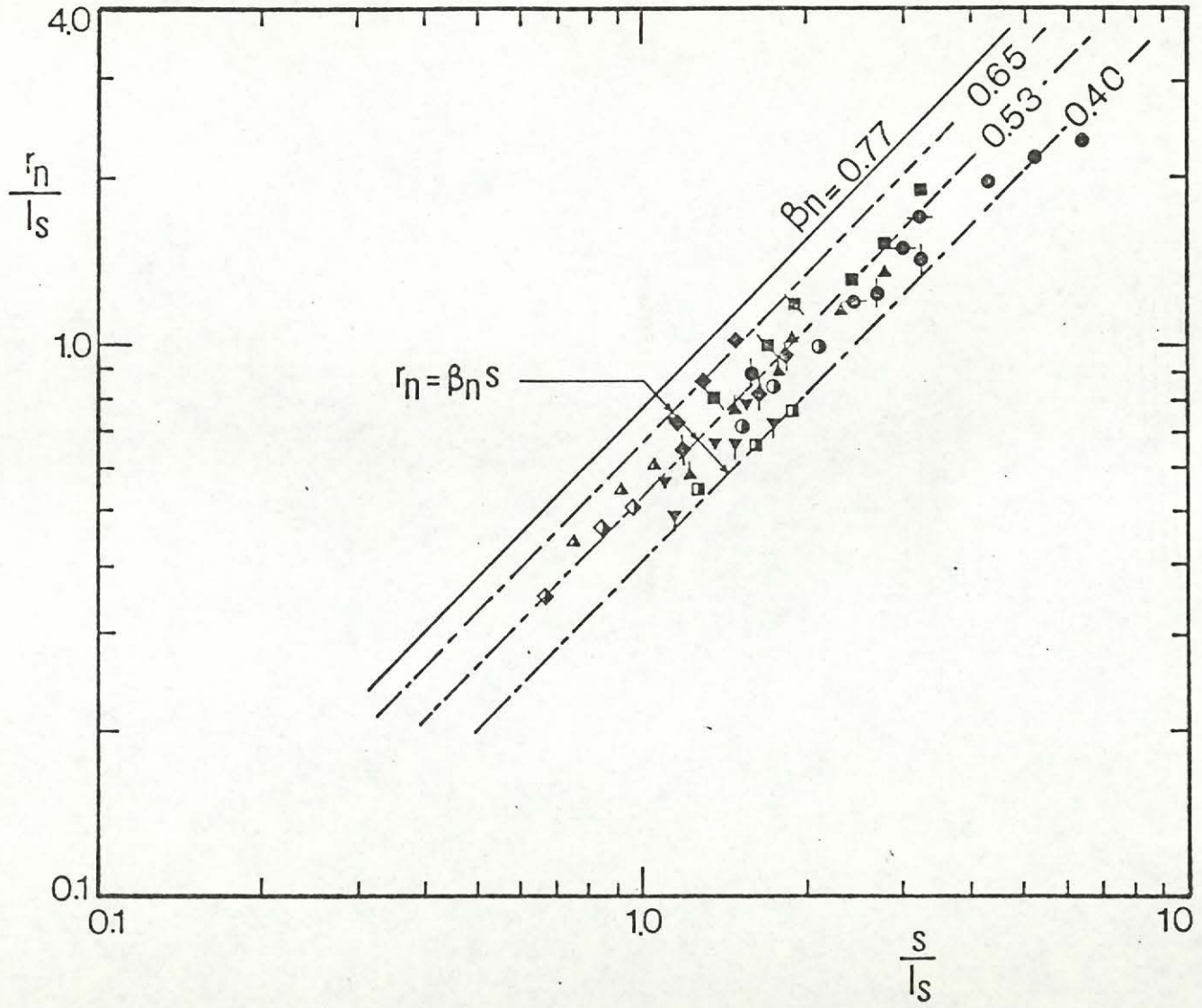

Fig. 29 Jet Width r_s of Bifurcated Buoyant Jets ($\theta_B < 20°$)

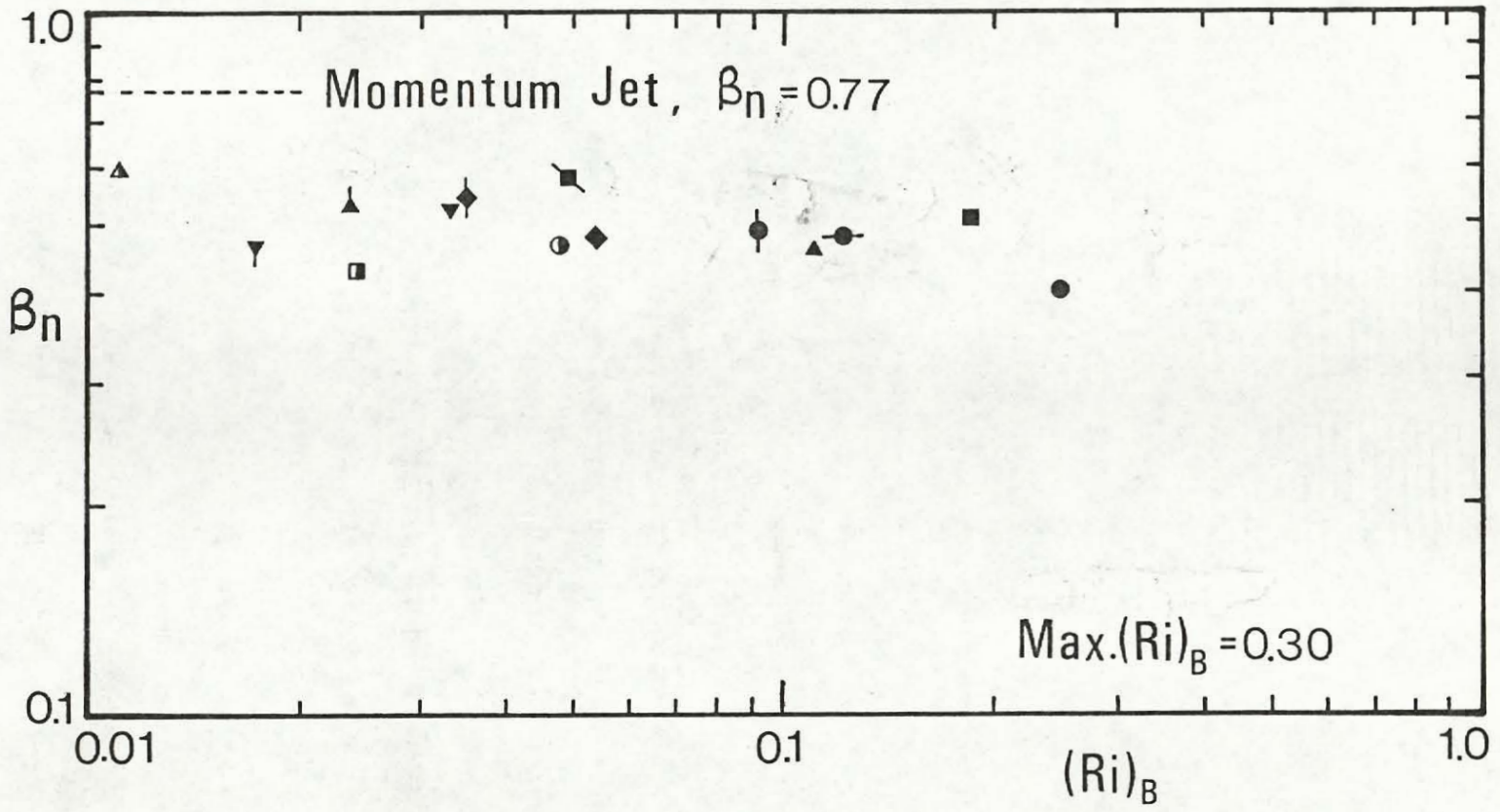

Fig. 30 Entrainment Coefficient as a Function of Richardson Number

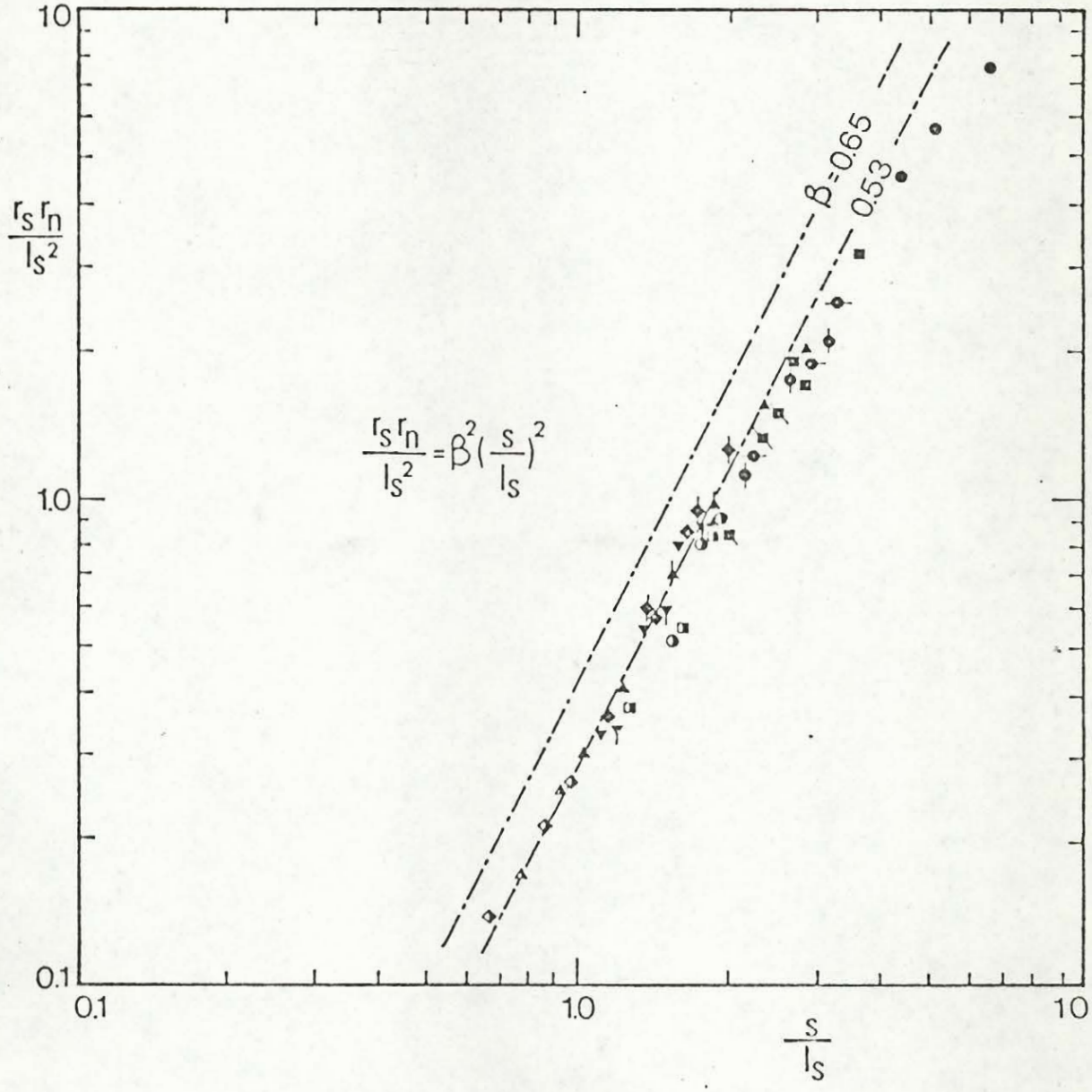

Fig. 31 Cross-Sectional Area of Bifurcated Buoyant Jets (θ_B < 20°)

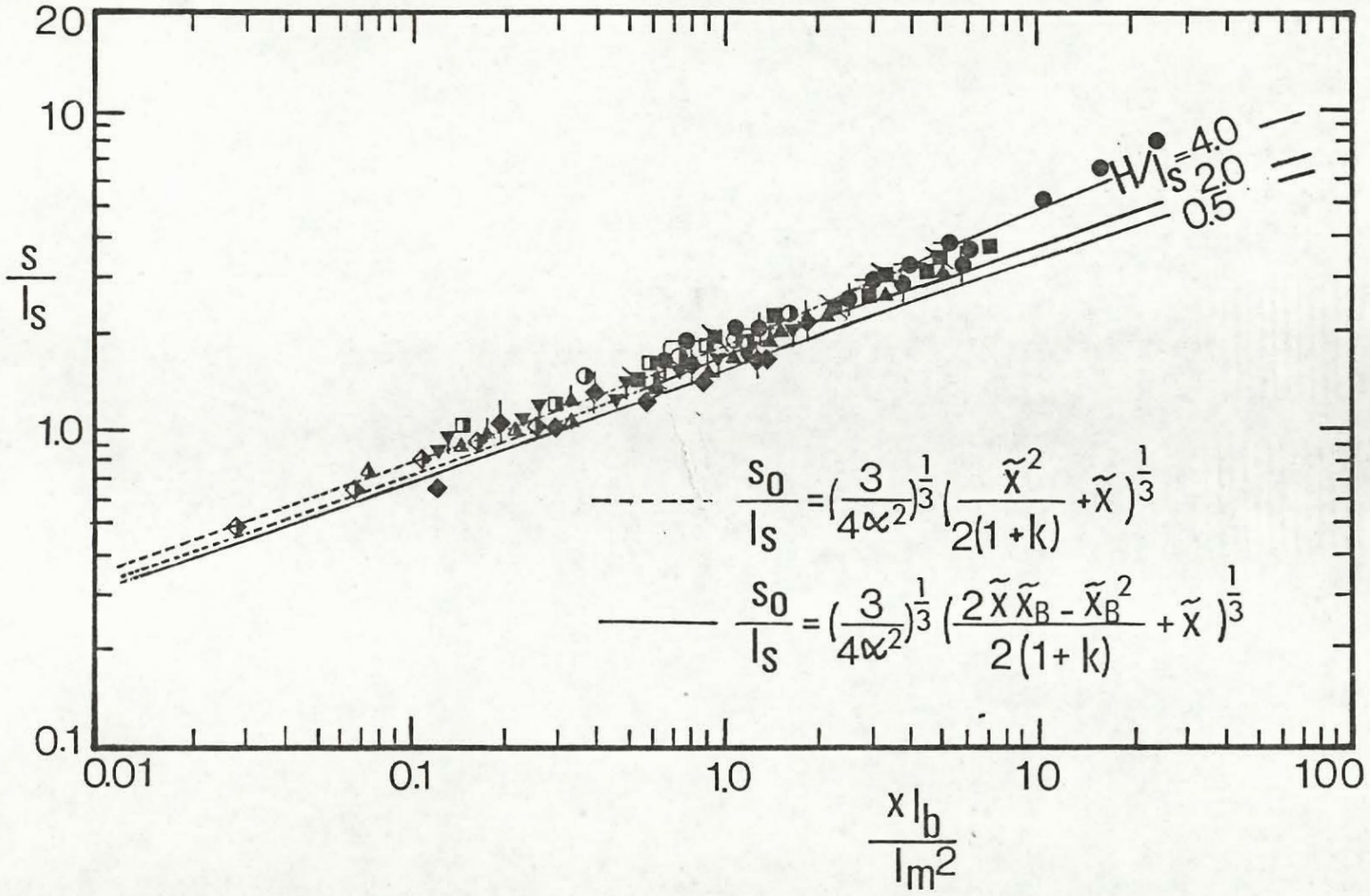

Fig. 32 Trajectory of Bifurcated Buoyant Jets ($\theta_B < 20°$)

The results for buoyant jets obtained so far were based on tests with $\theta_B < 20°$. The configuration of the radially spreading layer around the bifurcation point obtained from tests with $\theta_B > 20°$ is presented in Fig. 33. The length scale for normalization in this figure is based on momentum m_B at the bifurcation point:

$$\ell_{m_B} = \left[\frac{4m_B}{\rho\pi U}\right]^{\frac{1}{2}} = \ell_m \left[1 + \frac{x_B \ell_b}{(1+k)\ell_m^2}\right]^{1/2} \qquad (50)$$

In comparison with the momentum jet in Fig. 23, the radially spreading layer for buoyant jet is seen to have a slightly wider lateral dimension.

The experimental results in Fig.33 ($\theta_B > 20°$, $H/\ell_s = 0.5 \sim 2.0$) are replotted in Fig. 34 and compared with an equation deduced from test results of the lower impinging angle. The equation is obtained by adding $r_s/2$ to the jet center line trajectory given by Eq. 28:

$$\tilde{s}_o = (1+\beta_s)\left(\frac{3}{4\alpha^2}\right)^{1/3} \left[\frac{2\tilde{x}\,\tilde{x}_B - \tilde{x}_B^2}{2(1+k)} + \tilde{x}\right]^{1/3} \qquad (51)$$

where, for tests with $\theta_B < 20°$, $\alpha = 0.40$ and $\beta_s = 0.52$. Note that Eq. 51 does not include the thin spreading layer.

The vertical jet width r_n for all ranges of impinging angles is shown in Fig. 35. The growth of jet width is seen to follow nearly a one-third slope in the log-log plot. In the radial spreading region, the jet width r_n is affected by both the impinging angle and the Richardson number in a rather complicated manner.

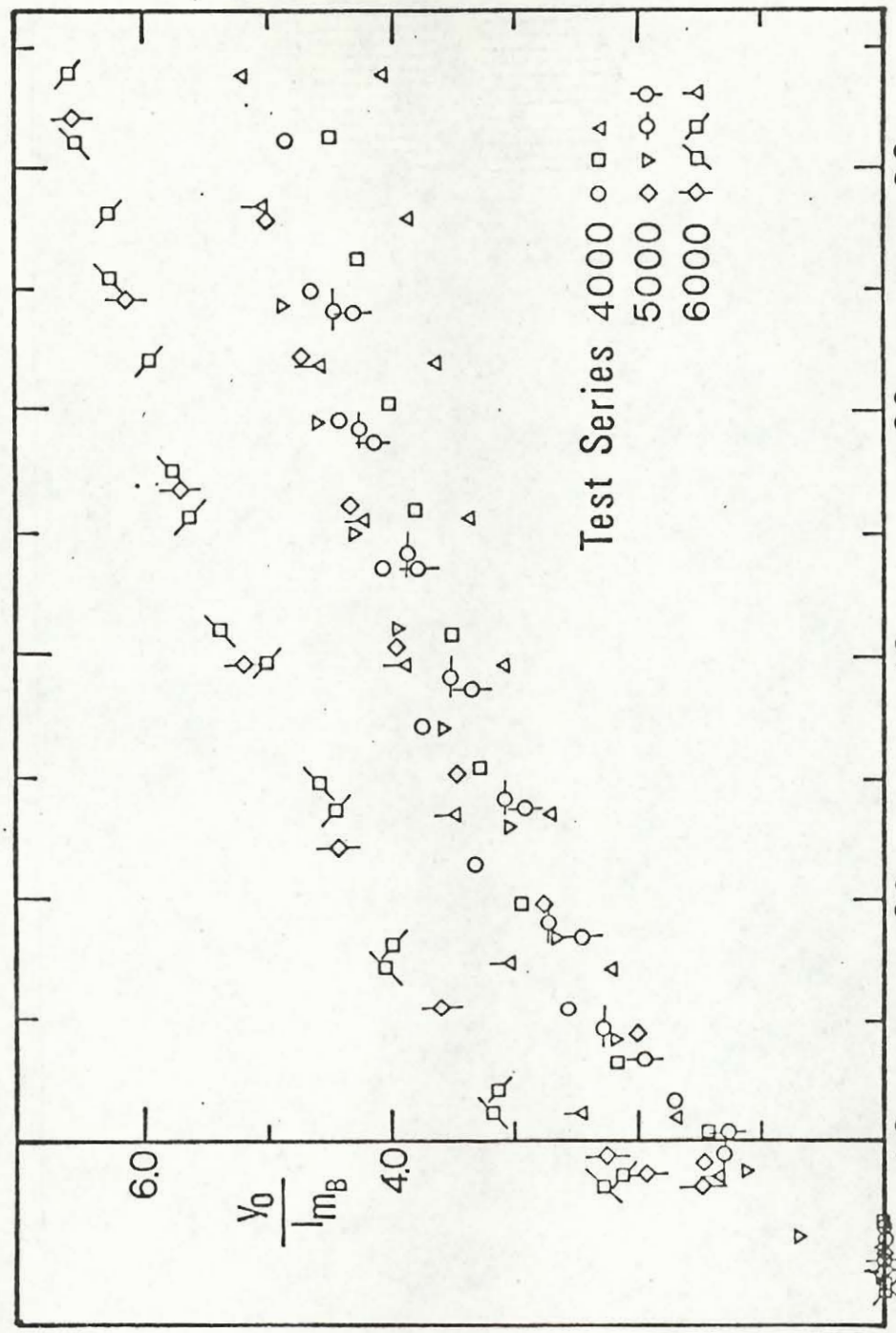

Fig 33 Buoyant Spreading Layer Around the Bifurcation Point ($\theta_B > 20°$)

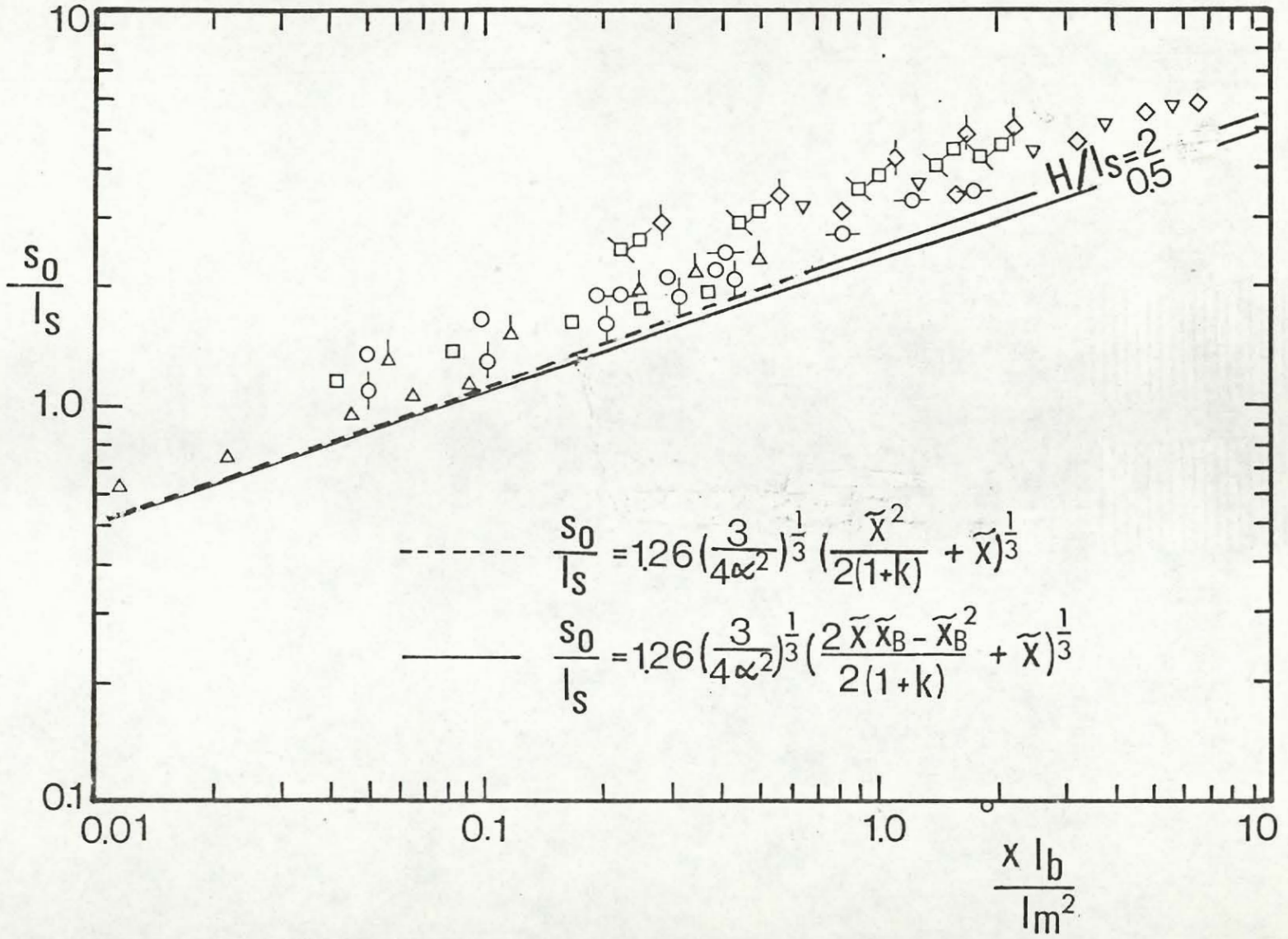

Fig. 34 Outer Boundary of the Bifurcated Buoyant Jets ($\theta_B > 20°$)

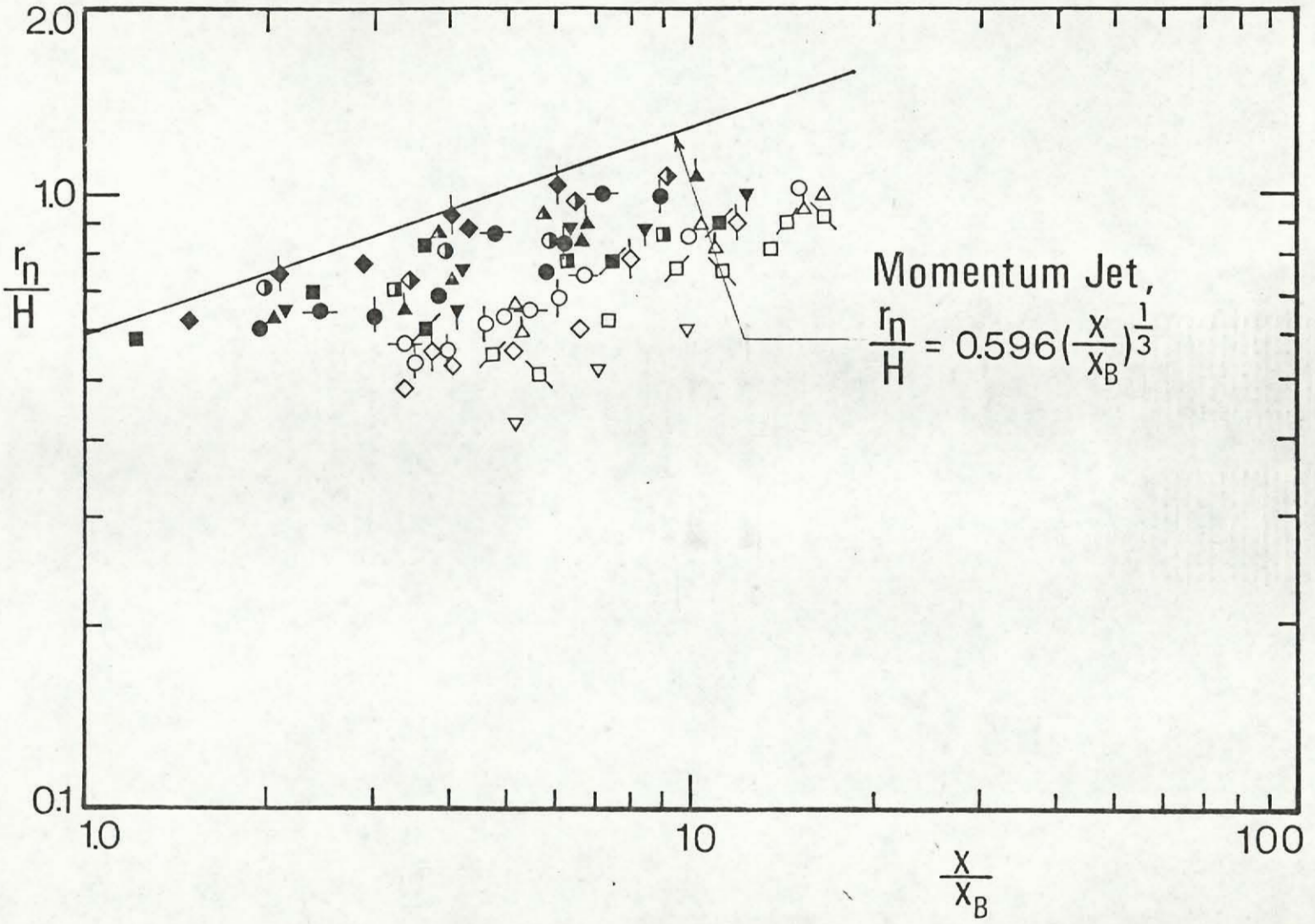

Fig. 35 Thickness of the Spreading Layer of the Buoyant Jet at various Θ_B

CHAPTER 5

SUMMARY AND CONCLUSIONS

Experimental investigation was carried out to study the bifurcation phenomena of buoyant jets in a cross-flow. The jet was observed to consist of three regions, namely: the non-bifurcated region upstream, the impinging region around the bifurcation point, and the downstream region where the jet split up into two separated elements.

The development in the impinging region near the bifurcation point is most complicated. A radially spreading layer was observed to form around the bifurcation point. The layer would eventually bifurcate into two separate elements at some downstream region.

In the limiting case when buoyancy is zero, the entrainment and spreading characteristics of each of the bifurcated elements were found to behave exactly the same as non-bifurcated jets in a cross-flow. The width of the element was observed to grow linearly with a lateral migration distance. The trajectory of the element was found to follow a simple one-third power law.

The bifurcation processes under the influence of buoyancy are more complicated. The entrainment coefficients, within the present range of experiments, were found weakly dependent on the Richardson number.

The entrainment coefficients and added-mass coefficients determined from the center line trajectory and growth of jet widths are summarized in Table 9 for NB ("non-bifurcated" jets), BM ("bifurcated momentum" jets), and BB ("bifurcated buoyant" jets), respectively.

	NB	BM	BB
k =	1.00	-	1.00
α =	0.45	0.50	0.40
β =	0.66	0.65	0.53
β_s =	0.58	0.55	0.52
β_n =	0.77	0.77	0.54

TABLE 9. Entrainment and Added-Mass Coefficients for NB, BM and BB

Note that the entrainment coefficients in Table 9 were determined for large exit to cross-flow velocity ratios (i.e., for $R > 6$) only. The entrainment coefficients for BB are weakly dependent on the Richardson number. The values in Table 9 are the average over the range of the Richardson numbers covered in the present experiment.

The experimental investigation for buoyant jets is incomplete. It has not been established with certainty whether the bifurcated vortex elements may, in some cases due to vortex interaction, merge back into a single thin layer in the downstream region. The problem is an

important one because it determines, for example, in the submerged discharge of pollutants, the maximum area of contamination. Further experiment in a wider channel is obviously needed to resolve this question.

The observation in the present experiment has been restricted to only widths and trajectory of the bifurcated jets. However, the more important information concerning the concentration and dilution of the bifurcated jet can be inferred from the dilution measurement in non-bifurcated jets. Chu (1978) reanalysed the experimental result of non-bifurcated jets by Fan (1967) and found the following relationship between the jet width r_s and minimum dilution ratio on the center plane of symmetry:

$$\frac{D_c Q_o}{U \ell_s^2} = 1.47 \left(\frac{r_s}{\ell_s}\right)^2 \tag{52}$$

Assuming that the minimum dilution ratio D_{min} at the vortex core is about $0.6\ D_c$ and that $r_n r_s / r_s^2 = 1.33$,

$$\frac{D_{min} Q_o}{U \ell_s^2} = 0.66 \left(\frac{r_n r_s}{\ell_s^2}\right)$$

$$= 0.66\ \beta^2 \left(\frac{s}{\ell_s}\right)^2 \tag{53}$$

Because entrainment characteristics between bifurcated and non-bifurcated jets were similar, Eq. 53 could be used to estimate dilution in bifurcated jets as well.

REFERENCES

1. Acton, E. "The Modelling of Large Eddies in Two-Dimensional Shear Layer". Journal of Fluid Mechanics, Vol. 76, 1976, pp. 561-592.
2. Briggs, G.A. "A Plume Rise Model Compared with Observations". Journal of the Air Pollution Control Association, Vol. 15, 1965, pp. 433-442.
3. Bringfelt, B. "A Study of Buoyant Chimney Plumes in Neutral and Stable Atmospheres". Atmospheric Environment, Vol. 3, 1969, pp. 609-618.
4. Chu, V.H. "Turbulent Dense Plumes in Laminar Cross Flow". Journal of Hydraulic Research, V. B, 1975, pp. 253-279.
5. Chu, V.H. "A Line-Impulse Model for Buoyant Jets in a Cross Flow", in Turbulent Buoyant Convection, Spalding, D.B. ed., Hemisphere Publishing Co., Washington, D.C., 1976, pp. 625-636.
6. Chu, V.H. and Goldberg,M.B. "Buoyant Force Plumes in Cross Flow", Journal of Hydraulic Division, ASCE, Vol. 100, HY 9, 1974, pp. 1203-1214.
7. Chu, V.H. and Vanvari, M.R. "Experimental Study of Turbulent Stratified Shearing Flow". Journal of Hydraulic Division, Proc. ASCE, Vol. 102, HY 6, 1976, pp. 691-706.
8. Chu, V.H. "Analysis of F.L. Fan's Data on Buoyant Jets in Cross Flow". Submitted for Publication.
9. Crow, S.C. and Bate, E.R. "Lifespan of Trailing Vortices in a Turbulent Atmosphere". Journal of Aircraft, Vol. 13, No. 7, pp. 476-482.

10. Csanady, G.T. "Some Observations on Smoke Plume". International Journal of Air and Water Pollution, Vol. 4, pp. 47-61.

11. Csanady, G.T. "The Buoyant Motion within a Hot Gas Plume in a Horizontal Wind". Journal of Fluid Mechanics, Vol. 22, 1965, pp. 225-239.

12. Daily and Harleman, Fluid Dynamics. Addison-Wesly Publishing Co., U.S.A., 1966.

13. Durando, N.A. "Vortices induced in a Jet by a Subsonic Cross Flow". AIAA Journal, Vol. 9, No. 2, 1971, pp. 325-327.

14. Escudier, M.P. and Maxworthy, T. "On the Motion of Turbulent Thermals". Journal of Fluid Mechanics, Vol. 61, 1973, pp. 541-552.

15. Fan, L.N. "Turbulent Buoyant Jets into Stratified or Flowing Ambient Fluids". W.M. Kech Laboratory Report KH-R-15, California Institute of Technology, Pasadena, California, 1967.

16. Fay, J.A., Escudier, M. and Hoult, D.P. "A Correlation of Field Observations of Plume Rise". Journal of the Air Pollution Control Association, Vol. 20, 1970, pp. 391-404.

17. Hayashi, T. "Turbulent Buoyant Jets of Effluent Discharged Vertically Upwards from an Orifice in a Cross Current in the Ocean". Proc. of the Fourteenth Congress of I.A.H.R., France 1971, Vol. 1, A-19, pp. 1-9.

18. Hoult, B.R., Fay, J.A. and Forney, L.J. "A Theory of Plums Rise Compared with Field Observations". Journal of Air Pollution Control Association, Vol. 19, 1969, pp. 585-590.

19. Keffer, J.F. and Baines, W.D. "The Round Turbulent Jet in a Cross Wind". Journal of Fluid Mechanics, Vol. 15, 1963, pp. 481-496.

20. Lamb, H. "Hydrodynamics" 6th ed., Dover, New York, 1945.

21. Morton, B.R., Taylor, G.I. and Turner, J.S. "Turbulent Gravitational Convection from Maintained and Instantaneous Sources". Proceeding of the Royal Society, London, England, Vol. A234, 1956, pp. 1-23.

22. Pratte, B.D. and Baines, W.D. "Profiles of the Round Turbulent Jet in a Cross Flow". Journal of the Hydraulic Division, ASCE, Vol. 92, HY 6, 1967, pp. 53-64;
See also Correction, Vol. 93, HY 3, 1968, pp. 815-816.

23. Priestly, C.H.B. "A Working Theory of the Bent-Over Plume of Hot Gas". Quarterly Journal of The Royal Meteorological Society, Vol. 82, 1956, pp. 165-176.

24. Rajaratnam, N. "Turbulent Jets". Elsevier Scientific Publishing Co., 1976, pp. 184-192.

25. Scorer, R.S. "Natural Aerodynamics". Pergamon Press, London, England, 1958.

26. Scorer, R.S. and Davernport, L.J. "Contrails and Aircraft Downwash". Journal of Fluid Mechanics, Vol. 43, 1970, pp. 451-464.

27. Turner, J.S. "A Comparison between Buoyant Vortex Rings and Vortex Pairs". Journal of Fluid Mechanics, Vol. 7, 1960, pp. 419-432.

28. Wright, S.J. "Mean Behaviour of Buoyant Jets in a Cross Flow". Journal of the Hydrualic Division, ASCE, Vol. 103, N. HY 5, 1977, pp. 499-513. See also Discussion by V.H. Chu.

APPENDIX I

EXIT MOMENTUM CORRECTION FACTORS

The boundary layer development inside the nozzle affects the exit velocity profile. In order that the exit momentum flux can be calculated based on uniform velocity distribution, a momentum correction factor is evaluated in this Appendix. This factor depends on the nozzle length x, fluid kinematic viscosity ν, fluid density ρ and the exit velocity V_{max}.

The formulae given for the displacement thickness and the momentum thickness of the laminar boundary layer are (see Daily and Harleman (1966), pp. 195-198):

$$\delta^* = \frac{1.73x}{Rx^{\frac{1}{2}}} \qquad \text{(I-1)}$$

$$\Theta = \frac{0.664\ x}{Rx^{\frac{1}{2}}} \qquad \text{(I-2)}$$

where the Reynolds number based on the nozzle length Rx is given by:

$$Rx = \frac{V_{max} \cdot x}{\nu} \qquad \text{(I-3)}$$

The average velocity $V_{av.}$ is given as follows:

$$V_{av} = \frac{4\ Q}{\pi d^2} \qquad \text{(I-4)}$$

where Q and d are the discharge and the inner diameter of the nozzle, respectively.

The maximum velocity at the center core is estimated to be:

$$V_{max} = \frac{4\,Q}{\pi(d-2\delta^*)^2} \qquad \text{(I-5)}$$

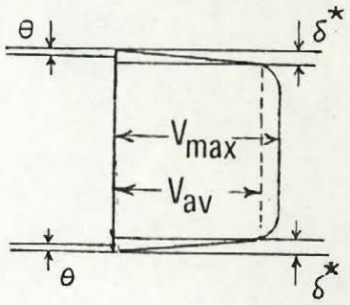

From Eqs. I-4 and I-5,

$$\left(\frac{V_{max}}{V_{av}}\right)^2 = 1 + \frac{8\delta^*}{d} + \ldots \qquad \text{(I-6)}$$

The actual exit momentum flux is

$$M_o = \frac{\pi}{4} V_{max}^2 (d-2\delta^*)^2 - V_{max}^2 \pi d\theta$$

$$= \frac{\pi}{4} V_{max}^2 d^2 \left[1 - 2\left(\frac{2\delta^*}{d}\right) + \left(\frac{2\delta^*}{d}\right) - \frac{4\theta}{d}\right] \qquad \text{(I-7)}$$

Neglecting $\left(\frac{2\delta^*}{d}\right)$, Eq. I-7 can be approximated to be:

$$M_o = \frac{\pi}{4} V_{max}^2 d^2 \left[1 - \frac{4}{d}(\delta^* - \theta\right] \qquad \text{(I-8)}$$

Since the momentum flux based on the average velocity is:

$$M_{av} = \frac{\pi}{4} V_{av}^2 d^2 \qquad \text{(I-9)}$$

From Eqs. I-6, I-8 and I-9

$$M_o = \frac{\pi}{4} V_{av}^2 d^2 \left[1 - \frac{4}{d}(\delta^* - \theta)\right]\left[1 + \frac{8\delta^*}{d} + \ldots\right]$$

$$= \frac{\pi}{4} V_{av}^2 d^2 \left[1 + \frac{4\delta^*}{d} - \frac{4\theta}{d} + \ldots\right]$$

Making use of Eqs. I-1, I-2 and I-3, the exit momentum flux can be calculated by:

$$M_o = \left[1 + \frac{1}{d}\left[4.264 \left(\frac{\nu x}{V}\right)^{\frac{1}{2}}\right]\right] V_{av} Q \qquad \text{(I-10)}$$

For the first nozzle, D = 0.20 cm, x = 0.40 cm,

$$M_o = \left[1 + 13.48 \left(\frac{\nu}{V}\right)^{\frac{1}{2}}\right] V_{av} Q \qquad \text{(I-11)}$$

For the second nozzle, D = 0.40 cm, x = 0.60 cm,

$$M_o = \left[1 + 8.26 \left(\frac{\nu}{V}\right)^{\frac{1}{2}}\right] V_{av} Q \qquad \text{(I-12)}$$

For the stack of length 3.00 cm, the above method of calculating the momentum correction factor is inaccurate. The velocity distribution at the exit of the stack is assumed to follow a power law:

$$\frac{V}{V_{max}} = \left(1 - \frac{2r}{d}\right)^{\alpha} \qquad \text{(I-13)}$$

where α is chosen to be $\frac{1}{6}$ for the range of Reynolds number of the discharging jet in the experiment.

Thus,

$$Q_o = \int_o^{\frac{d}{2}} 2 \pi V r \, d r \qquad \text{(I-14)}$$

Substituting from Eq. I-13 into Eq. I-14,

$$Q_o = \frac{\pi}{4} d^2 V_{max} \int_o^1 (1 - \frac{2r}{d})^{\frac{1}{6}} \, d \, (\frac{2r}{d})^2$$

$$= 0.198 \, \pi \, d^2 \, V_{max} \qquad \text{(I-15)}$$

Similarly, the actual exit momentum flux M_o will be calculated as follows:

$$M_o = \int_o^{\frac{d}{2}} 2 \pi V^2 \, r \, d \, r \qquad \text{(I-16)}$$

Again substituting from Eq. I-13 into Eq. I-16,

$$M_o = 0.161 \, \pi \, d^2 \, V_{max}^2 \qquad \text{(I-17)}$$

Since $V_{av} = 0.7912 \, V_{max}$, the exit momentum flux will be given as,

$$M_o = 1.03 \, \rho \, Q \, V_{av} \qquad \text{(I-18)}$$

Eqs. I-11 and I-12 were used to calculate the exit momentum flux in tests in which nozzles with diameters 0.20 cm and 0.40 cm are used while Eq. I-18 was used to calculate the exit momentum flux in tests with a stack.

SUMMARY OF EXPERIMENTAL RESULTS

Test No	M_o/ρ_o^2 (cm^4/sec^2)	F_o/ρ_o^3 (cm^4/sec^3)	ℓ_s (cm)	$(Re)_o$	$(Re)_a$	$\frac{x}{\ell_m}$	$\frac{s}{\ell_m}$	$\frac{s_o}{\ell_m}$	$\frac{s_i}{\ell_m}$	$\frac{r_s}{\ell_m}$	$\frac{r_n}{\ell_m}$
						3.535	2.506	3.086	1.926	1.160	1.826
						7.070	3.023	3.851	2.194	1.657	2.248
1001	1850.8	-	-	4723	12050	10.60	3.464	4.403	2.526	1.878	2.636
						14.14	3.683	4.731	2.636	2.095	
						17.67	3.906	5.066	2.746	2.320	
						3.497	2.461	2.952	1.969	0.984	2.104
						6.994	2.761	3.554	1.969	1.584	2.370
1002	453.20	-	-	2311	6092	10.49	3.226	4.045	2.406	1.639	2.708
						13.99	3.444	4.373	2.515	1.858	
						19.23	4.045	5.193	2.898	2.295	
						3.496	2.624	3.280	1.969	1.311	1.839
						6.992	2.843	3.717	1.969	1.748	2.146
1003	1780.3	-	-	4581	12078	10.49	3.239	4.181	2.296	1.885	2.676
						13.89	3.717	4.809	2.624	2.185	
						17.48	4.045	5.246	2.843	2.404	

Test No	M_o/ρ_o (cm^4/sec^2)	F_o/ρ_o (cm^4/sec^3)	ℓ_s (cm)	$(Re)_o$	$(Re)_a$	$\frac{x}{\ell_m}$	$\frac{s}{\ell_m}$	$\frac{s_o}{\ell_m}$	$\frac{s_i}{\ell_m}$	$\frac{r_s}{\ell_m}$	$\frac{r_n}{\ell_m}$
						3.445	2.640	3.340	1.940	1.400	2.174
						6.891	2.802	3.660	1.940	1.723	2.358
1004	458.36	-	-	2291	6040	10.34	3.259	4.201	2.317	1.884	2.646
						13.78	3.663	4.740	2.586	2.153	
						17.23	4.086	5.270	2.901	2.369	
						3.098	2.234	2.739	1.729	1.009	1.626
						6.196	2.754	3.391	2.117	1.275	1.929
1005	2407.5	-	-	5395	12045	9.294	3.424	4.354	2.494	1.860	2.290
						12.39	3.704	4.714	2.794	1.92	
						15.49	4.064	5.068	3.060	2.008	
						3.067	2.302	2.877	1.727	1.150	1.692
						6.134	2.709	3.452	1.967	1.486	1.952
1006	594.30	-	-	2654	6122	9.201	3.141	4.027	2.254	1.773	3.324
						12.27	3.38	4.411	2.350	2.061	
						15.33	3.62	4.794	2.446	2.348	

Test No	M_o/ρ_o (cm^4/sec^2)	F_o/ρ_o (cm^4/sec^3)	ℓ_s (cm)	$(Re)_o$	$(Re)_a$	$\frac{x}{\ell_m}$	$\frac{s}{\ell_m}$	$\frac{s_o}{\ell_m}$	$\frac{s_i}{\ell_m}$	$\frac{r_s}{\ell_m}$	$\frac{r_n}{\ell_m}$
						3.068	2.323	2.919	1.728	1.191	1.604
						6.137	2.707	3.494	1.920	1.575	1.843
1007	2487.7	-	-	5432	12531	7.671	3.186	4.166	2.207	1.958	2.076
						9.205	3.411	4.423	2.399	2.024	2.308
						12.27	3.565	4.635	2.495	2.140	
						1.513	2.157	2.61	1.704	0.906	
						3.026	2.406	3.068	1.744	1.324	1.532
1008	622.16	-	-	2679	6180	6.052	2.959	3.765	2.152	1.613	1.700
						9.078	3.302	4.148	2.456	1.692	2.194
						12.10	3.606	4.532	2.680	1.852	

Test No	M_o/ρ_o (cm^4/sec^2)	F_o/ρ_o (cm^4/sec^3)	ℓ_s (cm)	$(Re)_o$	$(Re)_a$	$\frac{x}{x_B}$	$\frac{x-x_B}{\ell_m}$	$\frac{y_o}{\ell_m}$	$\frac{r_n}{H}$
							-1.1365	0.4309	
							-0.4471	0.8618	
						2.426	0.2424	1.2065	0.7378
							0.9318	1.5512	
1009	3058.3	-	-	6089	12084	3.640	1.6212	1.8098	0.7724
							2.3107	2.0683	
						4.853	3.0001	2.3268	0.8426
							3.6895	2.5854	
						7.279	4.3789	2.6715	0.8776
							-1.1706	0.6738	
							-0.4968	1.0738	
						2.302	0.1769	1.4739	0.6796
							0.8507	1.7476	
1010	739.26	-	-	2926	6000	2.878	1.5245	2.0213	0.7680
							2.1983	2.1056	
						3.454	2.8721	2.1897	0.8038
							3.5458	2.2951	
						4.029	4.2196	2.4003	0.9170

Test No	M_b/ρ_o (cm^4/sec^2)	F_o/ρ_o (cm^4/sec^3)	ℓ_s (cm)	$(Re)_o$	$(Re)_a$	$\frac{x}{x_B}$	$\frac{x-x_B}{\ell_m}$	$\frac{y_o}{\ell_m}$	$\frac{r_n}{H}$
							-0.8315	0.6989	
							-0.2103	1.1648	
						2.989	0.4120	1.7473	0.7028
							1.322	1.9413	
1011	3793.1	-	-	6790	12126	3.736	1.6534	2.1743	0.7374
							2.2747	2.4073	
						4.483	2.8959	2.5626	0.7724
							3.5171	2.7955	
						5.977	4.1384	2.8512	0.8426
							-0.8927	0.4233	
							-0.2771	0.9234	
						2.758	0.3385	1.2697	0.6796
							0.9541	1.6159	
1012	926.12	-	-	3324	6135	4.137	1.5697	1.8084	0.7476
							2.1853	2.0010	
						5.516	2.8009	2.1546	0.8154
							3.4165	2.3085	
						8.275	4.0320	2.3854	0.8494

Test No	M_o/ρ_o (cm^4/sec^2)	F_o/ρ_o (cm^4/sec^3)	ℓ_s (cm)	$(Re)_o$	$(Re)_a$	$\frac{x}{x_B}$	$\frac{x-x_B}{\ell_m}$	$\frac{y_o}{\ell_m}$	$\frac{r_n}{H}$
							-0.8611	0.8363	
							-0.2529	1.3685	
						2.758	0.3554	1.8247	0.6796
							0.9636	2.1288	
1013	982.82	-	-	3384	6245	4.137	1.5718	2.3759	0.7476
							2.1801	2.4710	
						5.516	2.7883	2.5850	0.8154
							3.3965	2.6991	
						8.275	4.0047	2.8131	0.8494

Test No	M_o/ρ_o (cm^4/sec^2)	F_o/ρ_o (cm^4/sec^3)	ℓ_s (cm)	$(Re)_o$	$(Re)_a$	$\frac{x}{\ell_m}$	$\frac{s}{\ell_m}$	$\frac{s_o}{\ell_m}$	$\frac{s_i}{\ell_m}$	$\frac{r_s}{\ell_m}$	$\frac{r_n}{\ell_m}$
						4.096	2.957	3.533	2.381	1.152	
						8.193	3.195	4.009	2.381	1.628	2.220
2001	721.56	-	-	2929	9300	16.39	3.765	4.749	2.781	1.968	2.614
						24.58	4.141	5.197	3.085	2.112	3.114
						36.87	4.813	5.965	3.661	2.304	
						4.043	2.792	3.234	2.350	0.884	
						8.086	3.082	3.813	2.350	1.463	2.310
2002	185.74	-	-	1466	4656	16.17	3.547	4.443	2.650	1.793	2.762
						24.26	3.767	4.724	2.809	1.915	3.102
						36.39	4.111	5.177	3.045	2.132	
						4.042	2.854	3.360	2.349	1.010	
						8.083	3.017	3.686	2.349	1.337	2.296
2003	720.21	-	-	2887	9166	16.17	3.802	4.749	2.854	1.894	3.150
						24.25	4.307	5.307	3.307	2.000	3.788
						36.37	5.011	6.138	3.884	2.254	

Test No	M_o/ρ_{o_2} (cm^4/sec^2)	F_o/ρ_{o^3} (cm^4/sec^3)	ℓ_s (cm)	$(Re)_o$	$(Re)_a$	$\frac{x}{\ell_m}$	$\frac{s}{\ell_m}$	$\frac{s_o}{\ell_m}$	$\frac{s_i}{\ell_m}$	$\frac{r_s}{\ell_m}$	$\frac{r_n}{\ell_m}$
						3.973	2.827	3.344	2.309	1.035	
						7.946	3.034	3.758	2.309	1.449	1.916
2004	198.74	-	-	1491	4734	15.89	3.861	4.793	2.930	1.862	2.548
						23.84	4.394	5.443	3.344	2.099	3.122
						35.76	4.802	6.053	3.551	2.502	
						3.517	2.621	3.198	2.044	1.154	
						7.034	3.253	4.022	2.484	1.539	1.630
2005	1203.7	-	-	3798	9043	14.07	3.649	4.610	2.687	1.923	2.516
						21.10	4.293	5.396	3.190	2.206	3.248
						31.65	4.588	5.726	3.450	2.275	
						3.053	2.363	2.953	1.774	1.178	
						6.105	2.762	3.382	2.142	1.240	1.734
2006	354.48	-	-	2040	4858	12.21	3.447	4.336	2.559	1.778	3.522
						18.32	3.931	4.922	2.940	1.982	3.454
						27.47	4.170	5.304	3.036	2.268	

Test No	M_o/ρ_o (cm^4/sec^2)	F_o/ρ_o (cm^4/sec^3)	ℓ_s (cm)	$(Re)_o$	$(Re)_a$	$\frac{x}{\ell_m}$	$\frac{s}{\ell_m}$	$\frac{s_o}{\ell_m}$	$\frac{s_i}{\ell_m}$	$\frac{r_s}{\ell_m}$	$\frac{r_n}{\ell_m}$
						3.052	2.418	3.061	1.774	1.287	
						6.104	3.040	3.872	2.208	1.664	1.530
2007	1371.3	-	-	4011	9551	12.21	3.531	4.587	2.475	2.112	2.288
						18.31	4.151	5.255	3.047	2.208	2.822
						27.47	4.580	5.875	3.285	2.589	
						3.002	2.409	3.038	1.780	1.258	
						6.005	3.004	3.618	2.390	1.368	1.448
2008	335.28	-	-	1951	4646	12.01	3.712	4.666	2.758	1.908	2.148
						18.01	4.066	5.140	2.993	2.148	2.904
						27.02	4.462	5.78	3.144	2.636	

Test No	M_o/ρ_o (cm^4/sec^2)	F_o/ρ_o (cm^4/sec^3)	ℓ_s (cm)	$(Re)_o$	$(Re)_a$	$\frac{x}{x_B}$	$\frac{x-x_B}{\ell_m}$	$\frac{y_o}{\ell_m}$	$\frac{r_n}{H}$
							-0.9960	0.0000	
							0.2411	1.4690	
						4.968	1.4781	2.0877	1.0344
							2.7152	2.3965	
2009	1818.6	-	-	4681	8917	9.936	3.9523	2.6288	1.2758
							5.1893	2.8613	
						14.90	6.4264	3.1314	1.5862
							7.6634	3.3247	
							8.9005	3.4794	
							-0.9676	0.6126	
							0.2576	1.4549	
						5.065	1.4828	1.9145	1.0002
							2.7080	2.2973	
2010	511.50	-	-	2459	4684	10.13	3.9332	2.5271	1.3448
							5.1584	2.8333	
						15.19	6.3836	2.9866	1.5172
							7.6088	3.1014	
							8.8340	3.2162	

Test No	M_o/ρ_o (cm^4/sec^2)	F_o/ρ_o (cm^4/sec^3)	ℓ_s (cm)	$(Re)_o$	$(Re)_a$	$\frac{x}{x_B}$	$\frac{x-x_B}{\ell_m}$	$\frac{y_o}{\ell_m}$	$\frac{r_n}{H}$
							-0.9677	0.00	
							0.2575	1.3784	
							1.4827	1.8378	
							2.7080	2.2208	
2011	2049	-	-	4921	9374		3.9332	2.4504	
							5.1584	2.6036	
							6.3836	2.7567	
							7.6088	3.0630	
							8.8340	3.3694	
							-0.9225	1.0203	
							0.2833	1.8088	
						5.229	1.4892	2.3365	1.0000
							2.6950	2.7132	
2012	456.1	-	-	2285	4353	10.46	3.9009	2.9394	1.2758
							5.1067	3.0901	
						15.69	6.3126	3.2408	1.5518
							7.5184	3.3161	
							8.7243	3.3916	

Test No	M_o/ρ_o (cm^4/sec^2)	F_o/ρ_o (cm^4/sec^3)	ℓ_s (cm)	$(Re)_o$	$(Re)_a$	$\frac{x}{\ell_m}$	$\frac{s}{\ell_m}$	$\frac{s_o}{\ell_m}$	$\frac{s_i}{\ell_m}$	$\frac{r_s}{\ell_m}$	$\frac{r_n}{\ell_m}$
						3.845	2.935	3.626	2.244	1.382	
						7.691	3.529	4.394	2.664	1.729	2.160
3001	52.43	-	-	741	3245	15.38	3.845	4.785	2.905	1.881	3.008
						23.07	4.112	5.199	3.025	2.174	3.728
						34.61	4.515	5.885	3.145	2.700	
						3.845	2.845	3.445	2.244	1.202	
						7.690	3.085	3.806	2.364	1.442	2.388
3002	201.2	-	-	1451	6357	15.38	3.626	4.407	2.845	1.862	3.418
						23.07	4.173	5.368	2.978	2.390	4.066
						34.61	4.534	5.849	3.218	2.630	
						2.884	2.629	3.170	2.089	1.082	
						5.768	3.215	3.846	2.584	1.552	1.656
3003	86.73	-	-	953	3131	11.54	3.528	4.389	2.668	1.721	2.308
						17.30	3.692	4.671	2.713	1.958	2.986
						25.96	3.857	4.941	2.774	2.167	

Test No	M_o/ρ_o (cm^4/sec^2)	F_o/ρ_o (cm^4/sec^3)	ℓ_s (cm)	$(Re)_o$	$(Re)_a$	$\frac{x}{\ell_m}$	$\frac{s}{\ell_m}$	$\frac{s_o}{\ell_m}$	$\frac{s_i}{\ell_m}$	$\frac{r_s}{\ell_m}$	$\frac{r_n}{\ell_m}$
						2.884	2.487	3.021	1.953	1.068	
						5.768	2.994	3.697	2.291	1.406	1.513
3004	355.62	-	-	1929	6336	11.54	3.524	4.373	2.674	1.699	2.338
						17.30	3.974	4.914	3.035	1.879	2.796
						25.90	4.493	5.545	3.440	2.104	
						2.884	2.326	2.821	1.830	0.9913	
						5.768	2.794	3.533	2.055	1.477	1.284
3005	1377.7	-	-	3798	12294	11.54	3.243	4.142	2.343	1.798	1.842
						17.30	3.479	4.502	2.456	2.046	2.786
						25.90	3.848	5.088	2.608	2.300	

Test No	M_o/ρ_o (cm^4/sec^2)	F_o/ρ_o (cm^4/sec^3)	ℓ_s (cm)	$(Re)_o$	$(Re)_a$	$\frac{x}{x_B}$	$\frac{x-x_B}{\ell_m}$	$\frac{y_o}{\ell_m}$	$\frac{r_n}{H}$
							-0.2856	1.2978	
							0.8680	2.0188	
						5.874	2.0216	2.3794	0.8448
							3.1751	2.6678	
3006	143.1	-	-	1224	3184	11.75	4.3287	2.8720	1.0860
							5.4823	3.0562	
						17.62	6.6359	3.2023	1.3878
							7.7894	3.3887	
							8.9430	3.6043	
							-0.5014	1.0815	
							0.6521	2.0186	
						5.758	1.8056	2.5233	0.8392
							2.9691	2.8837	
3007	560.5	-	-	2423	6334	11.52	4.1126	3.1522	1.1790
							5.2661	3.3247	
						17.27	6.4196	3.5211	1.1388
							7.5731	3.7772	
							8.7266	3.7814	

Test No	M_o/ρ_o (cm^4/sec^2)	F_o/ρ_o (cm^4/sec^3)	ℓ_s (cm)	$(Re)_o$	$(Re)_a$	$\frac{x}{x_B}$	$\frac{x-x_B}{\ell_m}$	$\frac{y_o}{\ell_m}$	$\frac{r_n}{H}$
							0.0375	1.3521	
							0.7511	1.6075	
						5.759	1.6532	1.9623	0.6594
							2.4121	2.2743	
3008	2062.5	-	-	4648	12152	11.52	3.3913	2.6013	1.0096
							4.2832	2.7498	
						17.28	5.4892	2.9432	1.1578
							6.2832	3.0521	
							7.1983	3.1213	
							0.0547	1.4420	
							1.066	2.1029	
						8.458	1.9679	2.4033	0.7844
							2.9293	2.5836	
3009	200.16	-	-	1447	3138	16.32	3.8906	2.7638	1.0860
							4.8519	2.9740	
						25.37	5.8132	3.1544	1.3274
							6.7745	3.3345	
							7.7359	3.4848	

Test No	M_o/ρ_{o_2} (cm^4/sec^2)	F_o/ρ_{o_3} (cm^4/sec^3)	ℓ_s (cm)	$(Re)_o$	$(Re)_a$	$\frac{x\ell_b}{\ell_m^2}$	$\frac{s}{\ell_s}$	$\frac{s_o}{\ell_s}$	$\frac{s_i}{\ell_s}$	$\frac{r_s}{\ell_s}$	$\frac{r_n}{\ell_s}$
						0.1793	1.2470	1.500	0.9938	0.5064	
						0.3587	1.5210	1.883	1.1600	0.7228	0.7060
4001	190.1	20.32	7.185	1453	4712	0.7173	1.7490	2.217	1.2810	0.9360	0.8542
						1.0760	1.9380	2.440	1.4360	1.0040	0.9022
						1.6140	2.2160	2.753	1.6790	1.0740	
						0.1450	1.0620	1.398	0.7266	0.4711	
						0.2901	1.2510	1.595	0.9095	0.6875	0.7478
4002	313.3	26.27	9.297	1880	4571	0.5801	1.6160	2.202	1.2120	0.8081	1.0668
						0.8702	1.8270	2.323	1.3320	0.9920	1.6398
						1.1600	1.9240	2.465	1.3830	1.0820	
						0.0370	0.6498	0.7686	0.5309	0.2377	
						0.0740	0.7684	0.9531	0.5837	0.3694	0.4570
4003	696.1	29.90	12.02	2831	8988	0.1480	0.8941	1.125	0.6630	0.4622	0.5624
						0.2220	1.0330	1.291	0.7950	0.4960	0.6176
						0.3330	1.1040	1.393	0.8149	0.5781	

Test No.	M_o/ρ_{o_2} (cm^4/sec^2)	F_o/ρ_{o_3} (cm^4/sec^3)	ℓ_s (cm)	$(Re)_o$	$(Re)_a$	$\frac{x\ell_b}{\ell m^2}$	$\frac{s}{\ell_s}$	$\frac{s_o}{\ell_s}$	$\frac{s_i}{\ell_s}$	$\frac{r_s}{\ell_s}$	$\frac{r_n}{\ell_s}$
						0.0275	0.5268	0.6500	0.4036	0.2464	
						0.0550	0.6618	0.8687	0.4549	0.4138	0.3394
4004	1248.4	40.29	16.01	3815	9085	0.1100	0.8383	1.0500	0.5868	0.4631	0.4766
						0.1650	0.9592	1.2120	0.7061	0.5062	0.5188
						0.2475	1.0160	1.3060	0.7259	0.5800	

Test No	M_o/ρ_o (cm^4/sec^2)	F_o/ρ_o (cm^4/sec^3)	ℓ_s (cm)	$(Re)_o$	$(Re)_a$	$\frac{x}{x_B}$	$\frac{x-x_B}{\ell_s}$	$\frac{y_o}{\ell_s}$	$\frac{r_n}{H}$
							0.3211	1.693	
							1.1411	2.554	
						4.999	2.2480	3.326	0.6512
							3.4550	3.742	
4005	501.9	29.31	12.20	2394	4657	9.997	4.6620	4.039	0.9434
							5.8690	4.395	
						15.00	7.0760	4.633	1.0448
							8.2820	4.870	
							9.4890	5.108	
							0.0721	1.495	
							0.6732	2.189	
						7.075	1.9790	2.834	0.7132
							3.1020	3.233	
4006	730.2	35.51	14.65	2901	4702	14.15	4.2700	3.481	0.9296
							5.2810	3.670	
						21.23	6.1910	3.928	1.0512
							7.2010	4.227	
							8.2120	4.475	

Test No	M_o/ρ_o (cm^4/sec^2)	F_o/ρ_o (cm^4/sec^3)	ℓ_s (cm)	$(Re)_o$	$(Re)_a$	$\frac{x}{x_B}$	$\frac{x-x_B}{\ell_s}$	$\frac{y_o}{\ell_s}$	$\frac{r_n}{H}$
							-0.0874	0.000	
							0.2625	1.627	
						5.092	1.4870	2.169	0.6466
							2.7120	2.651	
4007	1929.2	50.29	19.88	4762	9071	10.18	3.9360	3.073	0.9156
							5.1610	3.375	
						15.28	6.3850	3.616	0.9744
							7.6100	3.796	
							8.8340	3.977	

Test No	M_o/ρ_o (cm^4/sec^2)	F_o/ρ_o (cm^4/sec^3)	ℓ_s (cm)	$(Re)_o$	$(Re)_a$	$\frac{x\ell b}{\ell m^2}$	$\frac{s}{\ell_s}$	$\frac{s_o}{\ell_s}$	$\frac{s_i}{\ell_s}$	$\frac{r_s}{\ell_s}$	$\frac{r_n}{\ell_s}$
						2.6520	3.492	4.141	2.843	1.2980	
						5.3030	4.292	5.404	3.181	2.2230	2.104
5001	50.78	40.22	2.975	729	3126	10.610	5.610	6.464	3.857	2.6070	2.174
						15.910	6.188	7.808	4.568	3.2400	2.318
						23.860	7.855	9.825	5.884	3.9410	
						0.7352	2.183	2.572	1.794	0.7775	
						1.4700	2.327	2.819	1.836	0.9835	1.338
5002	183.2	78.21	4.492	1416	6137	2.9410	2.715	3.353	2.077	1.2760	1.518
						4.4110	3.120	3.985	2.254	1.7320	2.032
						6.6170	3.918	4.911	2.925	1.9860	
						0.5321	1.566	1.892	1.239	0.6543	
						1.0640	1.843	2.295	1.392	0.9030	1.024
5003	415.9	130.7	6.51	2159	6238	2.1280	2.311	3.010	1.611	1.3990	1.160
						3.1930	2.715	3.476	1.953	1.5230	1.330
						4.7890	3.119	3.937	2.301	1.6360	

Test No	M_o/ρ_o (cm^4/sec^2)	F_o/ρ_o (cm^4/sec^3)	ℓ_s (cm)	$(Re)_o$	$(Re)_a$	$\frac{x\ell_b}{\ell m^2}$	$\frac{s}{\ell_s}$	$\frac{s_o}{\ell_s}$	$\frac{s_i}{\ell_s}$	$\frac{r_s}{\ell_s}$	$\frac{r_n}{\ell_s}$
						0.1469	1.0800	1.283	0.8759	0.4074	
						0.2938	1.1530	1.395	0.9106	0.4840	0.7456
5004	1260.8	216.9	9.16	3807	12314	0.5877	1.2710	1.614	0.9279	0.6856	0.8890
						0.8815	1.4500	1.886	1.0150	0.8715	1.0552
						1.3220	1.6500	2.181	1.1190	1.0620	
						0.1194	0.9264	1.147	0.7063	0.4403	
						0.2388	1.0960	1.389	0.8042	0.5846	0.5772
5005	1939.3	270.1	9.51	4742	12268	0.4775	1.3430	1.763	0.9230	0.8400	0.6654
						0.7163	1.5460	2.071	1.0210	1.0500	0.7860
						1.0740	1.8090	2.423	1.1960	1.2280	

Test No	M_o/ρ_o (cm^4/sec^2)	F_o/ρ_o (cm^4/sec^3)	ℓ_s (cm)	$(Re)_o$	$(Re)_a$	$\frac{x}{x_B}$	$\frac{x-x_B}{\ell_s}$	$\frac{y_o}{\ell_s}$	$\frac{r_n}{H}$
							-0.9830	0.000	
							-0.2511	1.572	
						3.273	0.8571	2.006	0.5720
							1.9590	2.765	
5006	135.14	64.76	4.88	1211	3117	4.092	3.0600	3.415	0.5821
							4.1620	3.903	
						4.910	5.2640	4.337	0.5828
							6.3650	4.771	
						6.547	7.4670	5.204	0.6032
							-0.2511	1.554	
							0.8676	2.209	
							1.7210	2.650	
							2.6110	3.027	
5007	262.33	97.08	6.62	1705	3134	5.212	3.4210	3.517	0.4346
							4.2130	3.926	
						6.515	5.0210	4.294	0.5316
							5.8800	4.581	
						9.121	6.8110	4.892	0.6382

Test No	M_o/ρ_{o_2} (cm^4/sec^2)	F_o/ρ_{o_3} (cm^4/sec^3)	ℓ_s (cm)	$(Re)_o$	$(Re)_a$	$\frac{x}{x_B}$	$\frac{x-x_B}{\ell_s}$	$\frac{y_o}{\ell_s}$	$\frac{r_n}{H}$
							-0.2417	0.000	
							-0.1621	1.352	
						3.284	0.7863	2.276	0.5942
							1.7920	2.672	
5008	721.56	168.17	8.652	2863	6204	4.926	2.7970	3.068	0.6726
							3.8030	3.464	
						6.568	4.8080	3.859	0.7744
							5.8140	4.156	
						9.031	6.8190	4.453	0.8796
							-0.0663	0.000	
							0.0542	1.410	
						3.034	0.6977	1.964	0.5560
							1.7210	2.417	
5009	2845.9	338.39	13.55	5763	12365	3.793	2.7440	2.921	0.5898
							3.7680	3.425	
						4.552	4.7910	3.878	0.6356
							5.8150	4.180	
						6.069	6.8380	4.382	0.6842

Test No	M_o/ρ_o (cm^4/sec^2)	F_o/ρ_o (cm^4/sec^3)	ℓ_s (cm)	$(Re)_o$	$(Re)_a$	$\frac{x\ell_b}{\ell_m^2}$	$\frac{s}{\ell_s}$	$\frac{s_o}{\ell_s}$	$\frac{s_i}{\ell_s}$	$\frac{r_s}{\ell_s}$	$\frac{r_n}{\ell_s}$
						0.7205	1.926	2.409	1.444	0.9654	
						1.4050	2.264	2.810	1.718	1.0920	1.122
6001	194.3	81.75	4.56	1460	4636	2.8100	2.900	3.550	2.250	1.3000	1.491
						4.2150	3.194	3.912	2.475	1.4370	1.734
						6.3220	3.723	4.609	2.837	1.7720	
						0.6265	1.733	2.170	1.296	0.8744	
						1.2530	2.151	2.772	1.530	1.2420	0.939
6002	262.2	98.34	5.23	1704	4636	2.5060	2.643	3.464	1.823	1.3600	1.263
						3.7590	3.143	3.891	2.395	1.4960	1.412
						5.6380	3.494	4.402	2.586	1.8160	
						0.1926	1.160	1.439	0.881	0.5589	
						0.3852	1.353	1.710	0.996	0.7139	0.824
6003	730.9	166.4	6.93	2882	9151	0.7704	1.674	2.139	1.209	0.9302	1.041
						1.1560	1.868	2.420	1.317	1.1030	1.195
						1.7330	2.193	2.890	1.537	1.3120	

Test No.	M_o/ρ_{o^2} (cm^4/sec^2)	F_o/ρ_{o^3} (cm^4/sec^3)	ℓ_s (cm)	$(Re)_o$	$(Re)_a$	$\frac{x\ell_b}{\ell_m^2}$	$\frac{s}{\ell_s}$	$\frac{s_o}{\ell_s}$	$\frac{s_i}{\ell_s}$	$\frac{r_s}{\ell_s}$	$\frac{r_n}{\ell_s}$
						0.1662	1.031	1.280	0.7829	0.4967	
						0.3324	1.197	1.519	0.8760	0.6425	0.6634
6004	988.2	194.11	8.05	3362	9151	0.6647	1.588	2.071	1.1060	0.9654	0.8622
						0.9971	1.767	2.270	1.2640	1.0060	1.0122
						1.4960	2.147	2.711	1.5840	1.1270	
						0.1418	1.035	1.394	0.6764	0.5179	
						0.2835	1.228	1.653	0.8232	0.6701	0.5564
6005	1283.8	215.13	9.27	3843	9151	0.5671	1.522	1.970	1.0740	0.8958	0.7640
						0.8506	1.787	2.332	1.2420	1.0900	0.8988
						1.2760	1.967	2.553	1.3820	1.1710	
						0.1266	1.000	1.321	0.6789	0.5025	
						0.2532	1.206	1.541	0.8703	0.6708	0.4842
6006	1617.7	242.03	10.39	4323	9151	0.5063	1.487	1.937	1.0371	0.8820	0.6642
						0.7595	1.753	2.334	1.1710	1.1630	0.7204
						1.1390	1.927	2.563	1.2920	1.2710	

Test No	M_o/ρ_o (cm^4/sec^2)	F_o/ρ_o (cm^4/sec^3)	ℓ_s (cm)	$(Re)_o$	$(Re)_a$	$\frac{x}{x_B}$	$\frac{x-x_B}{\ell_s}$	$\frac{y_o}{\ell_s}$	$\frac{r_n}{H}$
							-0.3851	1.909	
							-0.1532	3.523	
						3.721	1.1430	4.478	0.5822
							2.4240	5.182	
6007	339.0	112.09	5.95	1947	4636	7.612	4.0150	5.799	0.8024
							5.5070	6.166	
						11.521	6.9990	6.680	0.9344
							8.4900	7.047	
							9.9820	7.194	
							-0.3982	2.113	
							0.1930	3.317	
						4.761	1.5250	4.162	0.5500
							2.8570	4.261	
6008	427.6	122.63	6.74	2190	4636	9.421	4.1890	5.408	0.7782
							5.5210	5.801	
						14.23	6.8530	6.227	0.9024
							8.1850	6.555	
							9.5170	6.817	

Test No	M_o/ρ_o (cm^4/sec^2)	F_o/ρ_o (cm^4/sec^3)	ℓ_s (cm)	$(Re)_o$	$(Re)_a$	$\frac{x}{x_B}$	$\frac{x-x_B}{\ell_s}$	$\frac{y_o}{\ell_s}$	$\frac{r_n}{H}$
							-0.3013	2.281	
							0.3474	3.170	
						5.621	1.5510	3.940	0.5222
							2.7550	4.473	
6009	524.82	140.4	7.38	2434	4636	11.32	3.9590	5.066	0.7606
							5.1630	5.628	
						16.23	6.6370	5.895	0.9344
							7.5710	6.251	
							8.7750	6.576	
							-0.2812	1.386	
							0.2789	2.434	
						5.212	1.5030	2.928	0.6084
							2.7280	3.435	
6010	1989.5	268.9	11.5	4803	9151	10.48	3.9520	3.856	0.8402
							5.1760	4.248	
						16.12	6.4010	4.670	1.0024
							7.6250	5.001	
							8.8400	5.242	

Test No	$\frac{x}{\ell_m}$	$\frac{s_o}{\ell_m}$
	1.379	2.063
	2.758	3.226
1009	4.137	3.916
	5.515	4.347
	8.273	4.605
	1.348	2.865
	2.695	3.539
1010	3.369	3.707
	4.043	3.876
	4.716	3.960
	1.242	2.907
	2.485	3.528
1011	3.106	3.917
	3.727	4.227
	4.970	4.460

Test No	$\frac{x}{\ell_m}$	$\frac{s_o}{\ell_m}$
	1.231	2.618
	2.462	3.233
1012	3.694	3.541
	4.925	3.810
	7.387	4.157
	1.216	3.043
	1.825	3.613
1013	2.433	3.727
	3.041	4.259
	3.649	4.487

Test No	$\frac{x}{\ell_m}$	$\frac{s_o}{\ell_m}$
	2.474	3.332
	4.948	4.067
2009	9.896	4.917
	14.84	5.304
	22.27	5.729
	2.450	3.415
	4.901	4.028
2010	9.802	4.947
	14.70	5.176
	22.05	5.713
	2.450	3.300
	4.901	3.798
2011	9.802	4.870
	14.70	5.406
	22.05	5.866

Test No	$\frac{x}{\ell_m}$	$\frac{s_o}{\ell_m}$
	2.412	3.813
	4.823	4.303
2012	9.647	4.906
	14.47	5.547
	21.71	5.924

Test No	$\frac{x}{\ell_m}$	$\frac{s_o}{\ell_m}$
	2.307	3.492
	4.614	3.948
3006	9.229	4.501
	13.84	4.934
	24.23	5.474
	2.307	3.609
	4.614	4.378
3007	9.229	5.087
	13.84	5.663
	20.76	6.000
	2.307	3.032
	4.614	3.500
3008	9.228	4.041
	13.84	4.582
	20.76	5.159

Test No	$\frac{x}{\ell_m}$	$\frac{s_o}{\ell_m}$
	1.923	3.330
	3.845	3.781
3009	7.691	4.202
	11.54	4.382
	17.30	4.953

Test No	$\frac{x\ell_b}{\ell_{m^2}}$	$\frac{s_o}{\ell_s}$
	0.04956	1.376
	0.09911	1.642
4005	0.19820	1.888
	0.29730	2.093
	0.39650	2.257
	0.04087	1.149
	0.08174	1.385
4006	0.16350	1.607
	0.24520	1.760
	0.32700	1.948
	0.01112	0.637
	0.02225	0.750
4007	0.04450	0.939
	0.06675	1.052
	0.08899	1.127

Test No	$\frac{x\ell_b}{\ell_{m^2}}$	$\frac{s_o}{\ell_s}$
	0.8044	3.122
	1.6090	3.531
5006	3.2180	4.863
	4.8260	5.734
	6.4350	6.554
	0.6178	3.244
	1.2360	3.652
5007	2.4710	4.452
	3.707	5.169
	4.942	5.720
	0.1985	1.886
	0.3969	2.261
5008	0.7939	2.724
	1.1910	3.186
	1.5880	3.533

Test No	$\frac{x\ell_b}{\ell_{m^2}}$	$\frac{s_o}{\ell_s}$
	0.0503	1.106
	0.1006	1.309
5009	0.2013	1.660
	0.3019	2.010
	0.4025	2.195

Test No	$\frac{x\ell_b}{\ell_{m^2}}$	$\frac{s_o}{\ell_s}$
	0.2761	3.012
	0.5522	3.558
6007	1.1040	4.315
	1.6570	4.820
	2.2090	5.114
	0.2394	2.755
	0.4789	3.234
6008	0.9578	3.939
	1.4370	4.403
	1.9160	4.737
	0.2234	2.612
	0.4467	3.053
6009	0.8935	3.696
	1.3400	4.170
	1.7870	4.560

Test No	$\frac{x\ell_b}{\ell_{m^2}}$	$\frac{s_o}{\ell_s}$
	0.05718	1.390
	0.11440	1.567
6010	0.22870	1.902
	0.3431	2.195
	0.4570	2.401

Test No	$\frac{x\ell_b}{\ell_{m^2}}$	$\frac{s_o}{\ell_s}$

APPENDIX III

LENGTH OF THE POTENTIAL CORE

The length of the potential core z_p has been estimated from the measurements made by Pratte and Baines (1967). The results are summarized in the following table.

Test Series	d (cm)	z_p (cm)	$\frac{z_p}{cm}$
1000	0.20	1.10 ~ 1.14	0.075 ~ 0.078
	0.40	1.88 ~ 2.08	0.128 ~ 0.141
2000	0.20	0.94 ~ 1.04	0.123 ~ 0.136
	0.40	1.48 ~ 1.72	0.194 ~ 0.226
3000	0.4	1.48 ~ 1.88	0.195 ~ 0.247
4000	0.4	1.48 ~ 1.88	0.195 ~ 0.247
5000	0.4	1.48 ~ 1.92	0.143 ~ 0.186
6000	0.4	1.48 ~ 1.72	0.194 ~ 0.226